# A DETAILED ANALYSIS OF THE CHEMICAL ABUNDANCES FOR THE STAR THETA URSAE MAJORIS

By

MALCOLM LEE BRUCE WEEMS

Bachelor of Science
Kansas State Teachers College
Emporia, Kansas
1967

Master of Science
Kansas State Teachers College
Emporia, Kansas
1969

Submitted to the Faculty of the Graduate College
of the Oklahoma State University
in partial fulfillment of the requirements
for the Degree of
DOCTOR OF PHILOSOPHY
May, 1972

A DETAILED ANALYSIS OF THE CHEMICAL ABUNDANCES

FOR THE STAR THETA URSAE MAJORIS

Thesis Approved:

Leon W. Schroeder

Thesis Adviser

Delbert L. Rutledge

Kenneth E. Wiggins

E E Kohnke

N Durham

Dean of the Graduate College

## ACKNOWLEDGEMENTS

The author would like to acknowledge Dr. Leon W. Schroeder, my thesis adviser, for suggesting the topic, supplying the tracing used in this study, and providing invaluable guidance throughout the preparation of this dissertation.

I also wish to extend a special thanks to Dr. J. C. Evans of the Department of Physics, Kansas State University, for use of his unpublished computer programs used in this study and for his exceedingly helpful suggestions and comments.

In addition, the author acknowledges Dr. K. O. Wright for the spectrograms used in this study; Dr. H. O. Peebles and Dr. E. C. Mangold for their permission to use certain data from their theses; the contributions made by the other members of my graduate committee, Dr. D. L. Rutledge, Dr. E. E. Kohnke, and Dr. K. E. Wiggins for their counseling during the formulation of this study; and Oklahoma State University Research Foundation for financial support for the use of the computer.

Finally, I would like to express appreciation to my wife, Cheryl, for her understanding and assistance during the preparation of this investigation and to my parents for their interest, encouragement and assistance at all times during my educational career.

TABLE OF CONTENTS

TABLE OF CONTENTS (Continued)

LIST OF TABLES

## LIST OF FIGURES

LIST OF FIGURES (Continued)

LIST OF FIGURES (Continued)

CHAPTER I

# INTRODUCTION

## Introduction to the Topic

Abundance determinations from stellar spectra have long preoccupied investigators in the field of astrophysics. The value of abundance determinations lies in the clues which they give to the history of stellar matter. For a fixed set of abundances it is possible to make a one-to-one mapping between the net emergent flux and the surface gravity and the coordinates of the Hertzsprung Russell diagram--a diagram representing the evolutionary path of a stellar object. Generally, the characterization of the net emergent flux and the surface gravity is accomplished through a model atmosphere approach.

The analysis of stellar spectra has developed from the rudimentary curve of growth analysis, the relationship between the width of a line and the number of effective absorbing atoms, first introduced by Minnaert and Slob (1931). Essentially, this technique represents a method for the deduction of various atmospheric parameters such as the temperature, pressure and chemical composition, based on the approximation that spectral line formation can be treated as originating in an atmosphere of some fixed temperature and density.

An improvement upon the treatment of spectral analysis began with the model atmosphere technique of Stromgen (1940) and has since been significantly improved upon by more recent investigations.

Aller (1949) was the first to apply the model atmosphere method to stars other than the sun where he investigated the B2V star, $\gamma$ Pegasi, Wallerstein (1966), Greenstein (1948), and R. Cayrel and A. Cayrel de Strobel (1966) have catalogued a number of stars, upon which these techniques have been applied. Of significance is the fact that very little is known about stars falling near the spectral range of the sun--such as Theta Ursae Majoris.

The determination of the chemical abundance of a stellar atmosphere using the fine analysis approach is based upon a generalized procedure of successive approximation. First, a curve of growth analysis supplies rough estimates of the abundance of existing elements, the surface gravity, and the effective temperature of the star. Next, a grid of stellar atmospheres can be computed on the basis of this knowledge. Selection of the appropriate model for the stellar atmosphere finally rests upon a comparison between experimental and theoretical values of the energy distribution in the continuous spectrum, the color temperature of the star and the hydrogen line profiles. In addition, any correct stellar model should effectively reproduce the discontinuity in the energy distribution at the Balmer limit. From the model atmosphere, the stratification of the temperature, pressure, and opacity can be used in conjunction with an assumed mechanism for the formation of a spectral line to theoretically predict the line profile and its equivalent width. Once agreement between the observed and calculated profiles has been achieved, abundance may be determined.

## Purpose of the Study

The purpose of this investigation is to determine the chemical composition of the stellar atmosphere of the star Theta Ursae Majoris. The abundances of the elements employ a detailed description of the structuring of the atmosphere. Theoretical curves of growth, metal line profiles, and equivalent widths are utilized to assess the effects of the various line broadening agents which are present in the atmosphere.

## Previous Investigation of Theta Ursae Majoris

Theta Ursae Majoris ($\alpha(1900) = 9^h\ 26^m$, $\delta(1900) = 52^o 8'$, Keenan and Morgan, 1951) is listed in the catalogue of Johnson and Morgan (1953) as a subgiant star of spectral type F6, luminosity class IV, and visual magnitude of 3.3. Like most stars of its type, it exhibits a low rotational velocity and shows no evidence of the presence of a stellar magnetic field. These latter qualities make Theta Ursae Majoris well-suited for analysis since the treatment of these two mechanisms is a difficult problem to introduce in the formation of a spectral line.

In the case of Theta Ursae Majoris, the coarse analysis necessary for the model atmosphere techniques were performed by Greenstein (1948), Boyarchuk (1960), Peebles (1964), and Mangold (1968). Both Greenstein and Mangold utilized a differential curve of growth technique while Peebles considered an absolute curve of growth method. Boyarchuk compared observed curves of growth with the theoretical curves computed by Wrubel for the Milne-Eddington model. A summary of the pertinent physical parameters obtained by these investigators is shown in Table I.

Some of the peculiar features of this star can be found in the hydrogen line contours and the metallic line profiles. Both of these show an abnormal reduction in line intensity when compared to similar stars. A portion of this effect (Greenstein, 1948) can be attributed to an

TABLE I

THE PHYSICAL PARAMETERS OF θ URSAE MAJORIS DETERMINED

FROM CURVE OF GROWTH ANALYSES

| Parameter | Greenstein | Peebles | Mangold |
|---|---|---|---|
| $\theta^{o}_{exc}$ | 1.04 | none | 0.98 |
| $\theta^{*}_{exc}$ | 0.98 | numerous values | 0.88 |
| $\theta^{*}_{ion}$ | 0.87 | 0.81[1] | 0.81[1] |
| $\log c/v^{*}$ | 5.44 | 5.04(Fe I-NBS) | none |
| $\log P^{*}_{e}$ | 1.20[2] | 1.31(Ti I-NBS) | 1.07 |
| $\log k^{*}_{\lambda}$ | -1.00 | none | -0.70 |
| $\log a^{*}$ | -2.3 | -1.8 Both scattering models<br>-1.3 Both absorption models | none |

[1]Derived from the effective temperature.

[2]Derived for $\theta_{ion} = 0.80$.

o = Sun

* = Star

unusually high value of the continuous optical absorption coefficient. This reduces the intensity of the observed lines, and gives the effect of a higher-than-normal surface gravity. However, some atmospheric structuring is still necessary to explain this anomaly. A comparison of the abundance analyses of Mangold and Greenstein shows evidence of some variation, but on the whole, indicates that the photosphere of Theta Ursae Majoris has a chemical composition not too unlike the solar atmosphere. Mangold did find trends which suggested the metal content of this star was somewhat deficient relative to the solar values.

A fine analysis of the atmosphere of Theta Ursae Majoris was performed by Evans and Schroeder (1969) and Bulman (1971) using a pressure-opacity-flux model for a given temperature distribution. A grid of sixteen representative model atmospheres were computed using a scaled version of Elste's solar temperature distribution. Effective temperatures and logarithms of the surface gravities were taken to fall within the range 6200 $^{o}$K to 6650 $^{o}$K and from 3.8 to 4.4, respectively. Among the results reported was the fact that the computed UBV colors, corrected for line blanketing (Myrick, 1970), were not in agreement with the observed ones for the band-width difference U-B. An analysis of the hydrogen line profiles resulted in a choice of the representative model atmosphere for Theta Ursae Majoris having an effective temperature of 6500 $^{o}$K and a surface gravity of log g = 4.2.

In a further investigation, Evans, Schroeder, and Weems (1971) suggest that a revision of this atmospheric model is necessary when the multicolor photometry of Mitchell and Johnson (1969) is included with the previous information. A model atmosphere with an effective temperature of 6350 $^{o}$K and logarithm of the surface gravity of 4.0 seems to be more indicative of the conditions with the atmosphere of this star. For the purposes of this investigation this model of the atmosphere of Theta Ursae Majoris will be utilized for all computational procedures.

# CHAPTER II

## MODEL ATMOSPHERES

### The Description of a Stellar Atmosphere

For the purposes of this study, a stellar atmosphere is described by that portion of a star capable of being observed. In a general way this would refer to the regions of a star from which its components of the electromagnetic spectrum arise; and characteristically this implies the layers of a star from which the continuous and absorption-line spectrum are formed. The present interpretation of a stellar atmosphere implies a depth ranging from a few hundred to a few thousand kilometers; the solar atmosphere, for example, can be described as having a geometrical depth of approximately 330 kilometers (Aller, 1963). Of course it is because the actual processes occurring within the atmosphere determine the nature of the radiant energy emitted that one may deduce the physical properties of the stellar atmosphere from observations of the continuum and the strength and shape of the spectral absorption lines.

The representation of a stellar atmosphere in terms of a model proceeds from a postulation of the dependence of the physical quantities --temperature, pressure, and opacity--upon a specified depth-dependent variable to the computation of the net flux emerging from the star and the shape of the spectral absorption lines. A comparison of the computed data with stellar observations is made and the model altered to yield a best fit thereby defining the model atmosphere only to the extent of the agreement.

To relieve the complexity--and somewhat out of necessity--the situation of describing accurately a stellar atmosphere must be accompanied by certain symplifying assumptions governing the physical processes which are occurring. It is argued that the amount of imperfection introduced will only evidence itself in secondary roles.

For the detailed analysis of Theta Ursae Majoris, the star was assumed to be spherically symmetric, non-rotating, and the range of depth of the atmosphere negligible compared to the radius of the star. Further, the atmosphere is assumed to be partitioned in homogeneous, steady-state, plane-parallel layers of which the outer boundary is defined by the condition that no significant quantity of radiation flows inward across this boundary. The atmosphere is also constrained to provide no significant sources or sinks of energy. A state of hydrostatic equilibrium exists at all times and at all points in the atmosphere under the influence of a uniform gravitational field. No provision is made for radiation, magnetic, or other mechanical forces. This ensures that the total pressure at each layer is equivalent to the gas pressure of the layer.

Additional assumptions are placed upon the mechanism of the interaction of the radiation and gravitational field. The gases present in the atmosphere are assumed to be in local thermodynamic equilibrium. This implies that for the continuous spectrum a simple replacement of the source function by the Planck function of the local electron temperature may be made since then the ratio of the probability of the emission to absorption of a photon in a specified frequency interval would be unity. Pure absorption is then the only mechanism for the formation of the radiation field. In general this ratio is close to unity except for lines that are formed in high regions of the atmosphere so that this assumption is not altogether unrealistic for the problem (Böhm 1960; Aller 1963; Motz 1970). Finally the assertion is made that the formation of the line and continuous spectrum may be treated as separate entities.

While magnetic forces are formally neglected, they are incorporated in an approximate manner through the use of an effective surface gravity rather than of the dynamical quantity. Magnetic effects produce a distention in the atmosphere at its outermost layers and reduce the dynamical surface gravity in the process (Aller, 1953).

The method of computation of the corresponding pressure-opacity-flux model follows the computational procedure developed by Weidman (1955) and later refined by Elste and Evans (1966). For a given chemical composition, effective surface gravity and temperature distribution, the model atmosphere program will generate the electron and gas pressures as functions of a conveniently defined depth variable. Rather than the actual physical depth in the atmosphere, the logarithmic optical depth scale is used (Elste 1955; Weidmann 1955). The logarithmic optical depth scale is approximately linearly proportional to the physical depth of a layer in an atmosphere. Following common practice for the independent variable of depth, the logarithm of the optical depth at 5000Å is used. It can be related to the physical variable by the expression

$$X \equiv \log t_o = \log \left[\int_o^t \frac{K_o(t)}{m_o \sum_i \varepsilon_i \mu_i} \rho(t)dt\right], \qquad (2\text{-}1)$$

where

$t$ = the physical depth in the atmosphere,

$K_o(t)$ = the continuous absorption coefficient per hydrogen particle at 5000Å,

$m_o$ = the gram mass of a unit atomic weight,

$\mu_i$ = the atomic weight of species i,

$\varepsilon_i$ = the number abundance of species i relative to hydrogen,

$\rho(t)$ = the density of stellar material.

The atmosphere was stratified into twenty-seven layers each specified by a value of the logarithm of the optical depth ranging from $-4.00 \leq x \leq +1.20$. Evans (1966, 1969) and Bulman (1971) have discussed extensively the theory developed for computing the pressure-opacity-flux model used in this study and the necessary details are given in Appendix A.

## The Temperature Distribution

The temperature is related to the depth through some arbitrarily adopted temperature law obeying the constraint that it resemble as closely as possible the real star. This law is commonly established by requiring that the spectrum meet the condition of radiative equilibrium at each layer; that is, the total flux must be constant with depth. Of course, one could bypass this requirement by adopting an empirical temperature relation which is based upon solar limb-darkening measurements. The latter procedure is convenient for stars whose sources of continuous absorption coefficients and ionization equilibrium are not far removed from those of the sun.

For the purposes of this study an empirical solar temperature distribution by Elste (1955) was utilized. This distribution has been shown to fit solar observations of limb-darkening (Elste 1964), sodium

D lines (Mattig and Schröter, 1961; Mugglestone, 1964) and the Balmer lines (David, 1961). The extension to the desired stellar temperature distribution is accomplished by multiplying the empirical solar temperature by the ratio of the stellar to solar effective temperature for each layer of the atmosphere. The resulting effective temperature does not yield total integrated flux since it has been empirically derived; however, this approximation will be assigned as the model temperature.

It is well known that the best criterion for the specification of temperature in F, G, and K stars is through the Balmer-line profiles. Bulman (1971) computes a grid of sixteen representative model atmospheres for the star Theta Ursae Majoris, having effective temperatures between 6200 $^{\circ}$K and 6650 $^{\circ}$K and surface gravities between log g = 3.8 and 4.4. His analysis of the hydrogen line profiles predicts a model with an effective temperature of 6500 $^{\circ}$K and logarithm of the surface gravity of 4.2. However, when this model was compared to that predicted by the UBV colors which incorporated the line blanketing measurements of Myrick (1970), no single definitive model for Theta Ursae Majoris could be ascertained. Evans, Schroeder, and Weems (1970) have reported that using the multi-color photometry of Mitchell and Johnson (1969), the UBV colors, and the hydrogen line profiles, a revised model with an effective temperature of 6350 $^{\circ}$K and log g of 4.0 best represents the atmosphere of Theta Ursae Majoris. The detailed model atmosphere is shown in Table II. It represents the model atmosphere chosen for the computational analysis of Theta Ursae Majoris. Following the data table, the effective temperature, the surface gravity, the helium to hydrogen number density, B, and the logarithm of the number of hydrogen atoms to those of the metals, A = log $N_H/\Sigma$ N metals are listed, respectively. In the

TABLE II

THE REPRESENTATIVE MODEL ATMOSPHERE FOR THETA URSAE MAJORIS

| Log Tau (5000) | Theta Model | Temp. (K) | Log PE | Log PG | Log K/PE (5000) | Mean Mol. Wt. | Log Density | Geometrical Depth (KM) |
|---|---|---|---|---|---|---|---|---|
| -4.00 | 1.0404 | 4844 | -1.1407 | 2.8125 | -24.9813 | 1.3597 | -8.6592 | 0.0 |
| -3.80 | 1.0399 | 4847 | -1.0947 | 2.8768 | -24.9893 | 1.3597 | -8.5950 | 0.0 |
| -3.60 | 1.0389 | 4851 | -1.0026 | 3.0057 | -25.0036 | 1.3597 | -8.4665 | 0.0 |
| -3.40 | 1.0374 | 4858 | -0.9079 | 3.1324 | -25.0169 | 1.3597 | -8.3405 | 0.0 |
| -3.20 | 1.0357 | 4866 | -0.8122 | 3.2567 | -25.0289 | 1.3597 | -8.2168 | 0.0 |
| -3.00 | 1.0331 | 4879 | -0.7133 | 3.3787 | -25.0412 | 1.3598 | -8.0959 | 0.0 |
| -2.80 | 1.0294 | 4896 | -0.6113 | 3.4983 | -25.0541 | 1.3598 | -7.9779 | 0.0 |
| -2.60 | 1.0240 | 4922 | -0.5049 | 3.6155 | -25.0691 | 1.3598 | -7.8630 | 0.0 |
| -2.40 | 1.0176 | 4953 | -0.3965 | 3.7306 | -25.0848 | 1.3598 | -7.7506 | 0.0 |
| -2.20 | 1.0076 | 5002 | -0.2776 | 3.8433 | -25.1063 | 1.3598 | -7.6422 | 0.0 |
| -2.00 | 0.9948 | 5066 | -0.1503 | 3.9533 | -25.1320 | 1.3598 | -7.5378 | 0.0 |
| -1.80 | 0.9794 | 5146 | -0.0133 | 4.0601 | -25.1618 | 1.3597 | -7.4377 | 0.0 |
| -1.60 | 0.9612 | 5243 | 0.1364 | 4.1631 | -25.1963 | 1.3597 | -7.3429 | 0.0 |
| -1.40 | 0.9411 | 5355 | 0.2974 | 4.2615 | -25.2339 | 1.3597 | -7.2537 | 0.0 |
| -1.20 | 0.9184 | 5488 | 0.4754 | 4.3543 | -25.2762 | 1.3597 | -7.1715 | 0.0 |
| -1.00 | 0.8938 | 5639 | 0.6688 | 4.4407 | -25.3222 | 1.3596 | -7.0969 | 0.0 |
| -0.80 | 0.8665 | 5817 | 0.8834 | 4.5200 | -25.3736 | 1.3595 | -7.0311 | 0.0 |
| -0.60 | 0.8356 | 6032 | 1.1259 | 4.5909 | -25.4324 | 1.3594 | -6.9760 | 0.0 |
| -0.40 | 0.8001 | 6299 | 1.4039 | 4.6523 | -25.5008 | 1.3591 | -6.9336 | 0.0 |
| -0.20 | 0.7591 | 6639 | 1.7240 | 4.7033 | -25.5800 | 1.3584 | -6.9057 | 0.0 |
| 0.0 | 0.7136 | 7063 | 2.0786 | 4.7437 | -25.6656 | 1.3569 | -6.8925 | 0.0 |
| 0.20 | 0.6644 | 7586 | 2.4612 | 4.7745 | -25.7497 | 1.3533 | -6.8940 | 0.0 |
| 0.40 | 0.6144 | 8203 | 2.8489 | 4.7968 | -25.8140 | 1.3445 | -6.9084 | 0.0 |

TABLE II (Concluded)

| Log Tau (5000) | Theta Model | Temp. (K) | Log PE | Log PG | Log K/PE (5000) | Mean Mol. Wt. | Log Density | Geometrical Depth (KM) |
|---|---|---|---|---|---|---|---|---|
| 0.60 | 0.5762 | 8747 | 3.1456 | 4.8136 | -25.8379 | 1.3307 | -6.9240 | 0.0 |
| 0.80 | 0.5489 | 9182 | 3.3581 | 4.8283 | -25.8369 | 1.3138 | -6.9360 | 0.0 |
| 1.00 | 0.5316 | 9481 | 3.4947 | 4.8431 | -25.8286 | 1.2989 | -6.9400 | 0.0 |
| 1.20 | 0.5206 | 9681 | 3.5815 | 4.8526 | -25.8201 | 1.2872 | -6.9435 | 0.0 |

T(eff) = 6350 $^{\circ}$K  Log g = 4.00  B = 0.1250  A = 3.2306 succeeding columns, the logarithms of the electron pressure, gas pressure and the ratio of the absorption coefficient to the electron pressure are given as functions of the optical depth at 5000Å and the temperature, either as $\theta = 5040/T(^{o}K)$ or $T(^{o}K)$. The values located under the column for the geometrical depth have been initialized to zero since the geometrical depth was not used for calculation purposes. Also tabulated are mean molecular weights and logarithmic densities.

## CHAPTER III

## THE THEORY OF LINE FORMATION

In order to extract the most information possible about the atmosphere of a star there are two aspects of an absorption line which must be considered, the intensity of the line, generally expressed in terms of an equivalent width, and its shape or profile. The former is just the total amount of energy extracted by the absorption line itself while the latter feature depends principally upon the residual energy distribution in the line as a function of the frequency.

### Line Depth in Flux

If local thermodynamic equilibrium is assumed for line formation, then scattering processes may be neglected as compared to pure absorption processes so the net flux in the continuum is represented by Equation (A-13). The line depth in flux (Gussman, 1963) is defined as

$$R(\Delta\lambda) = 1 - \frac{F_T^{\ell}(0,\Delta\lambda)}{F_T^{c}(0,\lambda_m)} = \frac{F_T^{c}(0,\lambda_m) - F_T^{\ell}(0,\Delta\lambda)}{F_T^{c}(0,\lambda_m)}, \qquad (3\text{-}1)$$

where

$\lambda_m$ = the wavelength which defines a 150 Å wide region of the spectrum containing $\lambda$,

$F_T^c(0,\lambda_m)$ = the total continuum flux emerging from the atmosphere,

$F_T^\ell(0,\Delta\lambda)$ = the emergent flux in the line at a distance $\Delta\lambda$ from the line center,

Both $F(0,\lambda_m)$ and $\tau_{\lambda m}(x)$ have been specified as details of the calculations of the model atmosphere. If the mechanisms for line formation are independent of those for the formation of the continuum, then the flux in the line is

$$F_T^\ell(0,\Delta\lambda) = 2 \int_0^\infty B_{\lambda m}(\tau^c + \tau^\ell)\, E_2(\tau^c + \tau^\ell)\, d(\tau^c + \tau^\ell), \qquad (3\text{-}2)$$

since the optical depth $\tau$, is just the addition of the optical depth in the continuum, $\tau^c$, and the optical depth in the line.

The optical depth in the line is given by

$$\tau^\ell(x,\Delta\lambda) = \int_{-\infty}^{x} \frac{K^\ell}{K_o}\, \frac{\tau_o}{\text{Mod}}\, (1 - 10^{-\chi_{\lambda m}\theta})dx, \qquad (3\text{-}3)$$

where $K^\ell(x,\Delta\lambda)$ = the line absorption coefficient per hydrogen particle,

$\chi_{\lambda m}$ = $12397.67/\lambda_m$,

$1\text{-}10^{-\chi_{\lambda m}\theta}$ = the factor needed to account for stimulated emission.

$K_o(x)$, $\tau_o(x)$ and $\theta(x)$ are the parameters specified by the model atmosphere calculations.

## Line Broadening Mechanisms

The absorption lines in stellar spectra are broadened through several different mechanisms in addition to instrumental imperfections.

The major causes of intrinsically broadened lines are (Aller, 1963; van Regemorten, 1965): (a) a Doppler broadening due to random thermal motions of the gas atoms as well as a possible small scale mass motion, turbulence, in the atmosphere; (b) radiation or natural broadening, due to the existence of small but finite lifetimes of excited states of a gas atom; (c) Stark broadening, from the interaction of absorbing atoms with surrounding ions or electrons; (d) Van der Waals broadening, from the interaction of absorbing atom with neutral atoms of a different type; (e) Zeeman broadening, due to line-splitting in a magnetic field; (f) resonance broadening, due to interactions of the absorbing atom with atoms of the same type; (g) isotopic broadening, a type of pseudo-broadening occurring because of isotopic variations between atoms. The more important extrinsic causes for line broadening in stellar spectra are rotational broadening due to contributions to the line from different portions of a rotating stellar surface and large scale turbulent effects in the atmosphere.

The turbulence broadening effects are commonly distinguished as being of two types, <u>macroturbulence</u> or <u>microturbulence</u>. Macroturbulence is defined as mass motions whose linear extent is large compared with the mean free path of a photon. On the other hand, for microturbulence the mass eddies have a linear extent small as compared with the mean free path of a photon. Turbulence affects both the equivalent width and the line profiles, but in a different manner depending upon whether or not the diameter of the atmosphere is greater or smaller than the thickness of the line-forming region. Microturbulence elements moving with different velocities absorb radiation from the continous spectrum at different distances from the line center resulting in a broadening of the line profile and an increased equivalent width. The delaying of optical saturation then raises the flat portion of the curve of growth. Macroturbulence does not affect the equivalent width, since by definition it occurs after the line has been formed, and simply rounds out the line profile.

## Calculation of Theoretical Line Intensity and Flux

Consider an atmosphere which contains mass motions, arising from cells whose thickness is greater than that of the region in which the line is formed, whose velocity along the line of sight has the radial and tangential components

$$\varepsilon_i = \varepsilon_i^r \cos\theta + \varepsilon_i^t \sin\theta, \tag{3-4}$$

where $\theta$ = angle between the observer and the velocity component of the ith cell.

If the continuum intensity of the ith cell is $I_i^c$, and the line intensity of the ith cell is $I_i^\ell$, then the total continuum intensity arising from n distinct cells occupying an area A at a limb distance $\mu = \cos\theta$ is

$$I_T^c = \sum_{i=1}^{n} a_i I_i^c, \tag{3-5}$$

while the total line intensity is given by

$$I_T^\ell = \sum_{i=1}^{n} a_i I_i^\ell, \tag{3-6}$$

where $a_i$ = the fraction of area A occupied by cells with a velocity of $\varepsilon_i$.

The line depth expression for the emergent radiation from the region of interest is from Equations (3-5) and (3-6)

$$r_\lambda(\mu) = \frac{I_T^c - I_T^\ell}{I_T^c} = \sum_{i=1}^{n} a_i\left[\frac{I_i^c - I_i^\ell}{I_t^c}\right] . \tag{3-7}$$

Now if the continuum is formed according to the mechanism of pure absorption, and local thermodynamic equilibriums assumed, the equation for the specific intensity of a ray which emerges from the surface of the ith cell at angle $\theta$ with the normal is

$$I_i^c(0,\mu) = \int_o^\infty S_i^c\, e^{-\tau_i^c/\mu} \frac{d\tau^c}{\mu} = \int_{-\infty}^\infty S_i^c\, e^{-\tau_i^c/\mu} \frac{K_i^c}{K_o^c} \frac{10^x}{\text{Mod}} \frac{dx}{\mu} , \tag{3-8}$$

where $\tau_i^c(x)$ = the continuum optical depth,

$$= \int_{-\infty}^x \frac{K_i^c}{K_o^c} \frac{10^x}{\text{Mod}}\, dx ,$$

$x$ = logarithm of the optical depth at $\lambda = 5000\text{Å}$, for a non-moving ambient photosphere,

$S_i^c$ = the source function in the continuum of the ith cell, which in this case is the Planck function.

Likewise the specific line intensity of the emergent ray is

$$\begin{aligned} I_i^\ell(0,\mu) &= \int_o^\infty S_i\, e^{-\tau_i/\mu} \frac{d\tau_i}{\mu}, \\ &= \int_{-\infty}^\infty S_i\, e^{-\tau_i/\mu} \frac{K_i}{K_o^c} \left(\frac{10^x}{\text{Mod}}\right) \frac{dx}{\mu} , \end{aligned} \tag{3-9}$$

where $S_i$ = the source function of the ith cell at a point in the line.

$\tau_i$ = the optical depth for a point in the line

$$= \tau_i^c + \tau_i^\ell = \int_{-\infty}^{x} \frac{K_i^\ell + K_i^c}{K_o^c} \frac{10^x}{\mathrm{Mod}} \, dx \; .$$

In Equation (3-9) the mechanism for line formation has been assumed to be independent of that which produces the continuum (Motz, 1970), so that the source function $S_i$ becomes

$$S_i = \frac{S_i^c + \rho_i}{1 + \rho_i} S_i^\ell = S_i^c \left(\frac{1 + \rho_i\beta_i}{1 + \rho_i}\right) , \qquad (3\text{-}10)$$

where $\rho_i = K_i^\ell / K_i^c , \quad \beta_i = S_i^\ell / S_i^c ,$

and $K_i = K_i^\ell + K_i^c = K_i^c (1 + \rho_i) .$

Making use of Equations (3-8), (3-9), and (3-10), the line depth in intensity, from Equation (3-7), is

$$r_\lambda(\mu) = \sum_{i=1}^{n} \left\{\frac{a_i}{I_T^c} \int_{-\infty}^{+\infty} S_i^c \, e^{-\tau_i^c/\mu} \frac{K_i^c}{K_o^c} \frac{10^x}{\mathrm{Mod}} \frac{dx}{\mu}\right\}$$

$$- \sum_{i=1}^{n} \frac{a_i}{I_T^c} \int_{-\infty}^{\infty} S_i^c \, e^{-\tau_i^c/\mu} \, e^{-\tau_i^\ell/\mu} \frac{(1 + \rho_i\beta_i)}{(1 + \rho_i)} (1+\rho_i)$$

$$\cdot \frac{K_i^c}{K_o^c} \frac{10^x}{\mathrm{Mod}} \frac{dx}{\mu} ,$$

or

$$r_\lambda(\mu) = \int_{-\infty}^{\infty} \left[\sum_{i=1}^{n} \frac{a_i S_i^c}{I_T^c} e^{-\tau_i^c/\mu} \left(1 - [1 + \rho_i \beta_i] e^{-\tau_i^\ell/\mu}\right) \cdot \frac{K_i^c}{K_i^o}\right] \frac{10^x}{\text{Mod}} \frac{dx}{\mu} . \tag{3-11}$$

It is now of benefit to make simplifying assumptions concerning some of the quantities in Equation (3-11). The best observational evidence for the existence of macroturbulence appears in the granular structure of the atmosphere of the sun. There the continuous radiation from the bright granules is not altogether different in intensity from that produced by the inter-granular region surrounding the cells (Evans, 1971). Therefore, it will be assumed that the intensity of the cells $I_i^c = I^c$ for all i. This implies that the total continuum intensity, summed over all cells, is just the total intensity $I_T^c$. Throughout the part of the line that makes the major contribution to the equivalent width, the source function in the line is not very different from that in the continuum and if local thermodynamic equilibrium is invoked, they are identical. Further, Jugaku (1957) has shown that it is theoretically sound to assume the source function to be Planckian for main-sequence B stars. The last restriction is placed on the macroturbulent distribution itself. It will be assumed that all cells have the same temperature stratification and differ only in their velocity fields. This latter assumption constrains the Planck function and the optical depth in the continuum to be identical for all cells. With these conditions, Equation (3-11) for the line depth becomes

$$r_\lambda(\mu) = \int_{-\infty}^{\infty} \left[\frac{B\, e^{-\tau^c/\mu}}{I^e} \sum_{i=1}^{n} a_i \left(1 - (1 + \rho_i)\, e^{-\tau_i^\ell/\mu}\right)\right.$$

$$\left. \cdot \frac{K^c}{K_o^c}\right] \frac{10^x}{\text{Mod}} \frac{dx}{\mu}, \tag{3-12}$$

where $B = B_\lambda$ = the Planck function,

$K^c = K_\lambda^c$ = the continuous absorption coefficient,

$K_o^c$ = the continuous absorption coefficient for $\lambda = 5000\text{Å}$,

$\tau_i^\ell$ = the optical depth of a line occurring in the ith cell of the atmosphere.

Using the identity

$$\sum_{i=1}^{n} a_i\, (1 - \psi_i) = 1 - \sum_{i=1}^{n} a_i \psi_i,$$

Equation (3-12) may be written in the form

$$r_\lambda(\mu) = \int_{-\infty}^{+\infty} \frac{B\, e^{-\tau^c/\mu}}{I^c} \left[1 - \sum_{i=1}^{n} a_i\, (1 + \rho_i)\, e^{-\tau_i^\ell/\mu}\right] \frac{K^c}{K_o^c} \frac{10^x}{\text{Mod}}\, dx. \tag{3-13}$$

Except for the sun, it is impossible to observe separate portions of a stellar surface. The energy that is received from a stellar object is then proportional to the total amount of energy emitted from each small segment of area. This energy or the flux is then obtained by integration of the specific intensity, Equations (3-5) and (3-6) over all possible solid angles. Hence, from Equations (3-8) and (3-9), the total flux in the continuum is

$$F_T^c(0,\lambda_m) = \frac{1}{\pi} \int_{\phi=o}^{\phi=2\pi} \int_{\theta=o}^{\theta=\pi/2} I_T^c(0,\mu) \cos\theta \sin\theta \, d\theta d\phi$$

or

$$F_T^c(0,\lambda_m) = 2 \sum_{i=1}^{n} a_i \{\int_o^\infty S_i^c [\int_{y=1}^{y=\infty} e^{-\tau_i^c y} \frac{dy}{y^2}] d\tau_i^c\}, \qquad (3\text{-}14)$$

where $y = 1/\mu$. Likewise, the flux in the line becomes,

$$F_T^\ell(0,\Delta\lambda) = 2 \sum_{i=1}^{n} a_i \{\int_o^\infty S_i [\int_{y=1}^{y=\infty} e^{-\tau_i y} \frac{dy}{y^2}] d\tau_i\} . \qquad (3\text{-}15)$$

The quantity in brackets is just the second exponential integral (see Equation (A-13). So Equations (3-14) and (3-15) may be written as

$$F_\lambda^c(0,\lambda_m) = \sum_{i=1}^{n} 2a_i \int_{-\infty}^{\infty} S_i^c E_2(\tau_i^c) \frac{K_i^c}{K_o^c} \frac{10^x}{\text{Mod}} dx, \qquad (3\text{-}16)$$

and

$$F_T^\ell(0,\Delta\lambda) = \sum_{i=1}^{n} 2a_i \int_{-\infty}^{\infty} S_i E_2(\tau_i^c + \tau_i^\ell) \frac{K_i}{K_o^c} \frac{10^x}{\text{Mod}} dx. \qquad (3\text{-}17)$$

The line depth in flux is then

$$R_\lambda(\mu) = \frac{F_T^c(0,\lambda_m) - F_T^\ell(0,\Delta\lambda)}{F_T^c(0,\Delta\lambda_m)},$$

$$= \sum_{i=1}^{n} \frac{2a_i}{F_T^c(0,\Delta\lambda_m)} \int_{-\infty}^{\infty} [S_i^c E_2 (\tau_i^c) \frac{K_i^c}{K_o^c} - S_i$$

$$\cdot E_2\ (\tau_i^c + \tau_i^\ell)\ \frac{K_i^c}{K_o^c}]\ \frac{10^x}{\text{Mod}}\ dx\ .$$

Using Equation (3-10) this becomes

$$R_\lambda(\mu) = \sum_{i=1}^{n} \frac{2a_i}{F_T^c(0,\Delta\lambda_m)} \int_{-\infty}^{\infty} [S_i^c\ E_2(\tau_i^c)\ \frac{K_i^c}{K_o^c} - S_i^c\ \frac{(1+\rho_i\beta_i)}{(1+\rho_i)}\ E_2(\tau_i^c+\tau_i^\ell)$$

$$\cdot \frac{K_i^c}{K_o^c}\ (1+\rho_i)]\ \frac{10^x}{\text{Mod}}\ dx\ .$$

Which, for convenience may be expressed as

$$R_\lambda(\mu) = \int_{-\infty}^{\infty} \{\sum_{i=1}^{n} \frac{2a_i\ S_i^c\ E_2(\tau_i^c)}{F_T^c} [1 - \frac{(1+\rho_i\beta_i)\ E_2(\tau_i^c+\tau_i^\ell)}{E_2(\tau_i^c)}]$$

$$\cdot \frac{K_i^c}{K_o^c}\}\ \frac{10^x}{\text{Mod}}\ dx\ . \tag{3-18}$$

The solution of the line depth Equation (3-18) is based upon the method of the Planckian gradient of Mugglestone (1958) and later modified by Evans (1969, 1971). The method utilizes an integration by parts of the flux Equations (3-14) and (3-15), for the line and continuum. The general form of these equations is

$$\psi = 2 \int_0^\infty S(\tau)\ E_2(\tau)\ d\tau.$$

Letting $u = S(\tau)$, $dv = E_2(\tau)$, $v = -E_3(\tau)$ and

$$du = \frac{dS(\tau)}{d\tau}\, d\tau\, \frac{dS(\tau)}{d \log \tau}\, \frac{d \log \tau}{d\tau}\, d\tau = \frac{dS(\tau)}{dx}\, dx ,$$

the above integral then becomes

$$\psi = S(0) + 2\int_{-\infty}^{\infty} \frac{dS}{dx} \cdot E_3(\tau)\, dx . \tag{3-19}$$

From the results of Equation (3-19), the Planckian gradient form of the line depth becomes

$$R_\lambda(\mu) = \sum_{i=1}^{N} \frac{a_i}{F_T^c(0,\lambda_m)} \{(S_i^c(0) - S_i^\ell(0)) \tag{3-20}$$

$$+ 2 \int_{-\infty}^{\infty} \frac{dS_i^c}{dx}\, E_3(\tau_i^c)\, [1 - \Phi_i \frac{E_3(\tau_i^c + \tau_i^\ell)}{E_3(\tau_i^c)}]\, dx\} ,$$

where $\Phi_i = \frac{dS_i^\ell}{dx} / \frac{dS_i^c}{dx}$ . Under the same restrictions used to calculate the intensity form of the line depth, the following conditions will be assumed: (a) the source function in the line and continuum is the Planck function; (b) the optical depth in the continuum is the same for all cells. Thus, the Planckian gradient form of the line depth, Equation (3-20) may be expressed as

$$R_\lambda(\mu) = \int_{-\infty}^{+\infty} \{\sum_{i=1}^{N} \frac{2a_i}{F_T^c(0,\lambda_m)}\, \frac{dB}{dx}\, E_3(\tau^c)\, [1 - \frac{E_3(\tau^c + \tau_i^\ell)}{E_3(\tau^c)}]\}\, dx,$$

or

$$R_\lambda(\mu) = \frac{2}{F_T^c(0,\lambda_m)} \int_{-\infty}^{+\infty} \frac{dB}{dx}\, E_3(\tau^c)\, [1 - \sum_{i=1}^{N} \frac{a_i\, E_3(\tau^c + \tau_i^\ell)}{E_3(\tau^c)}]\, dx .$$

If the macroturbulent cells are assumed to produce a velocity dispersion function, the expression in the bracket may be replaced by a weighted mean for the line optical depth (Evans, 1971), so that the expression for the line depth becomes

$$R_\lambda(\mu) = \frac{2}{F_T^c(0,\lambda_m)} \int_{-\infty}^{+\infty} \frac{dB}{dx} E_3(\tau^c) \left[1 - \frac{E_3(\tau^c + \sum_{i=1}^{N} a_i \tau_i^\ell)}{E_3(\tau^c)}\right] dx \ . \qquad (3\text{-}21)$$

The Metal Absorption Coefficient

For the computation of the metal lines, only broadening mechanisms giving rise to Gaussian profiles or Lorentz profiles are included. In addition to the thermal Doppler broadening the absorption coefficient includes natural, Stark, van der Waals, and microturbulence broadening. Magnetic interactions have been neglected as well as rotational broadening although macroturbulence broadening could be made to simulate the latter effect. The profile of a line that results from a thermal Doppler effect is a Gaussian profile while that from natural or pressure broadening is a dispersion profile. Combination of these two mechanisms results from the convolution of the two profiles. Considering only Doppler broadening, the random thermal agitation in a stellar atmosphere is increased by any microturbulence, and the most probable velocity of the atoms is given by

$$v_{mp} = \sqrt{\varepsilon_{th}^2 + \varepsilon_{turb.}^2} \ , \qquad (3\text{-}22)$$

where $\varepsilon_{th}$ = the most probably thermal velocity,

$$= \sqrt{2KT/m} = \sqrt{2RT/\mu_i} = \sqrt{83.83/(\mu_i\theta)} \ .$$

$\varepsilon_{turb.}$ = the most probable velocity of the micro-turbulence.

The 1/e width of the resulting Gaussian profile is given by the Doppler width

$$\Delta\lambda_D = \frac{\lambda}{c} v_{mp} = \frac{\lambda}{c} \sqrt{\left(\frac{2KT}{m}\right) + \varepsilon^2_{turb.}} \tag{3-23}$$

Since the convolution of two Lorentz profiles again yields a Lorentz profile whose width is equal to the sum of the widths of the convoluted functions, the half-width of the dispersion profile for the other broadening mechanism is just the sum of the half-widths due to natural, Stark and van der Waals broadening,

$$\Gamma_{(x)} = \Gamma_{rad.} + \Gamma_{Stark} + \Gamma_{van\ der\ Waals}\ . \tag{3-24}$$

The radiation damping constant is obtained through classical means while the Stark broadening due to hydrogen and helium as well as van der Waals broadening by ions and electrons are approximated using the Lindholm theory as a basis (Evans, 1966). The line absorption coefficient per hydrogen particle is computed from the absorption coefficient per absorbing particle,

$$K^{\ell} = \left(\frac{n_{n,m}}{N_H}\right) K_{atomic}, \tag{3-25}$$

where the quantity in parenthesis represents the number of absorbing particles per hydrogen particle. For the case of doublets, the blending is calculated by adding the absorption coefficients for each line. More of the details of the calculations of the metal line absorption coefficient can be found in Appendix B.

## The Theoretical Curve of Growth

The curve of growth method is a concept representing the behavior of the equivalent width of a stellar spectral line as the number of effective absorbers in the atmosphere changes. However, for computational ease, the theoretical curve of growth will be defined as a plot of the saturated equivalent width as a function of the unsaturated equivalent width (Aller, Elste, and Jugaku, 1957; Aller 1960; Aller 1963). The unsaturated equivalent width is defined as

$$\left(\frac{W}{\lambda}\right)^{*} = \int_{-\infty}^{+\infty} \frac{K^{\ell c}}{K_{o}} \left(\frac{\tau_{o}}{\text{Mod}}\right) \left(1-10^{-\chi_{\lambda m}\theta}\right) G_{\lambda m}\, dx, \tag{3-26}$$

where $K^{\ell c}$ = the absorption coefficient at the line center,

$G_{\lambda m}$ = the flux weight function (see Appendix B).

The flux weight function has the advantage that it depends only upon the model atmosphere chosen and so can be computed once and for all for the various wavelength regions covering the observed spectrum. For weak lines the logarithm of the saturated equivalent width is proportional to the logarithm of the unsaturated width so that it is more convenient to plot these quantities for the theoretical curve of growth. The relative abundance can be removed from Equation (3-26) to get

$$\log\,(w/\lambda)^{*} = \log \varepsilon + \log C_{\lambda}, \tag{3-27}$$

where

$$\log C_\lambda = \log \left[\int_{-\infty}^{\infty} \frac{K^{\ell c}}{K_o^c} \cdot \frac{\tau_o}{\mathrm{Mod}} \frac{1}{\varepsilon} (1-10^{-\chi_{\lambda m}\theta}) G_{\lambda m}\, dx\right], \quad (3\text{-}28)$$

and $\varepsilon_i$ = the abundance of the element relative to hydrogen = N/N(H).

The saturated equivalent width describes the total absorption of a spectral line and is represented by the area of a strip which removes the same amount of energy from the continuum as the spectral line. In logarithmic form this can be expressed in terms of the line depth as,

$$\log(w/\lambda) = \log \left[\frac{1}{\lambda} \int_{o}^{+\infty} R_\lambda(\mu)\, d\lambda, \quad (3\text{-}29)$$

where $R_\lambda(\mu)$ is defined in Equation (3-21).

## The Metal Line Program

For the analysis of the absorption lines, both the line profile and the curve of growth are calculated with the aid of a computer program devised by Evans (1966, 1971). Details of the computations can be found in Appendix B. For each observed line, the program calculates from three to nine points on the curve of growth. The abundance for the observed equivalent width is then estimated from this curve of growth and the result is used to calculate the line depth and the median point of the line depth integrand for a range of different values of $\Delta\lambda$. In addition to this it also supplies the optical depth in the line, the damping parameters, the Doppler width at the median point, the half-width of the line profile, a plot of the theoretical line profile, and the model atmosphere and turbulence model chosen for the analysis. For a model atmosphere consisting of from one to ten elements, the program can compute, element by element, equivalent width and line profiles for as many lines as are needed for the analysis.

## Chemical Abundances and the Empirical Curve of Growth

Provided with an equivalent width, a set of oscillator strengths and an atmospheric model, the stellar abundance of an element can be obtained. The process is basically an interpolation between the observed equivalent width and the theoretically calculated value. From Equation (3-26), it is readily apparent that it is advantageous to define an empirical curve of growth as a plot of the logarithm of the saturated equivalent width as the ordinate and the quantity

$$\log C_\lambda \; = \; \log g_{r,s} f_{r,s} \; \lambda + \log L_\lambda^*(\chi_{r,s}), \qquad (3\text{-}30)$$

as the abscissa. Equation (3-30) is obtained directly from Equation (B-22) utilizing the fact that $L_{r,s}(\chi,\lambda)$ is independent of the variable of integration and the definition of $\log L_\lambda^*$,

$$\mathrm{Log}\; L_\lambda^*(\chi_{r,s}) \equiv \log \sqrt{\frac{\pi}{c}} \int_{-\infty}^{\infty} \left(\frac{\Delta\lambda_D}{\lambda}\right) M(x)\; N_i(x)\left(1-10^{-\chi_{\lambda m}\theta}\right) dx + \Delta\chi\theta. \qquad (3\text{-}31)$$

The empirical curve of growth can be fitted to the theoretical curve of growth by a horizontal translation. The amount of displacement then yields the relative abundance, $\log \varepsilon = \log N/N(H)$. Each point on the theoretical curve of growth represents an observed spectral line; and each line has its own theoretical curve of growth; consequently, its own abundance. Because in practice the curves of growth for many lines in certain spectral regions have the same shape, it is of use to define a mean abundance, derived from a mean curve of growth. The mean curve of growth is obtained by fitting the empirical curve of growth for all the observed lines falling with a wavelength region to the theoretical curve of growth for a representative line of the group. For a solar-type star, this procedure can be applied over wavelength regions of hundreds of angstroms. To aid the investigation, the abundance determination for an element was automatically produced by a computer program (Evans, 1971).

## The Abundance Program

Basically an adaptation of the metal line program, the abundance program will compute, for a single theoretical curve of growth, the abundance of from one to fifty individual lines. A turbulence model incorporating both line broadening effects due to macroturbulent and microturbulent motions can be varied at will to alter the abundance results. The program supplies the abscissa for the empirical curve of growth from which the empirical curve of growth can be constructed for the evaluation of the mean abundance. In addition a statistical weighting factor may be utilized for the computation of a mean weighted abundance for an element. The details of the calculation may be found in Appendix B.

## CHAPTER IV

## THE OBSERVATIONAL DATA

### Spectrograms and Tracings

The spectrograms used for the detailed analysis of Theta Ursae Majoris were obtained by Dr. K. O. Wright by exposing photographic plates at the cassegrain focus of the seventy-two inch telescope at Dominion Astrophysical Observatory, Victoria, Canada. A compromise focus was used, since the field of the grating was not flat over the entire plate, (K. O. Wright 1971) which produced well-focused lines at approximately $\lambda 5900\text{Å}$.

For the Littrow spectrograph with Wood grating, second order spectra in the range $\lambda\lambda 4800 - 6750$ were produced with a dispersion of approximately 7.5 Å/mm and in the third order spectra, between $\lambda\lambda 3750 - 4500$, a dispersion of 4.5 Å/mm was obtained. A Baush and Lomb grating No. 496 was used to gather spectra with a dispersion of 3.2 Å/mm. Finally, a three-prism spectrograph yielded a dispersion of from 5 Å/mm to 15 Å/mm over the observed spectral region.

Microphotometer and intensitometer tracings were obtained through Dr. Leon W. Schroeder, Department of Physics, Oklahoma State University. The magnification used for all the tracings was 200.

### The Instrumental Profile

An assessment of the effect which the instrumental profile had upon the equivalent widths and line profiles for the various spectrographs utilized for this study is based upon data published by Anne B. Underhill (1954) in her analysis of 31 Cygani. The instrumental profile of the spectrograph (see Figure 1) was estimated through analysis of the mean profile of a number of iron lines in an iron arc comparison spectrum.

The Litt GIII BL84 spectrograph is quite similar to that of the Wood grating and consequently was assigned to be the instrumental profile for the spectrograph used in this study. Both of the Bausch and Lomb gratings have lower glost intensities (Wright, 1971) than the BL 84 grating and would show a narrower instrumental profile.

Instrumental broadening can be described by a convolution of the true profile with the profile of the apparatus to yield the observed profile. If Voight functions are used to approximate the intensity distributions of all profiles, then the true profile may be extracted. The details of the computation are found in Appendix C. A computer program, Table XXVI , Appendix C, was developed to perform all the necessary calculations for the computation of the equivalent widths and halfwidths for as many spectral lines as are necessary. The Voight parameters for the apparatus were obtained from Figure 1 and are listed in Table III. Columns 1, 2, and 3 lists the width in milliangstoms of the profile at half the central-intensity, one-tenth the central-intensity and the ratio of these two values, respectively. The last 6 columns given the Voight parameters obtained from Table XXVI, Appendix C.

For data taken with the Bausch and Lomb Gratings No. 496 and 169, a narrower profile was assumed, and the corresponding reduced apparatus function was derived from the Litt GIII BL84 spectrograph by a simple

TABLE III

THE VOIGHT PARAMETERS FOR THE APPARATUS PROFILE USED FOR $\theta$ U Ma

| Spectrograph | Voight Parameters | | | | | | | | |
|---|---|---|---|---|---|---|---|---|---|
| | $h$ | $b_{0.1}$ | $b_{0.1}/h$ | $\beta_1/h$ | $\beta_2^2/h^2$ | $\alpha$ | $P$ | $\beta_1$ | $\beta_2^2$ |
| Prism | 164 | 381 | 2.32 | 0.235 | 0.190 | 0.505 | 1.295 | 38.6 | 5110 |
| Wood Grating - 2nd Order | 164 | 381 | 2.32 | 0.235 | 0.190 | 0.505 | 1.295 | 38.6 | 5110 |
| Wood Grating - 3rd Order | 100 | 232 | 2.32 | 0.235 | 0.190 | 0.505 | 1.295 | 23.5 | 1900 |
| Bausch and Lomb - 2nd Order | 100 | 232 | 2.32 | 0.235 | 0.190 | 0.505 | 1.295 | 23.5 | 1900 |

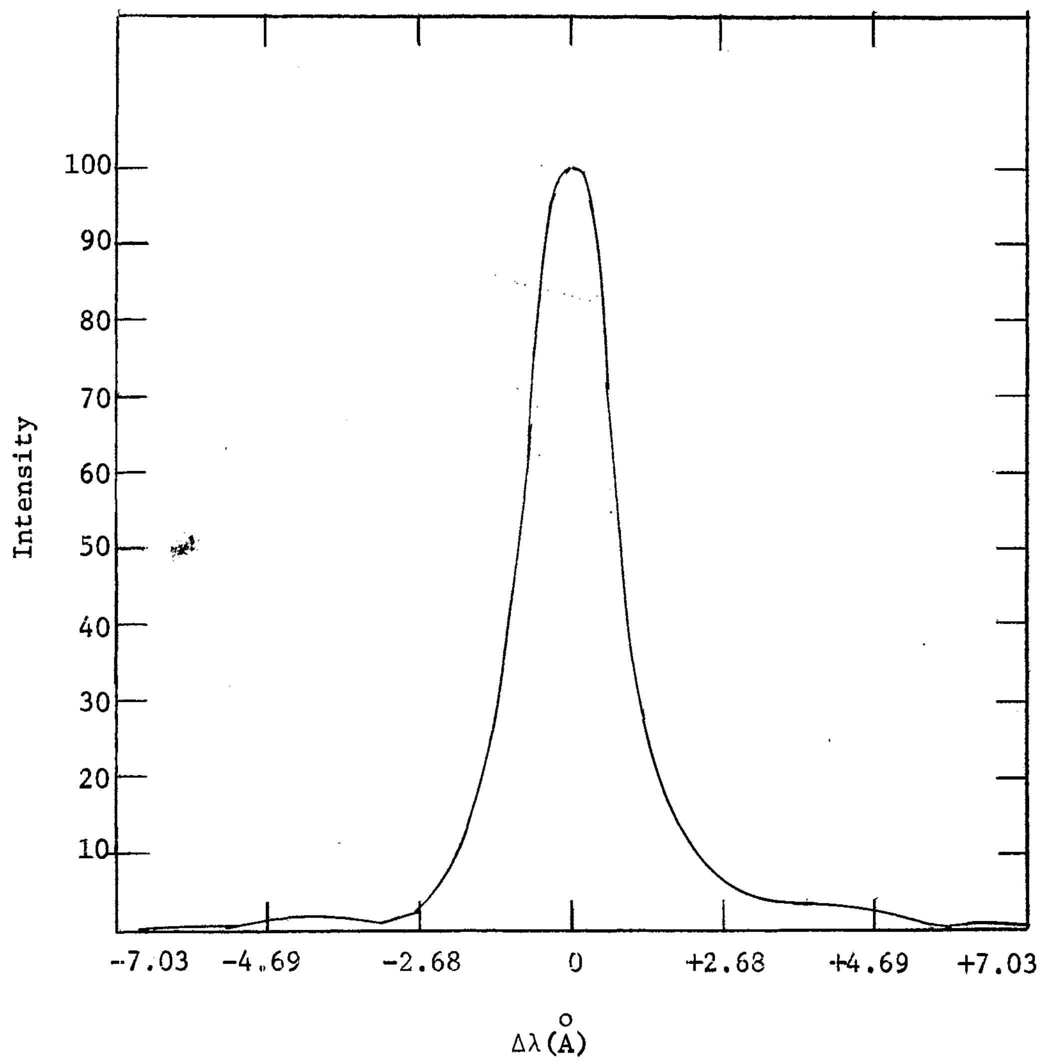


Figure 1. The Instrumental Profile for the Littrow GIII BL84 Spectrograph

scaling procedure. Since the Wood grating in the third order produces spectra having a dispersion of 4.5 Å/mm, it was also assigned Voight parameters of the reduced apparatus function.

## Equivalent Widths

Equivalent widths of spectral lines covering the region λλ3900 - 6700 Å were taken from the curve of growth analyses of Mangold (1968) and Peebles (1964). The equivalent widths reported were not corrected for instrumental effects. The selection of the lines was based upon the effects of blending, the availability of absolute f-values, and the number of lines available for a particular element. This restricted the observed equivalent widths primarily to lines of moderate strength. For the detailed analysis of the atmosphere of Theta Ursae Majoris, a number of weak lines are required to properly assess the effects of turbulent motion. So the turbulence analysis was supplemented by the determination of approximately one hundred iron lines in both the neutral and the first stage of ionization.

In measuring the equivalent width for each line, a profile was drawn directly upon the spectrogram tracing. Effects due to blending and the development of wings was introduced when necessary. The area enclosed by the profile was obtained using a planimeter and converted to square inches by multiplication with the planimeter conversion factor. When this result was multiplied by the dispersion of the spectrum and divided by the height of the continuum at the line center, the equivalent width of the observed line was obtained in milli-Angstrom units. Table IV shows the results of the measurement of the equivalent widths for the weak lines of neutral and singly ionized iron.

Column 1 lists the wavelength in Angstrom units taken from the <u>Revised Multiplet Table</u> (RMT) of Moore (1959).

Column 2 indicates the RMT multiplet number.

Column 3 gives the excitation potential in electron volts of the lower level of the transition.

Column 4 lists the number of profiles observed for the line.

Column 5 lists the logarithm of the ratio of equivalent width divided by the wavelength.

TABLE IV

LINE INTENSITIES FOR NEUTRAL AND SINGLY IONIZED IRON IN THETA URSAE MAJORIS

| Element | $\lambda$ | RMT | $\chi_{\ell}$ | No. of Meas. | Log w/$\lambda$ | Log h/$\lambda$ |
|---|---|---|---|---|---|---|
| Fe I | 4005.24 | 43 | 1.55 | 3 | -4.14 | -4.04 |
| Fe I | 4009.72 | 72 | 2.21 | 3 | -4.59 | -4.25 |
| Fe I | 4045.82 | 43 | 1.48 | 4 | -3.80 | -3.76 |
| Fe I | 4062.45 | 359 | 2.83 | 3 | -4.62 | -4.21 |
| Fe I | 4063.60 | 43 | 1.55 | 4 | -4.02 | -4.00 |
| Fe I | 4071.74 | 43 | 1.60 | 4 | -4.10 | -4.00 |
| Fe I | 4107.49 | 276 | 2.82 | 2 | -4.68 | -4.14 |
| Fe I | 4132.68 | 357 | 2.82 | 1 | -4.53 | -4.20 |
| Fe I | 4143.87 | 43 | 1.55 | 2 | -4.22 | -3.98 |
| Fe I | 4147.67 | 42 | 1.48 | 1 | -4.60 | -4.19 |
| Fe I | 4154.50 | 355 | 2.82 | 1 | -4.53 | -4.17 |
| Fe I | 4168.95 | 694 | 3.40 | 3 | -5.07 | -4.40 |
| Fe I | 4175.64 | 354 | 2.83 | 3 | -4.61 | -4.14 |
| Fe I | 4181.76 | 354 | 2.82 | 3 | -4.43 | -4.12 |
| Fe I | 4187.04 | 152 | 2.44 | 3 | -4.51 | -4.18 |
| Fe I | 4191.44 | 152 | 2.46 | 2 | -4.45 | -4.17 |
| Fe I | 4199.10 | 522 | 3.03 | 3 | -4.50 | -4.11 |
| Fe I | 4199.94 | 3 | 0.09 | 2 | -4.89 | -4.44 |
| Fe I | 4202.03 | 42 | 1.48 | 3 | -4.26 | -4.23 |
| Fe I | 4206.70 | 3 | 0.05 | 3 | -4.56 | -4.08 |
| Fe I | 4216.19 | 3 | 0.00 | 3 | -4.49 | -4.11 |
| Fe I | 4219.36 | 800 | 3.56 | 3 | -4.48 | -4.16 |
| Fe I | 4222.22 | 152 | 2.44 | 3 | -4.55 | -4.17 |
| Fe I | 4227.43 | 693 | 3.32 | 3 | -4.32 | -4.18 |
| Fe I | 4233.61 | 152 | 2.48 | 3 | -4.43 | -4.14 |
| Fe I | 4238.82 | 693 | 3.38 | 3 | -4.48 | -4.14 |
| Fe I | 4247.43 | 693 | 3.37 | 3 | -4.44 | -4.13 |
| Fe I | 4240.23 | 2 | 3.06 | 3 | -4.66 | -4.20 |
| Fe I | 4258.62 | 351 | 2.82 | 3 | -5.05 | -4.53 |
| Fe I | 4260.48 | 152 | 2.40 | 2 | -4.22 | -4.14 |
| Fe I | 4264.74 | 993 | 3.94 | 2 | -5.11 | -4.46 |
| Fe I | 4265.26 | 993 | 3.91 | 2 | -5.12 | -4.57 |
| Fe I | 4271.77 | 42 | 2.44 | 3 | -4.18 | -4.11 |
| Fe I | 4282.41 | 71 | 2.17 | 4 | -4.47 | -4.11 |
| Fe I | 4291.47 | 3 | 0.05 | 4 | -4.68 | -4.16 |
| Fe I | 4325.77 | 942 | 1.60 | 4 | -4.04 | -4.02 |
| Fe I | 4327.92 | 597 | 3.03 | 3 | -4.99 | -4.46 |
| Fe I | 4369.77 | 518 | 3.03 | 5 | -4.52 | -4.12 |
| Fe I | 4375.93 | 2 | 0.0 | 4 | -4.50 | -4.15 |
| Fe I | 4383.55 | 41 | 1.48 | 4 | -4.07 | -4.02 |
| Fe I | 4389.24 | 2 | 0.05 | 4 | -5.00 | -4.26 |
| Fe I | 4404.75 | 41 | 1.55 | 4 | -4.11 | -4.03 |
| Fe I | 4915.13 | 41 | 1.60 | 4 | -4.21 | -4.10 |
| Fe I | 4430.62 | 68 | 2.21 | 4 | -4.57 | -4.15 |
| Fe I | 4442.34 | 43 | 2.19 | 3 | -4.51 | -4.14 |

TABLE IV (Continued)

| Element | λ | RMT | $\chi_\ell$ | No. of Meas. | Log w/λ | Log h/λ |
|---|---|---|---|---|---|---|
| Fe I | 4443.20 | 350 | 2.85 | 3 | -4.57 | -4.13 |
| Fe I | 4447.72 | 68 | 2.21 | 3 | -4.52 | -4.18 |
| Fe I | 4454.38 | 350 | 2.82 | 3 | -4.61 | -4.19 |
| Fe I | 4489.74 | 2 | 0.12 | 3 | -4.60 | -4.14 |
| Fe I | 4531.15 | 39 | 1.48 | 1 | -4.14 | -3.86 |
| Fe I | 4602.94 | 39 | 1.48 | 2 | -4.59 | -4.12 |
| Fe I | 4871.32 | 318 | 2.85 | 4 | -4.40 | -3.95 |
| Fe I | 5006.13 | 318 | 2.83 | 1 | -4.54 | -4.15 |
| Fe I | 5051.64 | 16 | 0.91 | 2 | -4.51 | -4.02 |
| Fe I | 5068.77 | 383 | 2.93 | 2 | -4.64 | -4.06 |
| Fe I | 5083.34 | 16 | 0.95 | 2 | -4.63 | -4.03 |
| Fe I | 5110.41 | 1 | 0.0 | 2 | -4.50 | -4.00 |
| Fe I | 5133.69 | 1092 | 4.16 | 3 | -4.56 | -4.05 |
| Fe I | 5192.35 | 383 | 2.99 | 4 | -4.55 | -4.08 |
| Fe I | 5194.94 | 36 | 1.55 | 4 | -4.69 | -4.08 |
| Fe I | 5216.28 | 36 | 1.60 | 4 | -4.63 | -4.05 |
| Fe I | 5225.53 | 1 | 0.11 | 1 | -4.95 | -4.00 |
| Fe I | 5266.56 | 383 | 2.99 | 4 | -4.57 | -4.09 |
| Fe I | 5281.80 | 383 | 3.03 | 4 | -4.70 | -4.11 |
| Fe I | 5283.63 | 553 | 3.24 | 3 | -4.52 | -4.20 |
| Fe I | 5307.37 | 36 | 1.60 | 4 | -4.85 | -4.10 |
| Fe I | 5339.94 | 553 | 3.26 | 4 | -4.72 | -4.05 |
| Fe I | 5364.87 | 1146 | 4.44 | 3 | -4.77 | -4.18 |
| Fe I | 5367.47 | 1146 | 4.41 | 3 | -4.75 | -4.12 |
| Fe I | 5369.97 | 1146 | 4.35 | 3 | -4.66 | -4.23 |
| Fe I | 5383.37 | 1146 | 4.29 | 3 | -4.60 | -3.99 |
| Fe I | 5393.17 | 553 | 3.23 | 3 | -4.69 | -4.05 |
| Fe I | 5397.13 | 15 | 0.91 | 3 | -4.50 | -3.97 |
| Fe I | 5405.78 | 15 | 0.99 | 3 | -4.51 | -4.37 |
| Fe I | 5410.91 | 1165 | 4.45 | 3 | -4.70 | -4.04 |
| Fe I | 5424.07 | 1146 | 4.32 | 3 | -4.54 | -3.95 |
| Fe I | 5429.70 | 15 | 0.95 | 3 | -4.49 | -4.25 |
| Fe I | 5434.53 | 15 | 1.01 | 3 | -4.53 | -3.93 |
| Fe I | 5445.05 | 1156 | 4.37 | 3 | -4.72 | -4.00 |
| Fe I | 5497.52 | 15 | 1.01 | 2 | -4.50 | -3.86 |
| Fe I | 5501.47 | 15 | 0.95 | 2 | -4.58 | -3.89 |
| Fe I | 5506.78 | 15 | 0.99 | 1 | -4.55 | -3.92 |
| Fe I | 5569.63 | 686 | 3.42 | 1 | -4.65 | -3.92 |
| Fe I | 5572.85 | 686 | 3.40 | 1 | -4.58 | -3.86 |
| Fe I | 5576.10 | 686 | 3.43 | 1 | -4.81 | -4.06 |
| Fe I | 5562.99 | 1107 | 4.19 | 1 | -4.71 | -4.12 |
| Fe I | 5976.80 | 959 | 3.93 | 1 | -5.00 | -4.30 |
| Fe I | 6003.08 | 959 | 3.86 | 1 | -4.97 | -4.33 |
| Fe I | 6024.07 | 1178 | 4.53 | 1 | -4.90 | -4.24 |
| Fe I | 6065.53 | 207 | 2.60 | 1 | -4.74 | -4.16 |
| Fe I | 6055.99 | 1259 | 4.71 | 1 | -5.08 | -4.32 |
| Fe I | 6137.70 | 207 | 2.58 | 1 | -4.73 | -4.18 |
| Fe I | 6213.40 | 62 | 2.21 | 1 | -4.95 | -4.37 |

TABLE IV (Concluded)

| Element | λ | RMT | $\chi_\ell$ | No. of Meas. | Log w/λ | Log h/λ |
|---|---|---|---|---|---|---|
| Fe I | 6230.73 | 207 | 2.25 | 2 | -4.67 | -4.10 |
| Fe I | 6246.33 | 816 | 3.59 | 2 | -4.91 | -4.23 |
| Fe I | 6252.56 | 169 | 2.39 | 2 | -4.76 | -4.12 |
| Fe I | 6265.14 | 62 | 2.17 | 2 | -4.99 | -4.22 |
| Fe I | 6301.54 | 816 | 3.64 | 2 | -4.79 | -4.19 |
| Fe I | 6318.02 | 168 | 2.44 | 2 | -4.90 | -4.21 |
| Fe I | 6393.61 | 168 | 2.42 | 1 | -4.74 | -4.09 |
| Fe I | 6411.66 | 816 | 3.64 | 1 | -4.71 | -4.04 |
| Fe I | 6421.36 | 111 | 2.27 | 1 | -4.84 | -4.17 |
| Fe I | 6494.99 | 168 | 2.39 | 1 | -4.70 | -4.14 |
| Fe I | 6430.85 | 62 | 2.17 | 1 | -4.84 | -4.19 |
| Fe II | 4128.74 | 27 | 2.58 | 2 | -4.92 | -4.39 |
| Fe II | 4178.86 | 28 | 2.57 | 2 | -4.76 | -4.16 |
| Fe II | 4273.32 | 27 | 2.69 | 3 | -4.65 | -4.15 |
| Fe II | 4303.17 | 27 | 2.70 | 3 | -4.64 | -4.23 |
| Fe II | 4369.40 | 28 | 2.77 | 2 | -4.95 | -4.29 |
| Fe II | 4576.33 | 38 | 2.85 | 3 | -4.61 | -4.06 |
| Fe II | 4620.51 | 38 | 2.82 | 1 | -4.86 | -4.01 |
| Fe II | 5197.57 | 49 | 3.22 | 4 | -4.57 | -4.13 |
| Fe II | 5234.62 | 49 | 3.21 | 3 | -4.64 | -4.17 |
| Fe II | 5264.80 | 48 | 3.22 | 2 | -4.94 | -4.29 |
| Fe II | 5284.09 | 41 | 2.88 | 2 | -4.88 | -4.19 |
| Fe II | 5325.56 | 49 | 3.21 | 3 | -4.95 | -4.24 |
| Fe II | 5362.86 | 48 | 3.19 | 4 | -4.73 | -4.03 |
| Fe II | 5414.09 | 48 | 3.21 | 1 | -5.29 | -4.23 |
| Fe II | 5425.27 | 49 | 3.19 | 1 | -4.98 | -4.01 |
| Fe II | 6247.56 | 74 | 3.87 | 2 | -4.94 | -4.24 |
| Fe II | 6432.65 | 40 | 2.88 | 1 | -5.00 | -4.20 |
| Fe II | 6456.38 | 74 | 3.89 | 1 | -4.65 | -4.05 |

Column 6 gives the logarithm of the ratio of the halfwidth to the wavelength of the transition.

The equivalent widths measured in this study were eventually corrected for instrumental effects using the method of Voight functions. However, the nature of the correction produces only secondary changes in the equivalent widths while major changes occurs in the halfwidth of the profile. Therefore, it was not found advantageous to correct the equivalent width data of Mangold and Peebles for this broadening phenomena.

## Line Profiles

Line profiles of neutral and singly ionized iron were obtained from the profiles constructed for the measurement of the equivalent widths. The line depth was measured at representative distances from the line center for those profiles which were later to be fitted with a theoretical profile, calculated on the basis of a postulated model of the atmosphere. Table V indicates the data from these measurements. In addition, the requirements of the instrumental broadening program made it necessary to measure the width of the profile at certain depths. In Table VI are reproduced the data used for the assessment of the true profile from the observed one. Table VI also gives the halfwidths of the iron lines utilized for the macroturbulence analysis.

Column 1 lists the wavelength given by Moore's (1959) Revised Multiplet Table (RMT).

Column 2 gives the central depth of the line in centimeters.

Column 3 lists the halfwidth of the line in centimeters.

Column 4 gives the breadth in centimeters of the observed line at one tenth of the maximum intensity.

TABLE V

OBSERVED LINE PROFILES DATA FOR Fe I AND Fe II IN THETA URSAE MAJORIS

| Fe I λ4199.10 | | Fe I λ4202.03 | | Fe I λ4206.70 | | Fe I λ4219.36 | | Fe I λ4736.78 | |
|---|---|---|---|---|---|---|---|---|---|
| Δλ(Å) | Line Depth | Δλ(Å) | Line Depth | Δλ(Å) | Line Depth | Δλ(Å) | Line Depth | Δλ(Å) | Line Depth |
| 0 | 0.468 | 0 | 0.477 | 0 | 0.339 | 0 | 0.424 | 0 | 0.338 |
| 0.045 | 0.431 | 0.059 | 0.426 | 0.044 | 0.320 | 0.044 | 0.408 | 0.046 | 0.297 |
| 0.067 | 0.381 | 0.118 | 0.352 | 0.089 | 0.260 | 0.067 | 0.371 | 0.092 | 0.259 |
| 0.089 | 0.320 | 0.148 | 0.307 | 0.133 | 0.185 | 0.089 | 0.304 | 0.137 | 0.218 |
| 0.111 | 0.266 | 0.177 | 0.255 | 0.178 | 0.115 | 0.111 | 0.251 | 0.183 | 0.171 |
| 0.133 | 0.202 | 0.207 | 0.198 | 0.267 | 0.032 | 0.133 | 0.173 | 0.274 | 0.087 |
| 0.156 | 0.140 | 0.236 | 0.156 | 0.356 | 0.009 | 0.177 | 0.058 | 0.366 | 0.028 |
| 0.178 | 0.085 | 0.296 | 0.100 | 0.462 | 0 | 0.310 | 0.013 | | |
| 0.200 | 0.048 | 0.355 | 0.068 | | | 0.421 | 0 | | |
| 0.267 | 0.020 | 0.502 | 0.033 | | | | | | |
| 0.334 | 0.009 | 0.709 | 0 | | | | | | |
| 0.423 | 0 | | | | | | | | |

TABLE V (Concluded)

| Fe I $\lambda$4890.76 | | Fe I $\lambda$5434.53 | | Fe I $\lambda$5586.76 | | Fe II $\lambda$4122.64 | | Fe II $\lambda$4178.86 | | Fe II $\lambda$4731.44 | | Fe II $\lambda$5414.09 | | Fe II $\lambda$5425.27 | |
|---|---|---|---|---|---|---|---|---|---|---|---|---|---|---|---|
| $\Delta\lambda$ (Å) | Line Depth | $\Delta\lambda$ (Å) | Line Depth | $\Delta\lambda$ (Å) | Line Depth | $\Delta\lambda$ (Å) | Line Depth | $\Delta\lambda$ (Å) | Line Depth | $\Delta\lambda$ (Å) | Line Depth | $\Delta\lambda$ (Å) | Line Depth | $\Delta\lambda$ (Å) | Line Depth |
| 0 | 0.359 | 0 | 0.258 | 0 | 0.220 | 0 | 0.347 | 0 | 0.323 | 0 | 0.292 | 0 | 0.092 | 0 | 0.140 |
| 0.091 | 0.330 | 0.091 | 0.237 | 0.243 | 0.180 | 0.059 | 0.316 | 0.022 | 0.307 | 0.046 | 0.268 | 0.091 | 0.082 | 0.045 | 0.124 |
| 0.136 | 0.276 | 0.136 | 0.202 | 0.364 | 0.138 | 0.119 | 0.261 | 0.044 | 0.288 | 0.092 | 0.234 | 0.136 | 0.069 | 0.091 | 0.108 |
| 0.227 | 0.204 | 0.182 | 0.176 | 0.486 | 0.089 | 0.179 | 0.200 | 0.066 | 0.266 | 0.183 | 0.185 | 0.182 | 0.032 | 0.136 | 0.094 |
| 0.272 | 0.134 | 0.272 | 0.122 | 0.607 | 0.043 | 0.239 | 0.117 | 0.089 | 0.228 | 0.274 | 0.124 | 0.227 | 0.016 | 0.182 | 0.080 |
| 0.317 | 0.097 | 0.363 | 0.061 | 0.728 | 0.016 | 0.298 | 0.053 | 0.133 | 0.146 | 0.320 | 0.075 | 0.345 | 0 | 0.227 | 0.061 |
| 0.408 | 0.049 | 0.454 | 0.029 | 0.850 | 0 | 0.388 | 0 | 0.156 | 0.083 | 0.366 | 0.045 | | | 0.272 | 0.043 |
| 0.544 | 0.022 | 0.635 | 0.007 | | | | | 0.201 | 0.025 | 0.457 | 0 | | | 0.318 | 0.023 |
| 0.862 | 0 | 0.771 | 0 | | | | | 0.290 | 0 | | | | | 0.454 | 0 |

TABLE VI

INSTRUMENTAL BROADENING DATA FOR
OBSERVED LINES OF Fe I AND Fe II

| Element | λ | Co | Ho | B | Hc | Disp. |
|---|---|---|---|---|---|---|
| Fe I | 4005.25 | 4.40 | 2.20 | 4.30 | 7.00 | 0.4616 |
| Fe I | 4009.71 | 8.57 | 1.35 | 3.10 | 17.31 | 0.4576 |
| Fe I | 4009.71 | 3.13 | 1.32 | 2.62 | 7.08 | 0.4590 |
| Fe I | 4009.71 | 4.00 | 0.85 | 1.90 | 12.40 | 0.6042 |
| Fe I | 4045.82 | 6.60 | 2.45 | 5.65 | 8.10 | 0.4038 |
| Fe I | 4045.82 | 8.50 | 3.15 | 6.65 | 12.40 | 0.6017 |
| Fe I | 4062.45 | 7.45 | 1.48 | 3.02 | 16.60 | 0.4548 |
| Fe I | 4062.45 | 3.75 | 1.28 | 2.80 | 8.68 | 0.4610 |
| Fe I | 4062.45 | 3.14 | 1.08 | 2.32 | 12.24 | 0.6005 |
| Fe I | 4063.60 | 6.40 | 2.30 | 5.60 | 8.72 | 0.4062 |
| Fe I | 4063.60 | 7.00 | 2.40 | 5.00 | 12.30 | 0.6004 |
| Fe I | 4071.74 | 6.42 | 2.40 | 5.20 | 9.20 | 0.4067 |
| Fe I | 4071.74 | 6.70 | 2.20 | 5.00 | 12.30 | 0.5998 |
| Fe I | 4107.49 | 2.30 | 1.38 | 2.46 | 10.10 | 0.5974 |
| Fe I | 4143.87 | 5.80 | 2.00 | 3.75 | 12.05 | 0.5948 |
| Fe I | 4168.95 | 3.90 | 1.20 | 2.45 | 23.00 | 0.4470 |
| Fe I | 4175.64 | 3.10 | 1.42 | 3.00 | 11.33 | 0.5974 |
| Fe I | 4175.64 | 7.70 | 1.58 | 3.88 | 22.60 | 0.4465 |
| Fe I | 4181.76 | 4.60 | 1.38 | 3.15 | 11.23 | 0.5922 |
| Fe I | 4181.76 | 11.20 | 1.60 | 3.35 | 22.15 | 0.4461 |
| Fe I | 4187.04 | 3.90 | 1.02 | 2.20 | 11.18 | 0.5918 |
| Fe I | 4187.04 | 10.20 | 1.44 | 2.95 | 21.70 | 0.4457 |
| Fe I | 4199.10 | 3.70 | 1.70 | 3.34 | 11.15 | 0.5910 |
| Fe I | 4199.10 | 9.70 | 1.42 | 3.43 | 20.60 | 0.4448 |
| Fe I | 4199.94 | 4.40 | 1.12 | 2.22 | 20.60 | 0.4448 |
| Fe I | 4202.03 | 11.50 | 1.70 | 4.00 | 20.40 | 0.4446 |
| Fe I | 4206.70 | 3.48 | 1.48 | 3.02 | 11.18 | 0.5906 |
| Fe I | 4206.70 | 6.80 | 1.68 | 3.50 | 20.00 | 0.4443 |
| Fe I | 4216.19 | 7.40 | 1.50 | 3.02 | 19.48 | 0.4436 |
| Fe I | 4216.19 | 5.20 | 1.72 | 3.58 | 14.19 | 0.4451 |
| Fe I | 4227.43 | 7.90 | 2.05 | 3.55 | 14.30 | 0.4441 |
| Fe I | 4227.43 | 11.20 | 1.80 | 3.45 | 19.50 | 0.4428 |
| Fe I | 4258.63 | 3.12 | 1.18 | 2.25 | 19.40 | 0.4406 |
| Fe I | 4258.63 | 2.50 | 1.00 | 2.05 | 14.21 | 0.4411 |
| Fe I | 4260.48 | 8.45 | 2.30 | 3.70 | 14.25 | 0.4409 |
| Fe I | 4260.48 | 12.00 | 2.00 | 4.00 | 19.45 | 0.4405 |
| Fe I | 4264.73 | 2.62 | 1.30 | 3.50 | 19.40 | 0.4402 |
| Fe I | 4264.73 | 1.80 | 1.64 | 3.05 | 14.20 | 0.4405 |
| Fe I | 4265.27 | 3.70 | 0.96 | 2.20 | 19.40 | 0.4401 |
| Fe I | 4265.27 | 2.52 | 1.02 | 2.15 | 14.20 | 0.4404 |
| Fe I | 4271.76 | 13.15 | 2.10 | 4.00 | 19.30 | 0.4396 |
| Fe I | 4271.76 | 9.50 | 2.20 | 3.95 | 14.20 | 0.4398 |
| Fe I | 4276.69 | 2.30 | 0.52 | 1.22 | 14.15 | 0.4393 |
| Fe I | 4276.69 | 1.40 | 0.52 | 1.12 | 9.10 | 0.5808 |
| Fe I | 4325.77 | 5.45 | 2.20 | 4.88 | 7.80 | 0.5780 |

TABLE VI (Continued)

| Element | λ | Co | Ho | B | Hc | Disp. |
|---|---|---|---|---|---|---|
| Fe I | 4325.77 | 8.40 | 2.40 | 4.85 | 12.10 | 0.4347 |
| Fe I | 4327.90 | 2.41 | 1.13 | 2.25 | 12.02 | 0.4344 |
| Fe I | 4327.90 | 2.08 | 0.85 | 1.65 | 7.78 | 0.5779 |
| Fe I | 4369.40 | 2.91 | 1.08 | 2.14 | 7.00 | 0.5755 |
| Fe I | 4383.57 | 4.85 | 2.00 | 3.84 | 6.65 | 0.5748 |
| Fe I | 4404.75 | 15.00 | 1.50 | 3.30 | 25.90 | 0.9314 |
| Fe I | 4404.75 | 4.20 | 1.65 | 3.45 | 6.20 | 0.5736 |
| Fe I | 4415.13 | 9.40 | 2.30 | 4.80 | 16.20 | 0.4269 |
| Fe I | 4415.65 | 3.45 | 1.70 | 3.45 | 5.95 | 0.5729 |
| Fe I | 4531.15 | 11.70 | 1.80 | 3.40 | 26.20 | 0.9283 |
| Fe I | 4871.32 | 9.00 | 1.30 | 2.60 | 23.60 | 0.9080 |
| Fe I | 5250.65 | 2.00 | 0.75 | 1.43 | 9.60 | 0.8998 |
| Fe I | 5307.37 | 1.80 | 0.64 | 1.45 | 9.50 | 0.8980 |
| Fe I | 5364.87 | 2.28 | 0.79 | 1.76 | 9.10 | 0.8961 |
| Fe I | 5367.47 | 2.32 | 0.50 | 1.24 | 9.07 | 0.8960 |
| Fe I | 5369.97 | 1.89 | 1.20 | 2.17 | 9.10 | 0.8960 |
| Fe I | 5393.17 | 2.08 | 0.84 | 1.80 | 9.07 | 0.8952 |
| Fe I | 5397.31 | 2.74 | 1.54 | 3.48 | 9.02 | 0.8951 |
| Fe I | 5405.78 | 3.34 | 0.83 | 2.30 | 8.95 | 0.8948 |
| Fe I | 5410.91 | 2.12 | 0.82 | 1.58 | 8.88 | 0.8946 |
| Fe I | 5429.70 | 3.20 | 1.00 | 2.30 | 8.80 | 0.8940 |
| Fe I | 5445.05 | 1.70 | 1.30 | 2.50 | 8.75 | 0.8936 |
| Fe I | 5976.72 | 2.02 | 1.00 | 2.22 | 15.20 | 0.8750 |
| Fe I | 6003.08 | 2.15 | 0.95 | 2.18 | 15.00 | 0.8750 |
| Fe I | 6024.11 | 2.90 | 0.98 | 2.10 | 14.60 | 0.8750 |
| Fe I | 6056.10 | 1.70 | 0.95 | 2.00 | 13.60 | 0.8750 |
| Fe I | 6065.53 | 2.95 | 1.20 | 2.55 | 13.70 | 0.8750 |
| Fe I | 6137.81 | 3.50 | 1.10 | 2.52 | 13.70 | 0.8750 |
| Fe I | 6213.40 | 2.00 | 0.90 | 2.02 | 11.70 | 0.8750 |
| Fe I | 6301.54 | 2.60 | 1.22 | 2.76 | 9.95 | 0.8750 |
| Fe I | 6393.61 | 2.20 | 1.50 | 2.90 | 10.16 | 0.8742 |
| Fe I | 6400.03 | 2.70 | 1.60 | 2.80 | 10.08 | 0.8740 |
| Fe I | 6430.84 | 2.10 | 1.10 | 2.22 | 9.86 | 0.8734 |
| Fe I | 6432.58 | 1.50 | 1.13 | 2.30 | 9.86 | 0.8732 |
| Fe I | 6421.41 | 2.00 | 1.25 | 2.60 | 9.90 | 0.8736 |
| Fe I | 6495.08 | 2.52 | 1.30 | 2.80 | 9.72 | 0.8720 |
| Fe II | 4128.74 | 3.00 | 0.84 | 1.95 | 12.04 | 0.5959 |
| Fe II | 4178.86 | 3.80 | 1.10 | 2.90 | 11.30 | 0.5924 |
| Fe II | 4178.86 | 8.05 | 1.40 | 3.42 | 22.30 | 0.4463 |
| Fe II | 4273.32 | 6.30 | 1.54 | 3.15 | 19.25 | 0.4396 |
| Fe II | 4273.32 | 2.90 | 1.30 | 2.68 | 9.22 | 0.5810 |
| Fe II | 4303.17 | 7.40 | 1.62 | 3.55 | 18.26 | 0.4375 |
| Fe II | 4303.17 | 5.34 | 1.60 | 3.54 | 13.24 | 0.4368 |
| Fe II | 4303.17 | 3.30 | 0.90 | 1.85 | 8.20 | 0.5793 |
| Fe II | 4369.40 | 2.04 | 0.70 | 1.55 | 7.00 | 0.5755 |
| Fe II | 4576.33 | 6.05 | 0.75 | 1.56 | 23.25 | 1.2495 |
| Fe II | 4576.33 | 6.88 | 1.15 | 2.58 | 26.10 | 0.9227 |
| Fe II | 4576.33 | 7.45 | 0.90 | 2.00 | 26.22 | 0.9253 |

TABLE VI (Concluded)

| Element | λ | Co | Ho | B | Hc | Disp. |
|---|---|---|---|---|---|---|
| Fe II | 4620.51 | 4.42 | 0.82 | 1.90 | 26.15 | 0.9206 |
| Fe II | 4620.51 | 5.92 | 1.20 | 2.40 | 26.28 | 0.9221 |
| Fe II | 5132.67 | 2.10 | 0.60 | 1.50 | 16.35 | 0.9000 |
| Fe II | 5197.57 | 2.50 | 1.20 | 2.44 | 9.70 | 0.9015 |
| Fe II | 5734.62 | 2.20 | 0.75 | 1.52 | 7.62 | 0.9000 |
| Fe II | 5234.62 | 4.80 | 0.98 | 2.00 | 17.90 | 0.9212 |
| Fe II | 5264.81 | 1.64 | 0.50 | 1.10 | 9.48 | 0.8993 |
| Fe II | 5284.09 | 1.48 | 0.70 | 1.50 | 7.20 | 0.8905 |
| Fe II | 5325.56 | 2.52 | 0.80 | 1.70 | 17.80 | 0.9150 |
| Fe II | 5362.86 | 1.70 | 0.70 | 1.68 | 9.50 | 2.0710 |
| Fe II | 5362.86 | 3.95 | 1.50 | 2.95 | 17.76 | 0.9124 |
| Fe II | 5414.09 | 1.60 | 0.90 | 1.85 | 17.60 | 0.9089 |
| Fe II | 5425.27 | 2.30 | 1.18 | 2.58 | 17.58 | 0.9081 |
| Fe II | 5425.27 | 1.60 | 0.42 | 1.30 | 8.80 | 0.8962 |
| Fe II | 6247.56 | 2.30 | 1.05 | 2.13 | 11.00 | 0.8585 |
| Fe II | 6432.65 | 1.50 | 1.13 | 2.30 | 9.86 | 0.8732 |
| Fe II | 6456.38 | 2.35 | 1.70 | 3.58 | 10.10 | 0.8730 |

Column 5 reproduces the height of the continuum at the line center in centimeters.

Column 6 gives the dispersion in Å per inch of the tracing for the transition under consideration.

## Assessment of Errors

The sources of error which arise from the spectrophotometric techniques are discussed in some detail by Wright (1948). Errors due to improper focus, ghosts, calibration of the photographic plate, finite slit width of the microphotometer and the development process can all be important but probably not as much as errors introduced during the reduction of the tracings themselves. The location of the continuum and the treatment of blending effects are probably the most significant factors affecting uncertainty in the equivalent width data. Typically, the uncertainty in the equivalent widths of weak lines (on the order of 20 mA) can be as great as twenty per cent; for moderately strong lines, the error may drop to about ten per cent.

## The Physical Constants

Abundances derived from the model atmosphere technique can be no better than the reliability of the system of physical constants used for the analysis. At the present time knowledge of the damping constants and oscillator strengths is still very uncertain. In the last few years the number and reliability of oscillator strength measurements have increased dramatically relieving some of the difficulty in the computation of stellar abundances.

The necessary atomic data, the partition functions, atomic weights, ionization potentials, etc., were obtained from the results published by Evans (1966) and the damping constants used for this analysis have been discussed elsewhere in this study (see Appendix B).

A number of authors have published results of both theoretically or experimentally determined oscillator strengths and extensive lists have been prepared in biographical form by Glennon and Wiese (1962) and more recently by Miles and Wise (1970). For this study, oscillator strengths were used extensively from the work of Corliss and Tech (1968), Corliss and Bozman (1962), Warner (1967), Warner (1968) and Wiese, Smith, and Miles (1969).

The results of recent investigations have given evidence for an excitation potential dependence in the log gf values reported by Corliss and Bozman (Takens, 1970) and by Corliss and Tech (Wares, Wolnik, and Berthel, 1970; Evans, Weems, and Schroeder, 1970). As a result, correction factors were employed to remove any traces of a systematic error due to the excitation level of the transition.

## Wavelengths and Excitation Potentials

The wavelengths for the observed lines in the Spectrum in Theta Ursae Majoris were identified from Charlotte Moore's tabulation _A Multiplet Table of Astrophysical Interest, Revised Edition_ (1959). In addition, the excitation potential of the lower level of the transition was also obtained from this source.

CHAPTER V

ANALYSIS OF THE OBSERVATIONS

The shape and breadth of the Fraunhofer lines in the spectrum of Theta Ursae Majoris are affected by the various line broadening agents mentioned in Chapter II. For Theta Ursae Majoris, the most important sources arise from non-thermal phenomena such as atmospheric turbulence. The existence of microturbulence can best be determined from the curve of growth. Microturbulence produce an effective Doppler broadening which tends to delay the onset of optical saturation and effects the transition region of curve of growth. Haung and Struve (1960) discuss this effect in some detail in their reviews on atmospheric turbulence. On the other hand, if the scale of the turbulence is large the effect upon the equivalent width is negligible but the line profile will be altered as in stellar rotation.

From the analysis of the profile of a line, Huang and Struve (1954) first developed a method for the separation of these two broadening mechanisms. Through a curve of half-width correlation, a plot of the functional dependence of the half-width of a spectral line upon its equivalent width, they developed a procedure whereby the shift in the vertical and horizontal axis necessary to fit the empirical to the theoretical curve could be combined to derive a value for both large and small scale turbulent effects. Van den Heuvel (1963) and Elste (1967) have employed a similar curve to distinguish between macroturbulence and microturbulence. However, their approach is to calculate the theoretical relation using a model atmosphere, and so gives a more exact relationship between log $h/\lambda$ and log $w/\lambda$ than did Struve and Huang.

## The Microturbulence Analysis

Line intensities of approximately one hundred and twenty-five neutral and singly ionized lines of iron were used for the curve of growth analysis. The results have been incorporated into Tables XII and XIII for convenience.

The f-values for neutral iron were taken from the compilation of Corliss and Tech (1968). Since the f-values of Corliss and Tech have been shown to contain a systematic dependence upon the excitation potential (Wares, Wolnik, and Berthel, 1970; Evans, Weems, and Schroeder, 1970) an attempt was introduced to correct for this uncertainty using the results of Evans, Weems, and Schroeder. For multiplets of Fe I falling within the wavelength region of $\lambda$4200, the f-values were lowered by 0.5 dex* for those multiplets with $\chi_{\ell}$ greater than 2.2 electron volts. Multiplets with $\chi_{\ell}$ less than 1.5 electron volts were left unchanged. In the spectral region $\lambda$5800, multiplets of Fe I with $\chi_{\ell}$ less than 1.0 electron volts were assigned the Corliss and Tech f-value, while for $\chi_{\ell}$ approximately equal to 1.5 ev, the values were reduced by 0.3 dex. For multiplets with excitation potentials exceeding 2.2 electron volts, the f-values have been altered by -0.5 dex. The correction factor for all cases was determined by increasing or decreasing the f-values of all multiplets until the data defined a single curve of growth. The oscil-

---

*The notation 0.5 dex corresponds to the quantity log x = 0.5.

lator strengths for the Fe II lines were obtained from the results published by Warner (1967, 1968).

The curves of growth for iron are shown in Figure 2, Figure 3, and Figure 4. All curves of growth have been computed for the center of the star's disk. The Fe I lines have been separated into two distinct wavelength regions, $\lambda5800$ and $\lambda4200$. The larger symbols indicate equivalent widths determined by Mangold (1968) and the smaller, values obtained in this study. No systematic trend could be established in the equivalent widths corrected for instrumental effects in this study and those established earlier by Mangold as far as the curve of growth is concerned.

In Figure 2, the lower curve represents the curve of growth for $\lambda4200$ broadened only by the random thermal motion of atoms in the stellar atmosphere. The fact that almost all the data lie above this line indicates an apparent macroturbulent velocity field for Theta Ursae Majoris. The upper curve represents the upper extent of the magnitude of the microturbulent velocity in this star; the curve of growth with a three kilometer per second microturbulent velocity seems to represent the average value over this wavelength range. Figure 3 represents the state of affairs around the spectral region $\lambda5800$. Theoretical curves of growth for $\lambda5800$ have been calculated for a thermally-broadened line (lower dashed line) and a line incorporating a four kilometer per second microturbulent velocity (upper dashed curve). Again the data suggest that a value closer to three kilometers per second (solid curve) represents the best estimate for all lines in this region of the effect due to small scale eddies. The microturbulent velocity fields used for the computation of the theoretical curves of growth were based upon a thermally homogeneous model independent of the optical depth in the atmos-

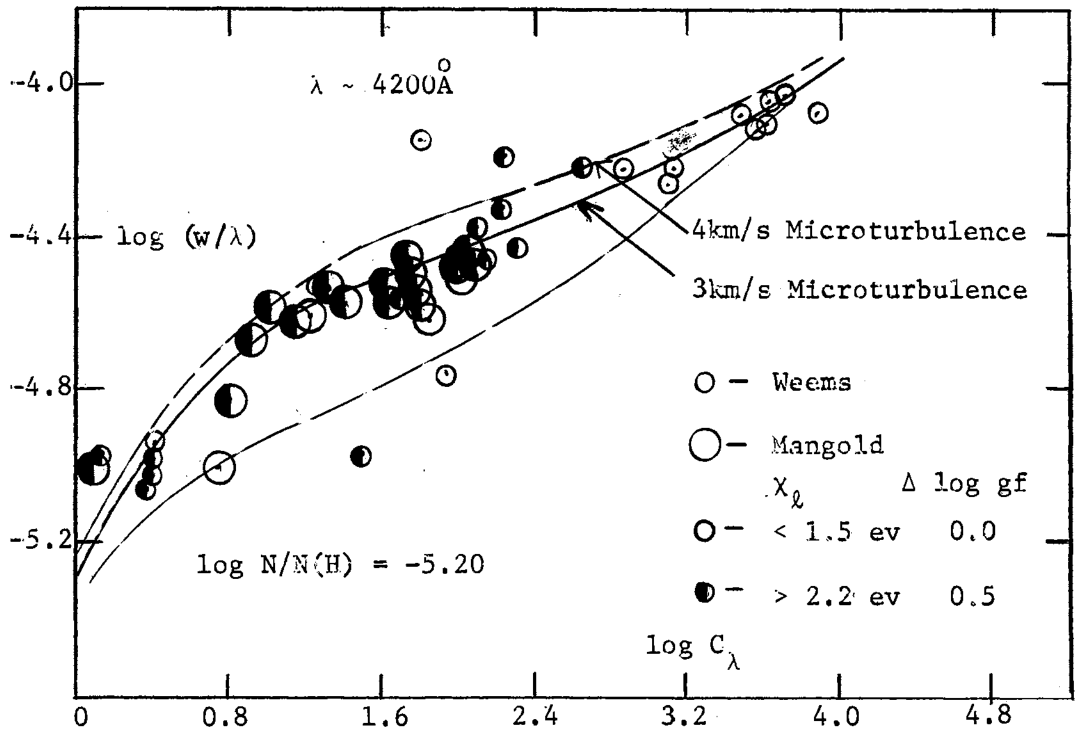


Figure 2. The Observed and Theoretical Center-of-the-Disk Curves of Growth for Fines in the Wavelength Region λ4200 for Fe I

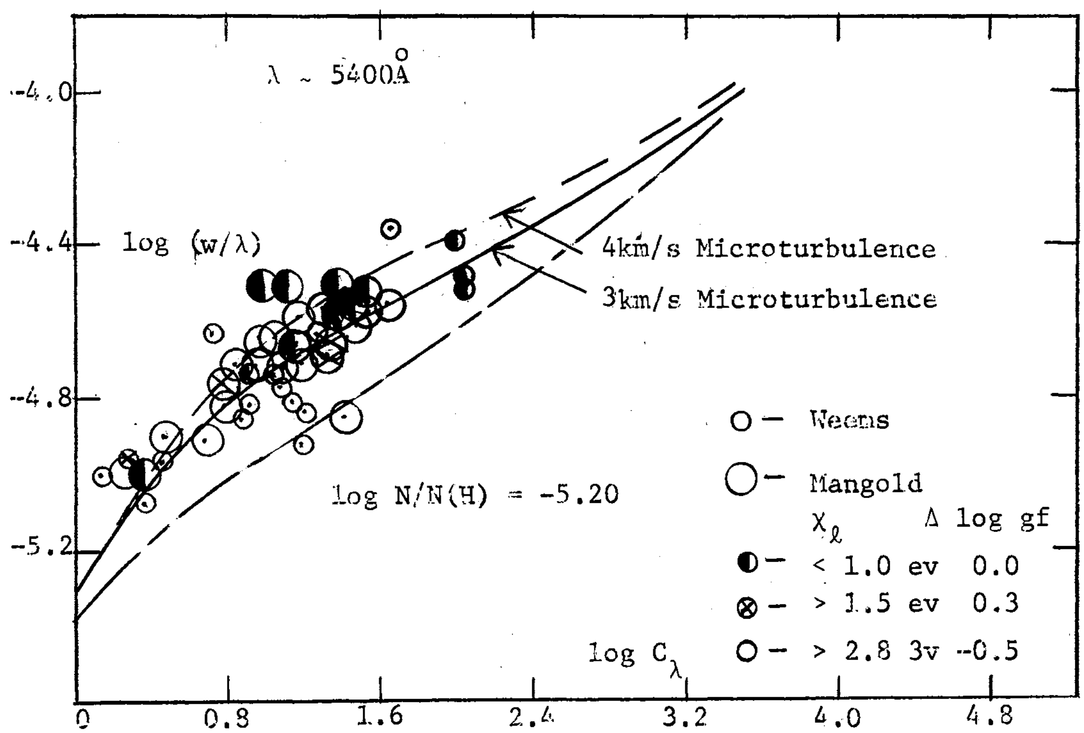


Figure 3. The Observed and Theoretical Center-of-the-Disk Curves of Growth for Lines in the Wavelength Region λ5400 for Fe I

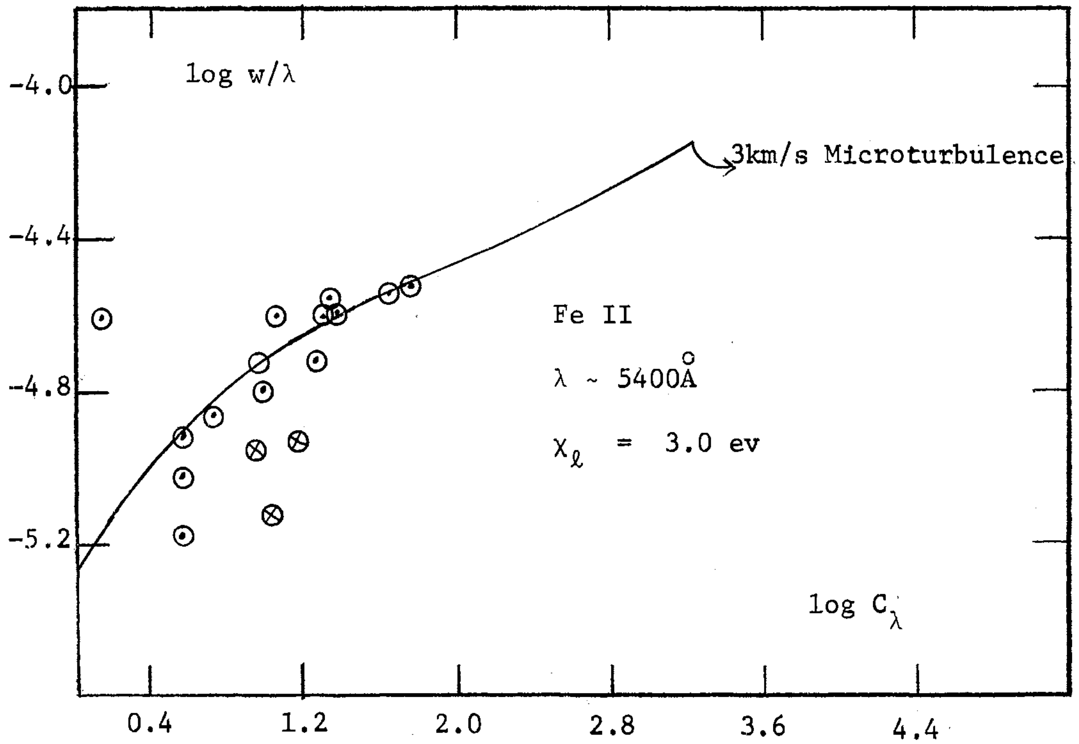


Figure 4. The Observed and Theoretical Center-of-the Disk Curves of Growth for Fe II.

phere. This eliminates any assessment of a possible microturbulent velocity stratification in the atmosphere and so the microturbulent velocity, as determined from the curve of growth, represents a value averaged over all layers of the atmosphere.

Figure 4 shows all the observed lines of Fe II regardless of the wavelength. A representative line ($\lambda$5414.09) was chosen for the group and the curve of growth calculated incorporating the results of the Fe I lines. The three observational points, indicated by the symbol x, yielded erroneous values of the abundance and so were weighted independently from the rest of the data. Again, the best fit to the empirical curve was obtained for a three kilometer per second microturbulent velocity.

## The Macroturbulence Analysis

In order to assess the contribution of any macroturbulent velocity field, only weak lines of relatively high excitation potential were selected. These lines are relatively insensitive to the temperature and electron pressure and, more important, yield halfwidths extremely sensitive to any line broadening agent present. Moderately strong lines show very little such dependence and are broadened principally by the amount of damping in the wings of the line. All equivalent widths and halfwidths have been corrected prior to the analysis using the method of Voight functions. The data derived from the observations listed in Table VII are plotted in Figure 5. As can be seen, there is relatively little change in the halfwidth for observed lines with $\log w/\lambda < -4.8$. For the stronger lines the halfwidth increases rapidly with increasing equivalent width. An estimation of the uncertainty involved in the observations of the weakest line is shown by the error bar on the weakest

TABLE VII

CORRECTED HALFWIDTHS AND EQUIVALENT WIDTHS FOR OBSERVED LINES OF Fe I AND Fe II

| Element | $\lambda$ | RMT | $\chi_{\ell}$ | Log $w/\lambda$ | Log $h/\lambda$ | Log gf |
|---|---|---|---|---|---|---|
| Fe I | 4005.25 | 43 | 1.55 | -4.14 | -4.04 | -0.09 |
| Fe I | 4009.71 | 72 | 2.21 | -4.52 | -4.35 | -0.93 |
| Fe I | 4045.82 | 43 | 1.48 | -3.80 | -3.76 | 0.66 |
| Fe I | 4062.45 | 359 | 2.83 | -4.55 | -4.34 | -0.45 |
| Fe I | 4063.60 | 43 | 1.55 | -4.02 | -3.99 | +0.44 |
| Fe I | 4071.74 | 43 | 1.60 | -4.10 | -3.99 | 0.37 |
| Fe I | 4143.87 | 43 | 1.55 | -4.22 | -3.98 | -0.42 |
| Fe I | 4168.95 | 694 | 3.40 | -4.98 | -4.40 | -1.23 |
| Fe I | 4175.64 | 354 | 2.83 | -4.53 | -4.21 | -0.41 |
| Fe I | 4181.76 | 354 | 2.82 | -4.37 | -4.21 | -0.05 |
| Fe I | 4187.04 | 152 | 2.44 | -4.46 | -4.30 | -0.33 |
| Fe I | 4199.10 | 522 | 3.03 | -4.42 | -4.20 | 0.34 |
| Fe I | 4199.94 | 3 | 0.09 | -4.93 | -4.44 | -4.21 |
| Fe I | 4202.03 | 42 | 1.48 | -4.26 | -4.23 | -0.25 |
| Fe I | 4206.70 | 3 | 0.05 | -4.52 | -4.18 | -3.42 |
| Fe I | 4216.19 | 3 | 0.00 | -4.52 | -4.24 | -2.98 |
| Fe I | 4227.43 | 693 | 3.32 | -4.32 | -4.18 | 0.51 |
| Fe I | 4258.63 | 351 | 2.82 | -5.06 | -4.53 | -1.76 |
| Fe I | 4260.48 | 152 | 2.39 | -4.22 | -4.14 | 0.13 |
| Fe I | 4264.73 | 993 | 3.94 | -4.97 | -4.46 | -1.06 |
| Fe I | 4265.27 | 993 | 3.94 | -5.02 | -4.57 | -0.80 |
| Fe I | 4271.76 | 42 | 2.44 | -4.18 | -4.11 | -0.25 |
| Fe I | 4276.69 | 976 | 2.69 | -4.59 | -4.25 | -0.88 |
| Fe I | 4325.77 | 942 | 1.60 | -4.04 | -4.02 | 0.36 |
| Fe I | 4327.90 | 597 | 3.27 | -4.97 | -4.46 | -0.48 |
| Fe I | 4383.57 | 41 | 1.48 | -4.07 | -4.02 | 0.51 |
| Fe I | 4404.75 | 41 | 1.55 | -4.11 | -4.03 | 0.25 |
| Fe I | 4415.13 | 41 | 1.60 | -4.20 | -4.10 | -0.13 |
| Fe I | 4415.65 | 41 | 1.60 | -4.22 | -4.11 | -0.13 |
| Fe I | 4531.15 | 39 | 1.48 | -4.14 | -3.86 | -1.57 |
| Fe I | 4871.32 | 318 | 2.85 | -4.36 | -4.05 | -0.39 |
| Fe I | 5307.37 | 36 | 1.60 | -4.96 | -4.48 | -2.76 |
| Fe I | 5364.87 | 1146 | 4.43 | -4.76 | -4.36 | 0.41 |
| Fe I | 5367.47 | 1146 | 4.40 | -4.92 | -4.70 | 0.49 |
| Fe I | 5393.17 | 553 | 3.23 | -4.80 | -4.33 | -0.60 |
| Fe I | 5397.31 | 15 | 0.91 | -5.39 | -4.57 | -1.88 |
| Fe I | 5405.78 | 15 | 0.99 | -4.51 | -4.37 | -1.75 |
| Fe I | 5410.91 | 1165 | 4.45 | -4.84 | -4.33 | 0.54 |
| Fe I | 5429.70 | 15 | 0.95 | -4.49 | -4.25 | -1.78 |
| Fe I | 5445.05 | 1163 | 4.37 | -4.73 | -4.11 | 0.17 |
| Fe I | 5976.72 | 959 | 3.93 | -5.00 | -4.30 | -1.03 |
| Fe I | 6003.08 | 959 | 3.86 | -4.97 | -4.33 | -0.91 |
| Fe I | 6024.11 | 1178 | 4.53 | -4.86 | -4.31 | 0.22 |
| Fe I | 6056.10 | 1259 | 4.71 | -5.08 | -4.32 | -0.12 |

TABLE VII (Concluded)

| Element | λ | RMT | $\chi_{\ell}$ | Log w/λ | Log h/λ | Log gf |
|---|---|---|---|---|---|---|
| Fe I | 6065.53 | 207 | 2.60 | -4.74 | -4.21 | -1.33 |
| Fe I | 6137.81 | 207 | 2.58 | -4.67 | -4.26 | -1.26 |
| Fe I | 6213.40 | 62 | 2.21 | -4.95 | -4.37 | -2.45 |
| Fe I | 6301.54 | 816 | 3.64 | -4.63 | -4.22 | -0.72 |
| Fe I | 6393.61 | 168 | 2.42 | -4.70 | -4.12 | -1.60 |
| Fe I | 6400.03 | 207 | 2.27 | -4.78 | -4.21 | -0.41 |
| Fe I | 6430.84 | 62 | 2.17 | -4.82 | -4.27 | -1.87 |
| Fe I | 6494.99 | 168 | 2.39 | -4.65 | -4.20 | -1.16 |
| Fe II | 4128.74 | 27 | 2.57 | -4.79 | -4.47 | -2.76 |
| Fe II | 4178.86 | 28 | 2.57 | -4.51 | -4.34 | -2.00 |
| Fe II | 4273.32 | 27 | 2.69 | -4.59 | -4.25 | -3.51 |
| Fe II | 4303.17 | 27 | 2.69 | -4.48 | -4.26 | -2.00 |
| Fe II | 4369.40 | 28 | 2.77 | -4.86 | -4.64 | -2.87 |
| Fe II | 4576.33 | 38 | 2.83 | -4.55 | -4.16 | -2.22 |
| Fe II | 4620.51 | 38 | 2.82 | -4.71 | -4.16 | -2.63 |
| Fe II | 5197.57 | 49 | 3.22 | -4.59 | -4.12 | -2.23 |
| Fe II | 5234.62 | 49 | 3.21 | -4.71 | -4.36 | -2.03 |
| Fe II | 5264.81 | 48 | 3.22 | -5.14 | -4.62 | -2.23 |
| Fe II | 5284.09 | 41 | 2.88 | -4.93 | -4.53 | -2.42 |
| Fe II | 5325.56 | 49 | 3.21 | -5.02 | -4.41 | -2.72 |
| Fe II | 5362.86 | 48 | 3.19 | -4.58 | -4.04 | -1.95 |
| Fe II | 5414.09 | 48 | 3.29 | -5.18 | -4.34 | -2.75 |
| Fe II | 5425.27 | 49 | 3.19 | -4.90 | -4.19 | -2.75 |
| Fe II | 6247.56 | 74 | 3.87 | -4.84 | -4.34 | -1.55 |
| Fe II | 6432.65 | 40 | 2.88 | -4.95 | -4.26 | -2.73 |
| Fe II | 6456.38 | 74 | 3.89 | -4.58 | -4.09 | -1.44 |

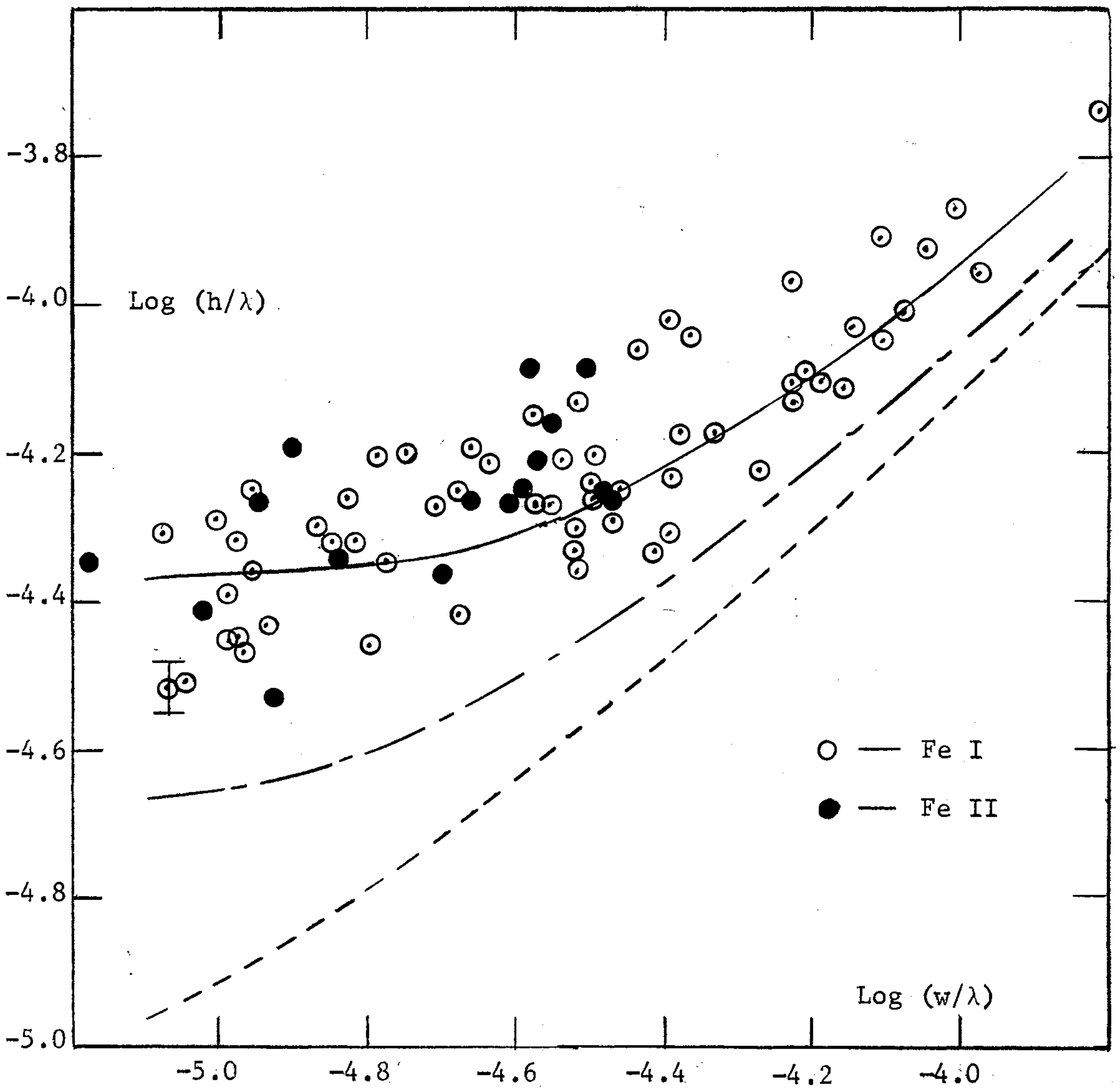


Figure 5. The Observed and Theoretical Correlation Between the Halfwidths and the Equivalent Widths for Fe I and Fe II

observational point which represents a 5% error in the measurement of the halfwidth.

The dashed curve on the lower portion of the diagram in Figure 5 shows the theoretically expected relation between the halfwidth and the equivalent width for a line in Theta Ursae Majoris broadened by thermal motions only. Even with the addition of 3 km/s microturbulence (middle curve), the halfwidth increases with an increase in the equivalent width for the weak lines. The upper curve (solid line) represents a line which has been broadened by a 3 km/s microturbulent velocity coupled with 3.5 km/s macroturbulent velocity. This velocity distribution for the macroturbulence was computed assuming the cells creating the disturbance to have a dispersion relationship for the velocity components (see Chapter II). No stratification effects were assumed. The data could have been fit by increasing the amount of microturbulence in the atmosphere; however, this would not be consistent with the results from the curve of growth analysis. The solid curve represents the best fit to the observations from a set of theoretical curves drawn by allowing the macroturbulence to be varied as a free parameter. The larger value of macroturbulence than microturbulence is also consistent with the results for the solar case reported by Elste (1967).

## The Analysis of the Line Profiles

The effect of microturbulence upon the shape of a stellar line would be to increase its Doppler core. Moving outward from the core, the presence of macroturbulence would most likely be seen as an increase in the halfwidth of the line. As a check on the derived values for the atmospheric turbulence of Theta Ursae Majoris, several profiles of Fe I and Fe II were theoretically calculated and compared with the observed quantities. Figures 6 through 18 show the results of this procedure. Since most of the observed stellar lines of Theta Ursae Majoris show an unusual wing developement--most of the lines are triangular in shape--the damping constants were treated as more or less free parameters to achieve a fit. This procedure is justified because of the rudimentary state of the theory used to treat line broadening from collisions with neutral atoms and Stark broadening of metallic lines. Cowley (1970) even suggests that empirical values determined from stellar sources might be better than the theoretical predictions at this time.

Using the derived atmospheric turbulence model, almost all observed profiles could be matched for distances of about 0.3 to 0.4 Angstroms from the line center. Striking differences between the computed and the observed line cores existed; many times they differed by a factor of about two. It is well known that the central depth (core) is extremely sensitive to the temperature and this could be the effect seen in the line profiles. The observed profiles indicate that the solar-type temperature distribution is not a complete description of the temperature stratification in Theta Ursae Majoris at least near the boundary of the atmosphere. Also, some of the discrepancy might rest in the initial assumption of local thermodynamic equilibrium for the line formation and the abnormally weak line intensities observed in the star. The important point is that even if the theoretical profiles were adjusted by changing the solar temperature distribution near the boundary of the atmosphere, turbulence would still be needed to fit the theoretical profiles with the observed ones.

No fit could be achieved for the line profiles in Figures 13 and

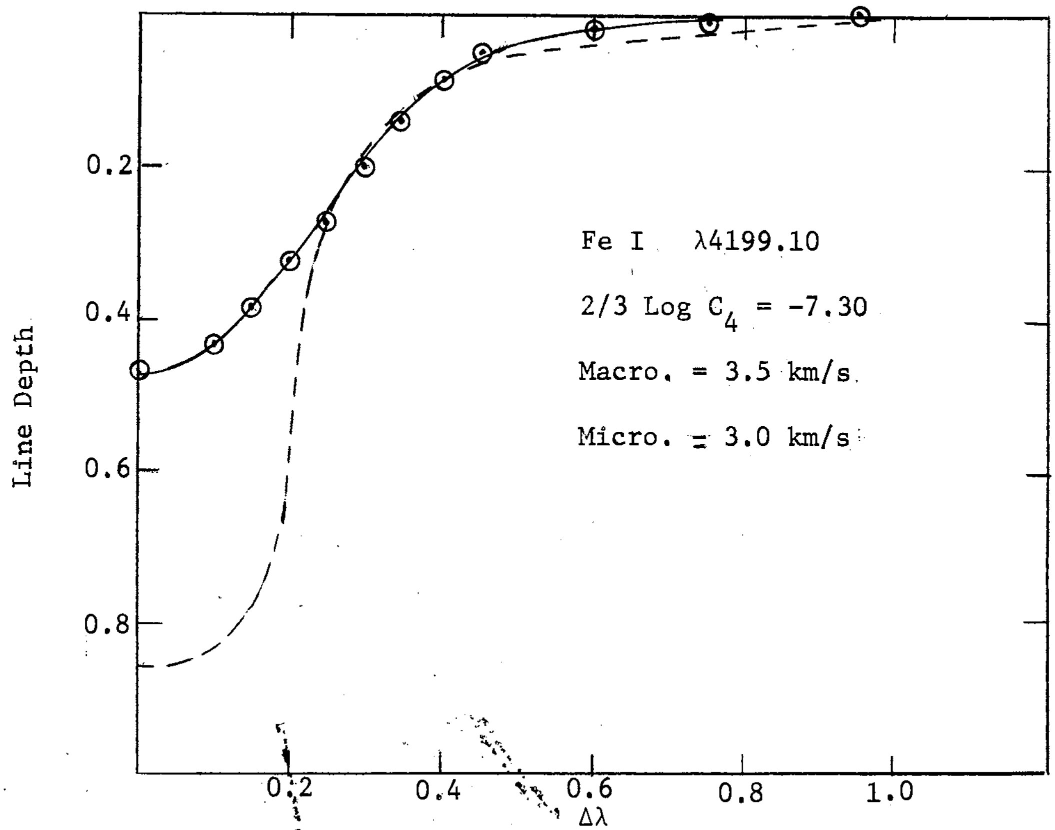


Figure 6. Observed and Calculated Line Profiles for Fe I λ4199.10

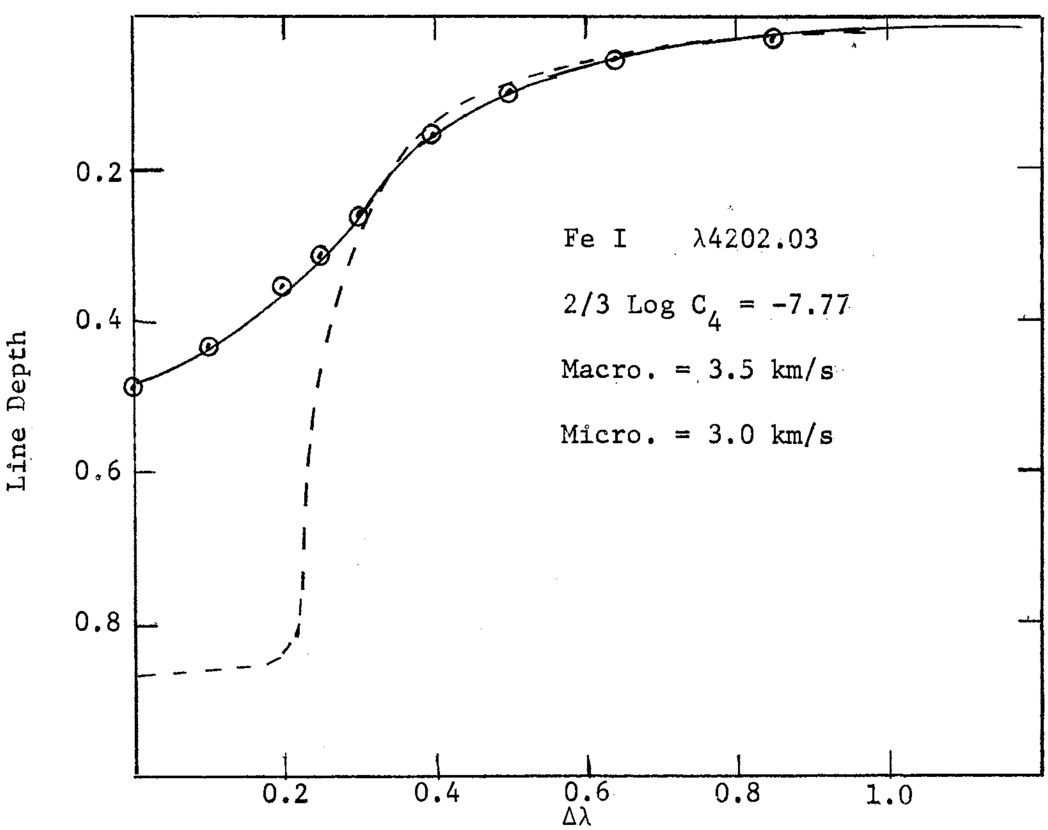


Figure 7. Observed and Calculated Line Profiles for Fe I λ4202.03

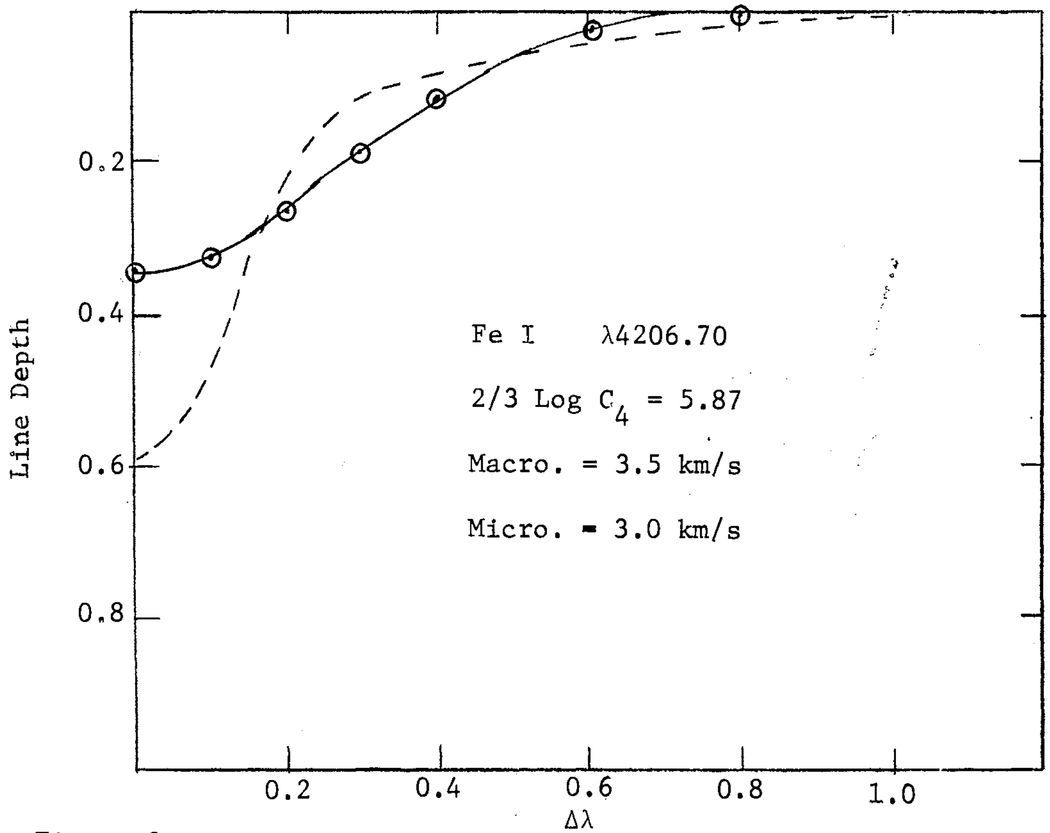


Figure 8. Observed and Calculated Line Profiles for Fe I λ4206.70

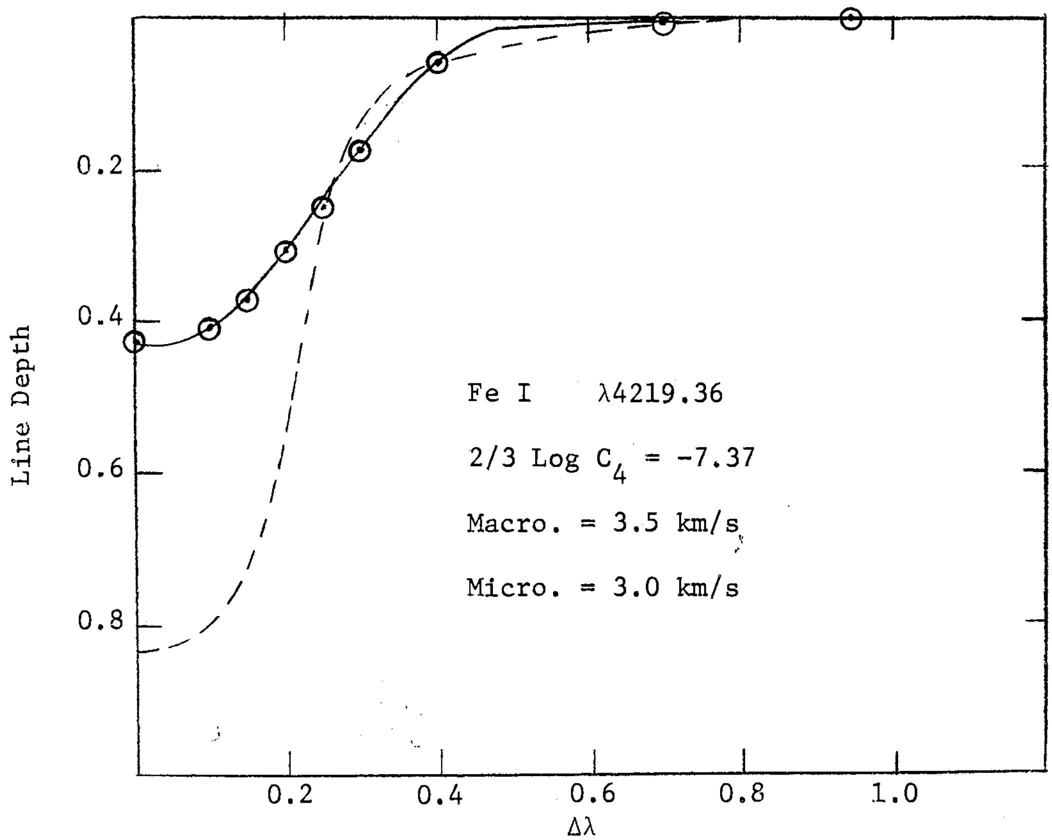


Figure 9. Observed and Calculated Line Profiles for Fe I λ4219.36

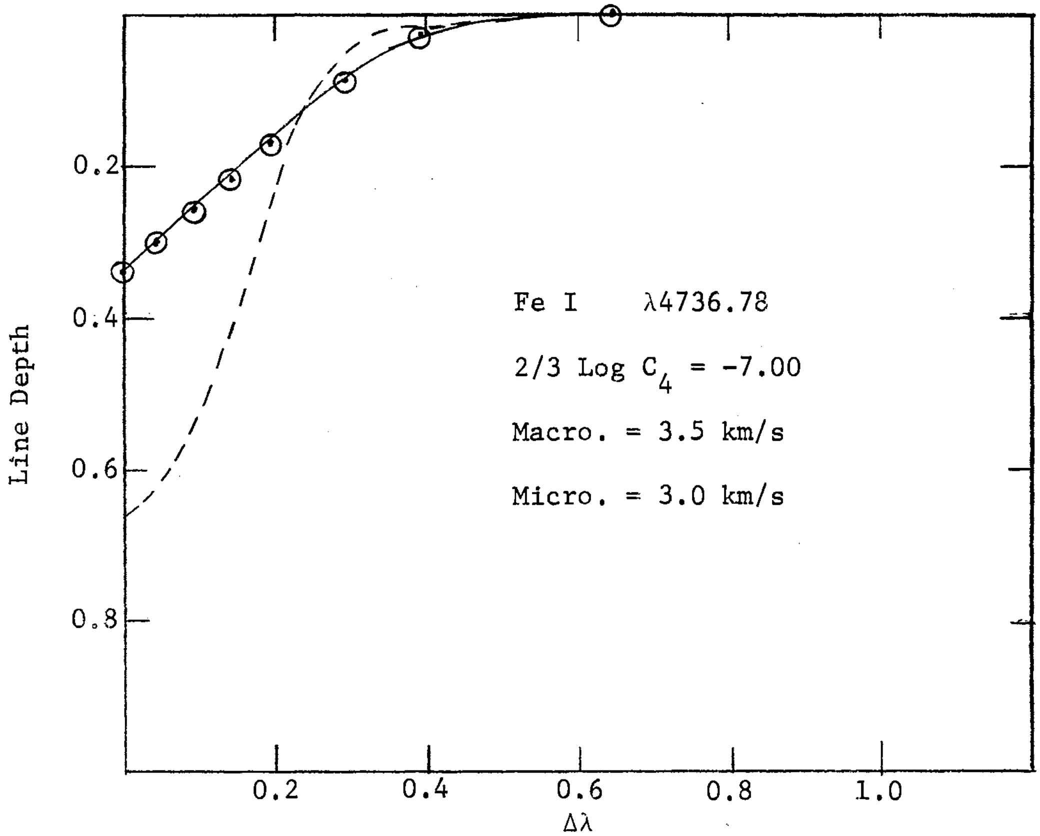


Figure 10. Observed and Calculated Line Profiles for Fe I λ4736.78

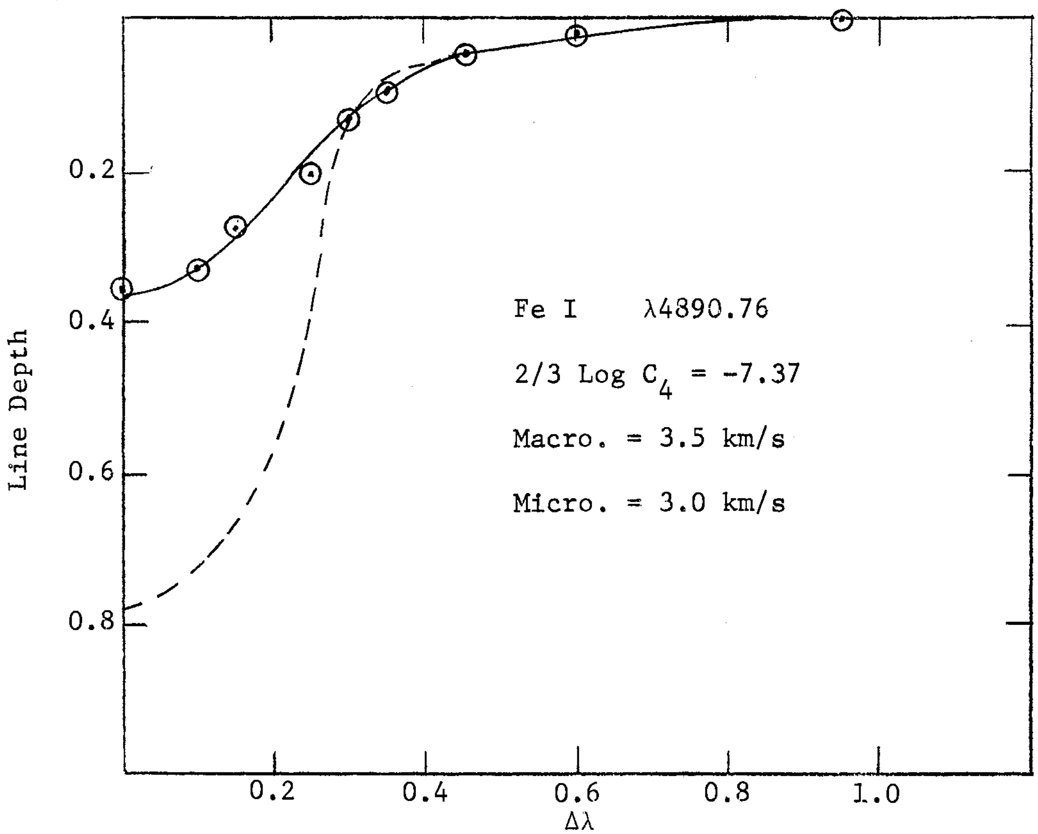


Figure 11. Observed and Calculated Line Profiles for Fe I λ4890.76

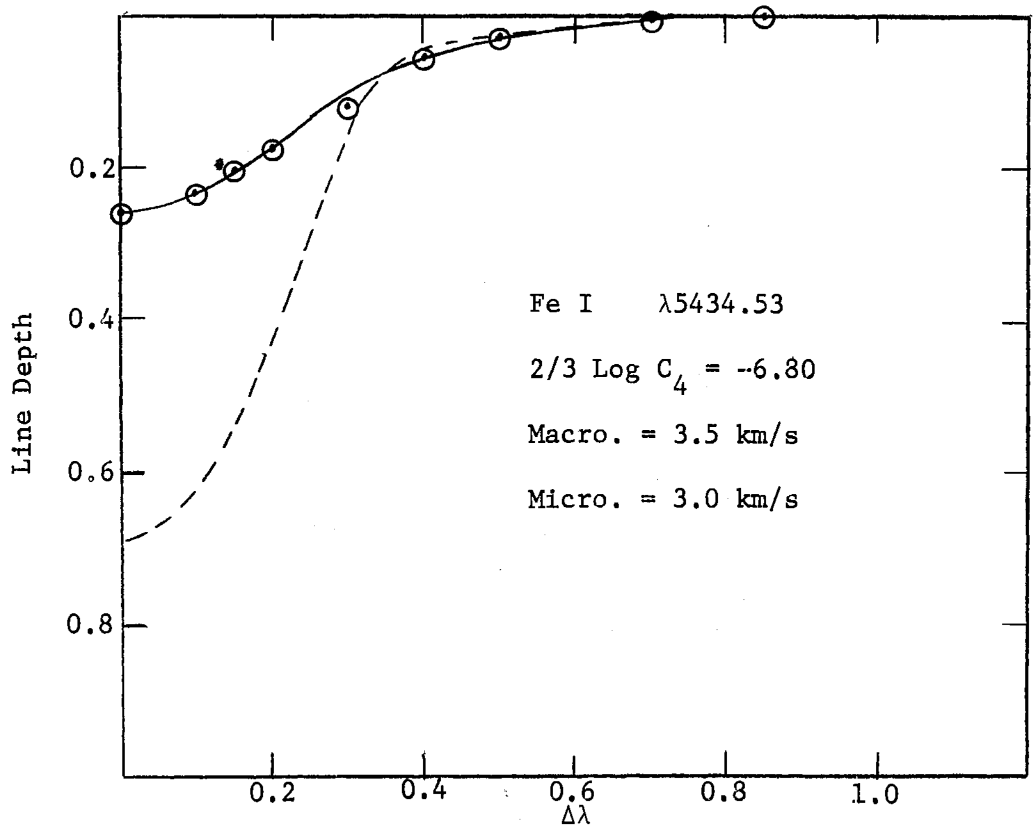


Figure 12. Observed and Calculated Line Profiles for Fe I λ5434.53

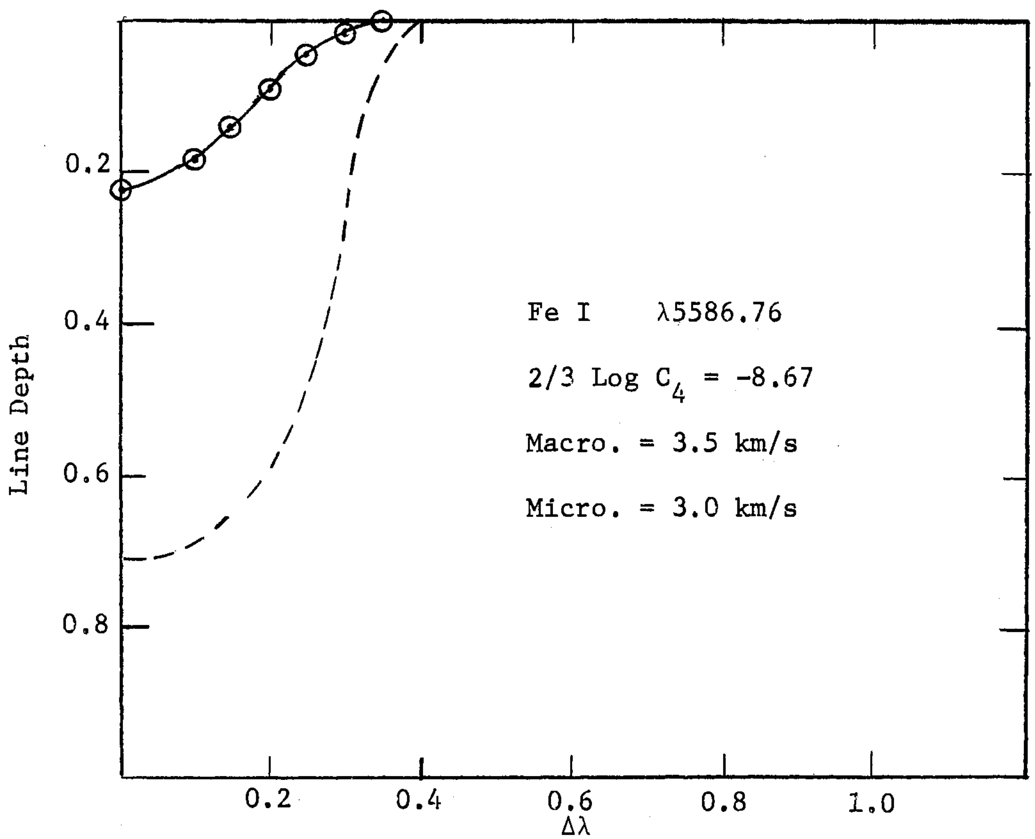


Figure 13. Observed and Calculated Line Profiles for Fe I λ5586.76

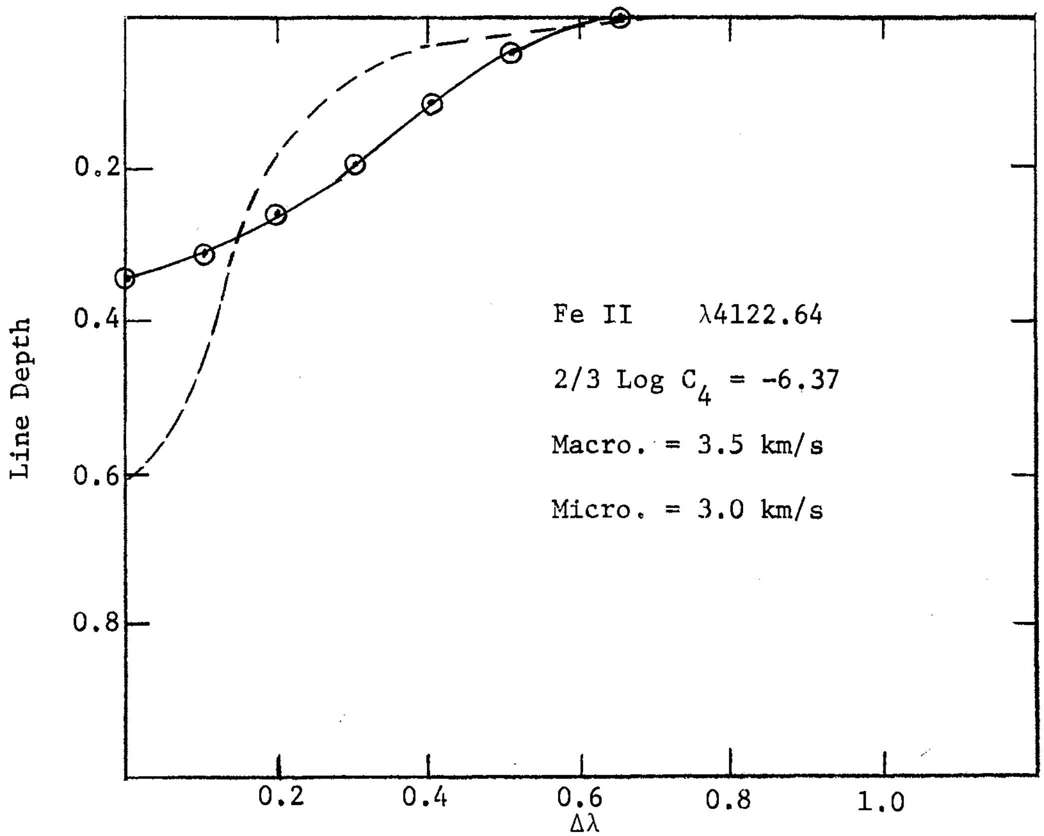


Figure 14. Observed and Calculated Line Profiles for Fe II λ4122.64

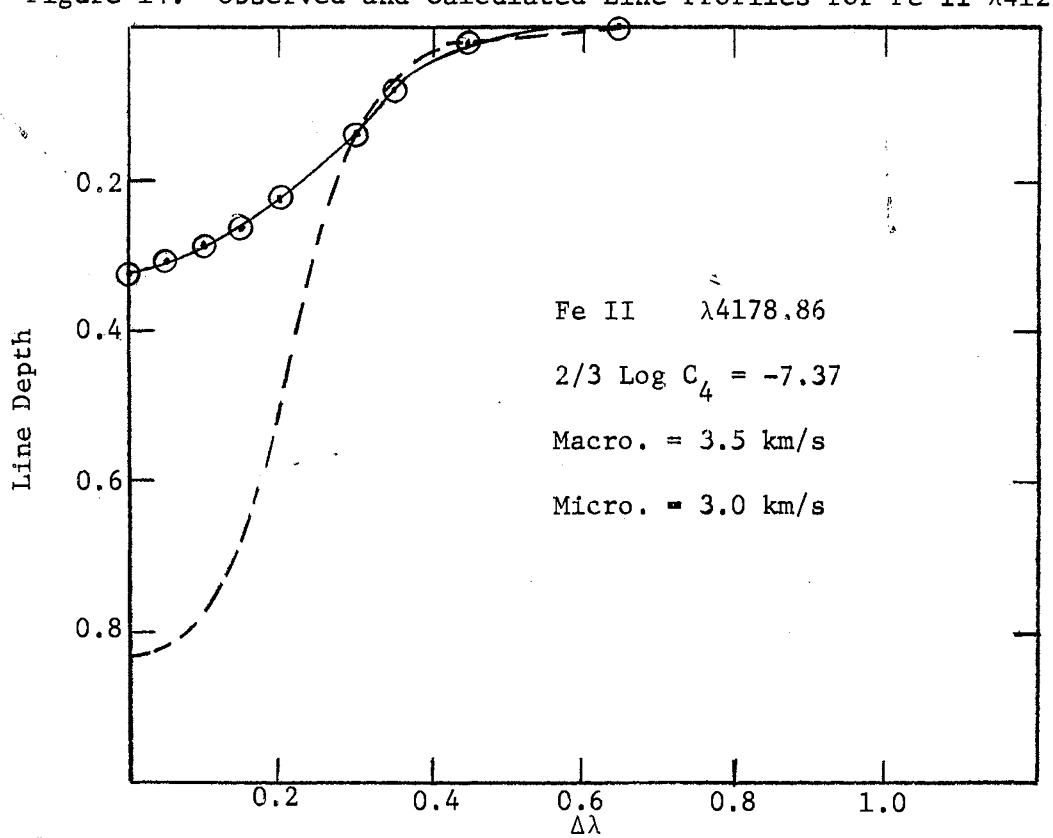


Figure 15. Observed and Calculated Line Profiles for Fe II λ4178.86

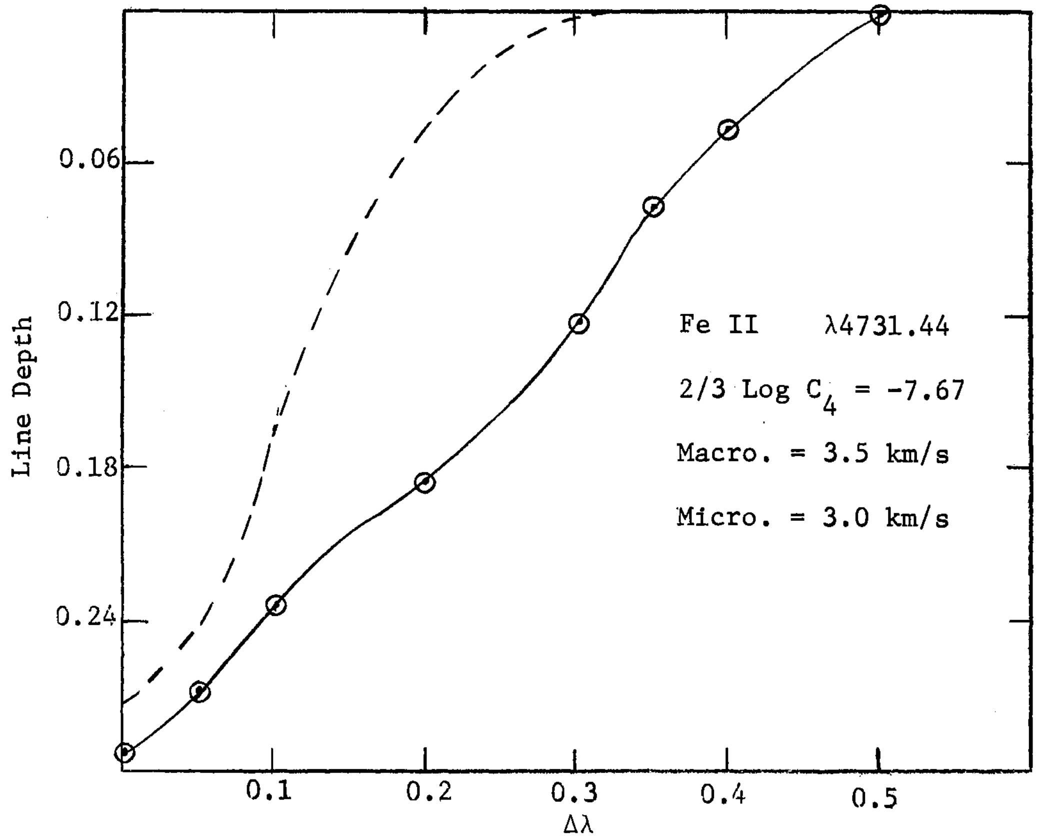


Figure 16. Observed and Calculated Line Profiles for Fe II λ4731.44.

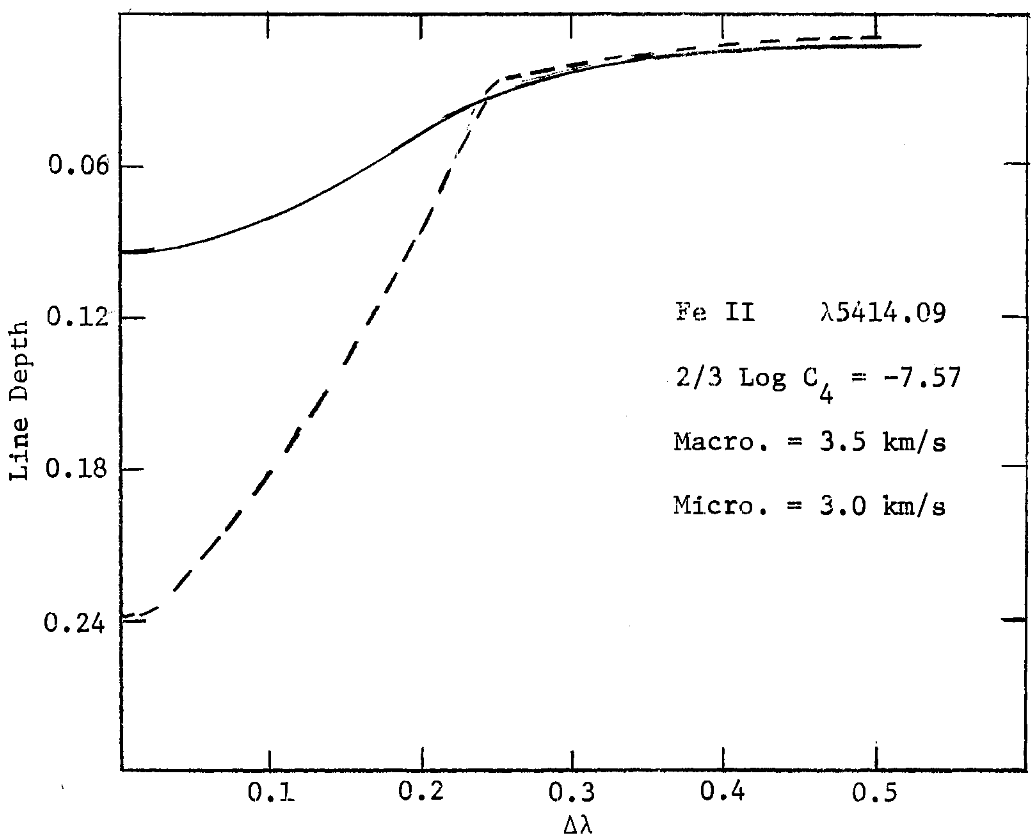


Figure 17. Observed and Calculated Line Profiles for Fe II λ5414.09

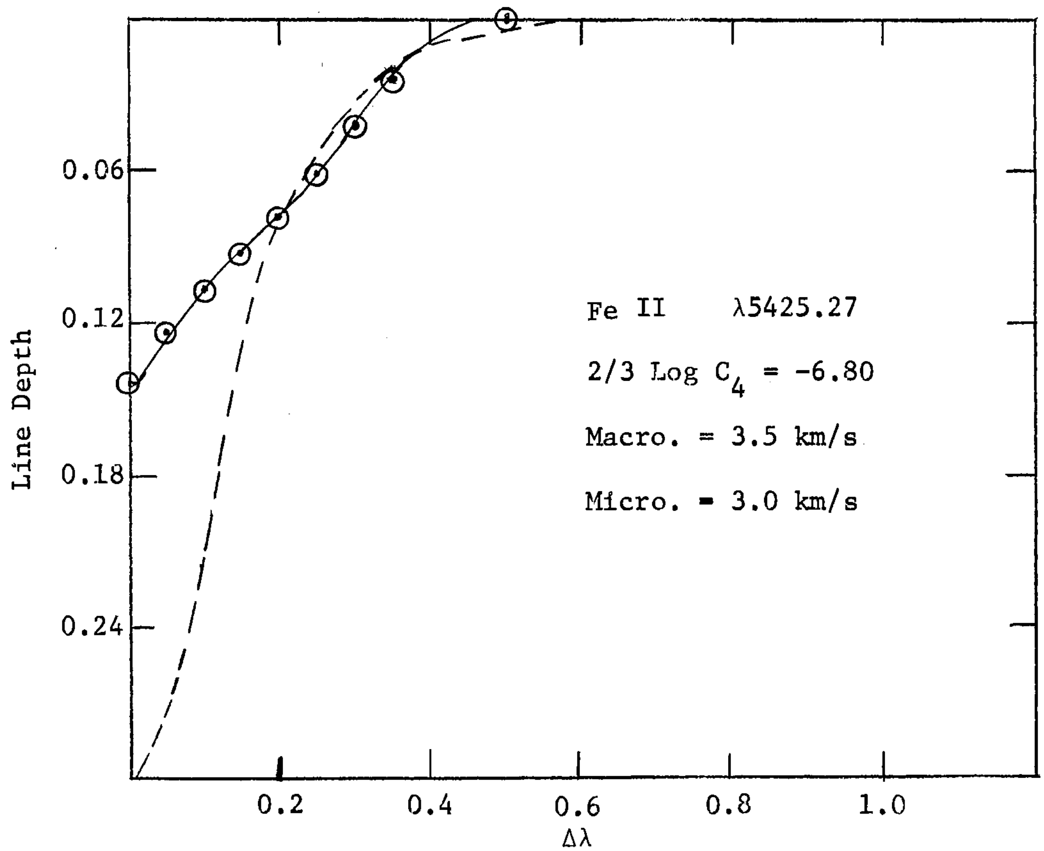


Figure 18. Observed and Calculated Line Profiles for Fe II λ5425.27

TABLE VIII

ABUNDANCE RESULTS FOR Ca I

| Element | RMT | λ | X(R,S) | Log GF | 2/3 Log $C_4$ | Log (H/L) | Log C | Log (W/L) | Wt. | Log N/N(H) |
|---|---|---|---|---|---|---|---|---|---|---|
| Ca I | 2 | 4226.73 | 0.0 | 0.24 | -8.79 | 0.0 | 4.5125 | -4.0200 | 2 | -7.0446 |
| Ca I | 5 | 4283.01 | 1.88 | -0.22 | -8.79 | 0.0 | 2.3541 | -4.5600 | 2 | -6.2999 |
| Ca I | 5 | 4289.36 | 1.87 | -0.30 | -8.79 | 0.0 | 2.2846 | -4.5800 | 2 | -6.2861 |
| Ca I | 5 | 4298.99 | 1.88 | -0.41 | -8.79 | 0.0 | 2.1677 | -4.5000 | 2 | -5.9419 |
| Ca I | 4 | 4425.44 | 1.88 | -0.38 | -8.79 | 0.0 | 2.2073 | -4.5200 | 2 | -6.0390 |
| Ca I | 4 | 4434.96 | 1.89 | -0.03 | -8.79 | 0.0 | 2.5553 | -4.4200 | 2 | -6.1144 |
| Ca I | 4 | 4435.69 | 1.89 | -0.50 | -8.79 | 0.0 | 2.0844 | -4.5200 | 2 | -5.9161 |
| Ca I | 36 | 4526.94 | 2.70 | -0.43 | -8.53 | 0.0 | 1.4495 | -4.7800 | 1 | -5.8849 |
| Ca I | 23 | 4578.56 | 2.51 | -0.56 | -8.53 | 0.0 | 1.4904 | -4.7600 | 1 | -5.8887 |
| Ca I | 22 | 5262.24 | 2.52 | -0.60 | -8.53 | 0.0 | 1.5021 | -4.6400 | 1 | -5.6515 |
| Ca I | 48 | 5512.98 | 2.93 | -0.29 | -7.52 | 0.0 | 1.4741 | -4.7100 | 1 | -5.7747 |
| Ca I | 21 | 5581.97 | 2.52 | -0.71 | -8.53 | 0.0 | 1.4177 | -4.8500 | 1 | -5.9752 |
| Ca I | 21 | 5588.76 | 2.52 | 0.21 | -8.53 | 0.0 | 2.3382 | -4.5000 | 1 | -6.1124 |
| Ca I | 21 | 5590.12 | 2.52 | -0.71 | -8.53 | 0.0 | 1.4183 | -4.9300 | 1 | -6.1059 |
| Ca I | 21 | 5601.29 | 2.52 | -0.69 | -8.53 | 0.0 | 1.4392 | -4.6600 | 1 | -5.6338 |
| Ca I | 23 | 6102.72 | 1.87 | -0.89 | -8.79 | 0.0 | 1.8508 | -4.7000 | 1 | -6.1309 |
| Ca I | 23 | 6122.22 | 1.88 | -0.41 | -8.79 | 0.0 | 2.3243 | -4.5500 | 1 | -6.2418 |
| Ca I | 20 | 6166.44 | 2.51 | -0.90 | -8.53 | 0.0 | 1.2797 | -5.2300 | 1 | -6.3909 |
| Ca I | 23 | 6162.17 | 1.89 | -0.22 | -8.79 | 0.0 | 2.5092 | -4.5300 | 1 | -6.3696 |
| Ca I | 18 | 6439.07 | 2.51 | 0.47 | -8.53 | 0.0 | 2.6685 | -4.5500 | 1 | -6.5860 |
| Ca I | 18 | 6493.78 | 2.51 | 0.14 | -8.53 | 0.0 | 2.3422 | -4.7300 | 1 | -6.6827 |

TABLE IX

ABUNDANCE RESULTS FOR Co I

| Element | RMT | $\lambda$ | X(R,S) | Log GF | 2/3 Log $C_4$ | Log (H/L) | Log C | Log (W/L) | Wt. | Log N/N(H) |
|---|---|---|---|---|---|---|---|---|---|---|
| Co I | 16 | 4020.90 | 0.43 | -2.16 | -8.87 | 0.0 | 2.2304 | -5.1400 | 3 | -7.2402 |
| Co I | 29 | 4092.39 | 0.92 | -1.36 | -8.87 | 0.0 | 2.5850 | -4.5600 | 2 | -6.4006 |
| Co I | 29 | 4110.53 | 1.04 | -1.42 | -8.87 | 0.0 | 2.4164 | -5.0400 | 2 | -7.2940 |
| Co I | 28 | 4121.32 | 0.92 | -0.65 | -8.87 | 0.0 | 3.2981 | -4.6600 | 3 | -7.4577 |
| Co I | 150 | 4517.09 | 3.11 | -0.90 | -8.67 | 0.0 | 1.1069 | -5.2900 | 1 | -6.3037 |
| Co I | 156 | 4693.19 | 3.22 | -0.51 | -8.67 | 0.0 | 1.4162 | -5.4800 | 1 | -6.8329 |
| Co I | 15 | 4727.94 | 0.43 | -3.70 | -8.87 | 0.0 | 0.7608 | -5.5400 | 1 | -6.2443 |
| Co I | 180 | 5156.37 | 4.04 | -0.13 | -8.57 | 0.0 | 1.1173 | -5.0100 | 2 | -5.9529 |
| Co I | 170 | 5212.70 | 3.50 | -0.12 | -8.67 | 0.0 | 1.6043 | -5.5400 | 1 | -7.0877 |
| Co I | 190 | 5342.70 | 4.00 | 0.33 | -8.57 | 0.0 | 1.6274 | -5.7700 | 1 | -7.3599 |
| Co I | 190 | 5343.38 | 4.01 | 0.03 | -8.57 | 0.0 | 1.3188 | -5.3400 | 1 | -6.5747 |
| Co I | 39 | 5369.59 | 1.73 | -1.87 | -8.72 | 0.0 | 1.4517 | -5.5100 | 1 | -6.9020 |

TABLE X

ABUNDANCE RESULTS FOR Cr I

| Element | RMT | λ | X(R,S) | Log GF | 2/3 Log $C_4$ | Log (H/L) | Log C | Log (W/L) | Wt. | Log N/N(H) |
|---|---|---|---|---|---|---|---|---|---|---|
| Cr I | 22 | 4373.25 | 0.98 | -1.99 | -8.77 | 0.0 | 1.5521 | -5.6600 | 1 | -7.1707 |
| Cr I | 64 | 4381.11 | 2.70 | -0.56 | -8.57 | 0.0 | 1.4480 | -5.9300 | 1 | -7.3514 |
| Cr I | 22 | 4384.98 | 1.03 | -1.08 | -8.77 | 0.0 | 2.4180 | -4.9800 | 4 | -7.2242 |
| Cr I | 103 | 4387.50 | 2.99 | -0.22 | -8.57 | 0.0 | 1.5343 | -5.0800 | 3 | -6.4761 |
| Cr I | 129 | 4410.30 | 3.00 | -0.60 | -8.57 | 0.0 | 1.1478 | -5.7900 | 1 | -6.9047 |
| Cr I | 22 | 4412.25 | 1.03 | -2.26 | -8.77 | 0.0 | 1.2406 | -5.5700 | 1 | -6.7618 |
| Cr I | 127 | 4458.54 | 3.00 | 0.04 | -8.57 | 0.0 | 1.7925 | -5.1000 | 3 | -6.7602 |
| Cr I | 150 | 4511.90 | 3.07 | 0.04 | -8.57 | 0.0 | 1.7369 | -5.0900 | 3 | -6.6916 |
| Cr I | 33 | 4535.15 | 2.53 | -0.64 | -8.67 | 0.0 | 1.5321 | -5.5000 | 1 | -6.9763 |
| Cr I | 10 | 4545.96 | 0.94 | -1.15 | -8.77 | 0.0 | 2.4453 | -4.7300 | 4 | -6.8131 |
| Cr I | 21 | 4591.39 | 0.96 | -1.36 | -8.77 | 0.0 | 2.2214 | -4.9000 | 4 | -6.9059 |
| Cr I | 21 | 4600.75 | 1.00 | -1.20 | -8.77 | 0.0 | 2.3459 | -4.7300 | 4 | -6.7137 |
| Cr I | 21 | 4616.14 | 0.98 | -1.13 | -8.77 | 0.0 | 2.4355 | -4.8200 | 4 | -6.9868 |
| Cr I | 21 | 4626.19 | 0.96 | -1.18 | -8.77 | 0.0 | 2.4047 | -4.8500 | 4 | -7.0081 |
| Cr I | 186 | 4639.54 | 3.10 | -0.27 | -8.57 | 0.0 | 1.4130 | -5.1200 | 1 | -6.4068 |
| Cr I | 21 | 4646.17 | 1.03 | -0.67 | -8.77 | 0.0 | 2.8531 | -4.5500 | 3 | -6.6586 |
| Cr I | 32 | 4649.46 | 2.53 | -0.90 | -8.67 | 0.0 | 1.2829 | -5.4900 | 1 | -6.7160 |
| Cr I | 21 | 4651.29 | 0.98 | -1.15 | -8.77 | 0.0 | 2.4188 | -4.8800 | 4 | -7.0710 |
| Cr I | 21 | 4652.16 | 1.00 | -0.97 | -8.77 | 0.0 | 2.5807 | -4.7900 | 4 | -7.0758 |
| Cr I | 186 | 4708.04 | 3.15 | 0.37 | -8.57 | 0.0 | 2.0160 | -5.0800 | 3 | -6.9578 |
| Cr I | 186 | 4718.43 | 3.18 | 0.49 | -8.57 | 0.0 | 2.1109 | -4.9300 | 4 | -6.8427 |
| Cr I | 145 | 4724.42 | 3.07 | -0.28 | -8.57 | 0.0 | 1.4369 | -5.5800 | 1 | -6.9689 |
| Cr I | 145 | 4730.71 | 3.07 | 0.09 | -8.57 | 0.0 | 1.8075 | -5.2100 | 2 | -6.9150 |
| Cr I | 61 | 4745.31 | 2.70 | -1.07 | -8.57 | 0.0 | 0.9727 | -5.6600 | 1 | -6.5913 |
| Cr I | 145 | 4756.11 | 3.09 | 0.54 | -8.57 | 0.0 | 2.2424 | -4.9400 | 4 | -6.9896 |
| Cr I | 231 | 4764.29 | 3.54 | 0.05 | -8.52 | 0.0 | 1.3630 | -5.3000 | 1 | -6.5786 |
| Cr I | 144 | 4836.86 | 3.09 | -0.83 | -8.57 | 0.0 | 0.8798 | -5.5600 | 1 | -6.3900 |
| Cr I | 143 | 4922.27 | 3.09 | 0.41 | -8.57 | 0.0 | 2.1274 | -4.5000 | 2 | -5.7018 |

TABLE X (Continued)

| Element | RMT | λ | X(R,S) | Log GF | 2/3 Log $C_4$ | Log (H/L) | Log C | Log (W/L) | Wt. | Log N/N(H) |
|---|---|---|---|---|---|---|---|---|---|---|
| Cr I | 166 | 4936.33 | 3.10 | 0.03 | -8.57 | 0.0 | 1.7399 | -5.0800 | 2 | -6.6817 |
| Cr I | 166 | 4954.81 | 3.11 | 0.03 | -8.57 | 0.0 | 1.7329 | -4.9200 | 3 | -6.4492 |
| Cr I | 9 | 4964.93 | 0.94 | -2.48 | -8.77 | 0.0 | 1.1536 | -5.2200 | 1 | -6.2734 |
| Cr I | 60 | 5110.75 | 2.70 | -0.93 | -8.57 | 0.0 | 1.1449 | -5.6600 | 1 | -6.7635 |
| Cr I | 7 | 5206.04 | 0.94 | -0.17 | -8.77 | 0.0 | 3.4842 | -4.5000 | 3 | -7.0586 |
| Cr I | 59 | 5238.97 | 2.70 | -1.05 | -8.57 | 0.0 | 1.0357 | -5.4300 | 1 | -6.4014 |
| Cr I | 201 | 5243.40 | 3.38 | -0.31 | -8.52 | 0.0 | 1.1831 | -5.2800 | 3 | -6.3751 |
| Cr I | 18 | 5247.56 | 0.96 | -1.62 | -8.77 | 0.0 | 2.0194 | -4.9800 | 4 | -6.8257 |
| Cr I | 18 | 5296.69 | 0.98 | -1.54 | -8.77 | 0.0 | 2.0853 | -4.8400 | 4 | -6.6717 |
| Cr I | 94 | 5297.36 | 2.89 | -0.40 | -8.57 | 0.0 | 1.5238 | -4.8100 | 4 | -6.0569 |
| Cr I | 18 | 5298.27 | 0.98 | -1.25 | -8.77 | 0.0 | 2.3754 | -4.5600 | 3 | -6.2223 |
| Cr I | 94 | 5329.12 | 2.90 | -0.39 | -8.57 | 0.0 | 1.5277 | -4.9700 | 4 | -6.3194 |
| Cr I | 18 | 5345.81 | 1.00 | -1.16 | -8.77 | 0.0 | 2.4511 | -4.8000 | 4 | -6.9654 |
| Cr I | 18 | 5348.32 | 1.00 | -1.47 | -8.77 | 0.0 | 2.1413 | -4.9900 | 4 | -6.9618 |
| Cr I | 191 | 5390.39 | 3.35 | -0.86 | -8.52 | 0.0 | 0.6711 | -5.3100 | 3 | -5.8985 |
| Cr I | 18 | 5409.79 | 1.03 | -0.88 | -8.77 | 0.0 | 2.7092 | -4.6600 | 4 | -6.8996 |
| Cr I | 119 | 5712.78 | 3.00 | -0.87 | -8.57 | 0.0 | 0.9902 | -5.7900 | 1 | -6.7471 |
| Cr I | 268 | 4001.44 | 3.87 | 1.07 | -8.47 | 0.0 | 2.0239 | -5.0400 | 2 | -6.9132 |
| Cr I | 268 | 4022.26 | 3.87 | 0.81 | -8.47 | 0.0 | 1.7661 | -5.4200 | 1 | -7.1205 |
| Cr I | 251 | 4039.10 | 3.83 | 1.15 | -8.47 | 0.0 | 2.1423 | -5.1500 | 2 | -7.1747 |
| Cr I | 279 | 4065.72 | 4.09 | -0.34 | -8.47 | 0.0 | 0.4328 | -5.8500 | 1 | -6.2527 |
| Cr I | 65 | 4120.61 | 2.70 | 0.09 | -8.57 | 0.0 | 2.0714 | -5.4000 | 1 | -7.4030 |
| Cr I | 35 | 4126.52 | 2.53 | -0.16 | -8.67 | 0.0 | 1.9711 | -5.4300 | 1 | -7.3368 |
| Cr I | 249 | 4197.23 | 3.83 | 0.27 | -8.47 | 0.0 | 1.2790 | -5.5800 | 1 | -6.8110 |
| Cr I | 249 | 4208.36 | 3.83 | 0.21 | -8.47 | 0.0 | 1.2201 | -6.0300 | 1 | -7.2272 |
| Cr I | 248 | 4209.37 | 3.83 | 0.68 | -8.47 | 0.0 | 1.6902 | -5.4500 | 1 | -7.0785 |
| Cr I | 137 | 4211.35 | 3.00 | -0.31 | -8.57 | 0.0 | 1.4177 | -5.6000 | 1 | -6.9715 |
| Cr I | 1 | 4254.35 | 0.0 | -0.45 | -8.87 | 0.0 | 3.9755 | -4.3700 | 3 | -6.8228 |
| Cr I | 96 | 4272.91 | 2.89 | -0.42 | -8.57 | 0.0 | 1.4105 | -5.4200 | 1 | -6.7649 |
| Cr I | 1 | 4274.80 | 0.0 | -0.57 | -8.87 | 0.0 | 3.8576 | -4.4000 | 3 | -6.8991 |

TABLE X (Concluded)

| Element | RMT | λ | X(R,S) | Log GF | 2/3 Log $C_4$ | Log (H/L) | Log C | Log (W/L) | Wt. | Log N/N(H) |
|---|---|---|---|---|---|---|---|---|---|---|
| Cr I | 1 | 4289.72 | 0.0 | -0.76 | -8.87 | 0.0 | 3.6691 | -4.2900 | 3 | -6.1032 |
| Cr I | 22 | 4337.57 | 0.96 | -0.96 | -8.77 | 0.0 | 2.5967 | -4.6700 | 4 | -6.8151 |
| Cr I | 22 | 4339.45 | 0.98 | -0.78 | -8.77 | 0.0 | 2.7587 | -4.9000 | 4 | -7.4432 |
| Cr I | 22 | 4339.72 | 0.96 | -1.27 | -8.77 | 0.0 | 2.2869 | -5.2300 | 3 | -7.4189 |
| Cr I | 22 | 4344.51 | 1.00 | -0.53 | -8.77 | 0.0 | 2.9910 | -4.6500 | 3 | -7.1525 |
| Cr I | 104 | 4346.83 | 2.97 | -0.13 | -8.57 | 0.0 | 1.6378 | -5.1800 | 3 | -6.7081 |
| Cr I | 22 | 4351.05 | 0.96 | -1.27 | -8.77 | 0.0 | 2.2881 | -4.9600 | 3 | -7.0652 |

TABLE XI

ABUNDANCE RESULTS FOR Cr II

| Element | RMT | λ | X(R,S) | Log GF | 2/3 Log $C_4$ | Log (H/L) | Log C | Log (W/L) | Wt. | Log N/N(H) |
|---|---|---|---|---|---|---|---|---|---|---|
| Cr II | 31 | 4242.38 | 3.85 | -1.02 | -8.52 | 0.0 | 2.4891 | -4.5500 | 3 | -6.2613 |
| Cr II | 31 | 4252.62 | 3.84 | -1.85 | -8.52 | 0.0 | 1.6687 | -5.0000 | 3 | -6.4836 |
| Cr II | 31 | 4261.92 | 3.85 | -1.21 | -8.52 | 0.0 | 2.3011 | -4.7600 | 3 | -6.6679 |
| Cr II | 31 | 4275.57 | 3.84 | -1.33 | -8.52 | 0.0 | 2.1911 | -4.6400 | 3 | -6.2575 |
| Cr II | 44 | 4555.02 | 4.05 | -1.44 | -8.47 | 0.0 | 1.9288 | -4.6700 | 3 | -6.0759 |
| Cr II | 44 | 4558.66 | 4.06 | -0.31 | -8.47 | 0.0 | 3.0506 | -4.5000 | 3 | -6.6246 |
| Cr II | 44 | 4588.22 | 4.05 | -0.65 | -8.47 | 0.0 | 2.7219 | -4.6100 | 4 | -6.7006 |
| Cr II | 44 | 4592.09 | 4.06 | -1.37 | -8.47 | 0.0 | 1.9938 | -4.8800 | 3 | -6.6066 |
| Cr II | 44 | 4616.64 | 4.05 | -1.51 | -8.47 | 0.0 | 1.8646 | -4.9800 | 3 | -6.6493 |
| Cr II | 44 | 4634.11 | 4.05 | -1.19 | -8.47 | 0.0 | 2.1862 | -4.7500 | 3 | -6.5304 |
| Cr II | 30 | 4812.35 | 3.85 | -1.99 | -8.52 | 0.0 | 1.5738 | -4.9600 | 4 | -6.3266 |
| Cr II | 30 | 4848.24 | 3.85 | -1.13 | -8.52 | 0.0 | 2.4371 | -4.6700 | 4 | -6.5842 |
| Cr II | 30 | 4876.41 | 3.85 | -1.56 | -8.52 | 0.0 | 2.0096 | -4.6000 | 4 | -5.9572 |

TABLE XII

ABUNDANCE RESULTS FOR Fe I

| Element | RMT | λ | X(R,S) | Log GF | 2/3 Log $C_4$ | Log (H/L) | Log C | Log (W/L) | Wt. | Log N/N(H) |
|---|---|---|---|---|---|---|---|---|---|---|
| Fe I | 43 | 4005.24 | 1.55 | -0.09 | -8.72 | -4.0400 | 3.1717 | -4.1400 | 3 | -5.0724 |
| Fe I | 72 | 4009.72 | 2.21 | -0.93 | -8.78 | -4.3500 | 1.7377 | -4.5200 | 3 | -5.4726 |
| Fe I | 276 | 4040.09 | 2.72 | -2.11 | -8.67 | 0.0 | 0.1065 | -5.0000 | 3 | -4.9537 |
| Fe I | 43 | 4045.82 | 1.48 | 0.66 | -8.72 | -3.7600 | 0.0 | -3.8000 | 0 | 0.0 |
| Fe I | 359 | 4062.45 | 2.83 | -0.45 | -8.67 | -4.3400 | 1.6714 | -4.5500 | 3 | -5.5382 |
| Fe I | 43 | 4063.60 | 1.55 | 0.44 | -8.72 | -4.0000 | 3.7080 | -4.0200 | 3 | -5.2748 |
| Fe I | 43 | 4071.74 | 1.60 | 0.37 | -8.72 | -4.0000 | 3.5937 | -4.1000 | 3 | -5.3769 |
| Fe I | 558 | 4080.22 | 3.27 | -0.81 | -8.67 | 0.0 | 0.9259 | -4.8200 | 3 | -5.5024 |
| Fe I | 276 | 4107.49 | 2.82 | -0.32 | -8.67 | -4.1400 | 1.8151 | -4.6800 | 2 | -6.1049 |
| Fe I | 357 | 4134.68 | 2.82 | -0.32 | -8.78 | -4.2000 | 1.8180 | -4.5300 | 2 | -5.5982 |
| Fe I | 43 | 4143.87 | 1.55 | -0.42 | -8.72 | -3.9800 | 2.8565 | -4.2200 | 2 | -5.0382 |
| Fe I | 42 | 4147.67 | 1.48 | -1.50 | -8.72 | -4.1900 | 1.8402 | -4.6000 | 2 | -5.8952 |
| Fe I | 355 | 4154.50 | 2.82 | -0.36 | -8.62 | -4.1700 | 1.7800 | -4.5300 | 2 | -5.5602 |
| Fe I | 694 | 4168.95 | 3.40 | -1.23 | -8.67 | -4.4000 | 0.4012 | -4.9800 | 3 | -5.2204 |
| Fe I | 354 | 4175.64 | 2.83 | -0.41 | -8.67 | -4.2100 | 1.7234 | -4.5300 | 3 | -5.5036 |
| Fe I | 354 | 4181.76 | 2.82 | -0.05 | -8.67 | -4.2100 | 2.0929 | -4.3700 | 3 | -5.0572 |
| Fe I | 152 | 4187.04 | 2.44 | -0.33 | -8.67 | -4.3000 | 2.1507 | -4.4600 | 3 | -5.5846 |
| Fe I | 152 | 4191.44 | 2.46 | -0.44 | -8.67 | -4.1700 | 2.0232 | -4.4500 | 2 | -5.4039 |
| Fe I | 522 | 4199.10 | 3.03 | 0.34 | -8.67 | -4.2000 | 2.2989 | -4.4200 | 3 | -5.5263 |
| Fe I | 3 | 4199.94 | 0.09 | -4.21 | -8.87 | -4.4400 | 0.4120 | -4.9300 | 2 | -5.1620 |
| Fe I | 42 | 4202.03 | 1.48 | -0.25 | -8.72 | -4.2300 | 3.0959 | -4.2600 | 3 | -5.4512 |
| Fe I | 3 | 4206.70 | 0.05 | -3.42 | -8.87 | -4.1800 | 1.2397 | -4.5200 | 3 | -4.9746 |
| Fe I | 3 | 4216.19 | 0.0 | -2.98 | -8.87 | -4.2400 | 1.7270 | -4.5200 | 3 | -5.4619 |
| Fe I | 800 | 4219.36 | 3.56 | 0.51 | -8.67 | -4.1600 | 2.0067 | -4.4800 | 3 | -5.5460 |
| Fe I | 152 | 4222.22 | 2.44 | -0.85 | -8.67 | -4.1700 | 1.6343 | -4.5500 | 3 | -5.5011 |
| Fe I | 693 | 4227.43 | 3.32 | 0.51 | -8.67 | -4.1800 | 2.2175 | -4.3200 | 3 | -4.8771 |
| Fe I | 152 | 4233.61 | 2.48 | -0.41 | -8.67 | -4.1400 | 2.0397 | -4.4300 | 3 | -5.3163 |
| Fe I | 693 | 4238.82 | 3.38 | 0.10 | -8.67 | -4.1400 | 1.7560 | -4.4800 | 3 | -5.2953 |

TABLE XII (Continued)

| Element | RMT | λ | X(R,S) | Log GF | 2/3 Log $C_4$ | Log (H/L) | Log C | Log (W/L) | Wt. | Log N/N(H) |
|---|---|---|---|---|---|---|---|---|---|---|
| Fe I | 693 | 4247.43 | 3.37 | 0.07 | -8.67 | -4.1300 | 1.7357 | -4.4400 | 3 | -5.0630 |
| Fe I | 2 | 4240.23 | 3.06 | -1.01 | -8.67 | -4.2000 | 0.9276 | -4.6600 | 3 | -5.1650 |
| Fe I | 351 | 4258.62 | 2.82 | -1.76 | -8.67 | -4.5300 | 0.3908 | -5.0600 | 3 | -5.3188 |
| Fe I | 152 | 4260.48 | 2.40 | 0.13 | -8.67 | -4.1400 | 2.6540 | -4.2200 | 2 | -4.8358 |
| Fe I | 993 | 4264.74 | 3.94 | -1.06 | -8.57 | -4.4600 | 0.1118 | -4.9700 | 2 | -4.9172 |
| Fe I | 993 | 4265.26 | 3.91 | -0.80 | -8.57 | -4.5700 | 0.3978 | -5.0200 | 2 | -5.2725 |
| Fe I | 42 | 4271.77 | 2.44 | -0.25 | -8.67 | -4.1100 | 2.2394 | -4.1800 | 3 | -4.2705 |
| Fe I | 976 | 4276.69 | 3.86 | -0.88 | -8.57 | 0.0 | 0.3624 | -5.3700 | 2 | -5.6647 |
| Fe I | 71 | 4282.41 | 2.17 | -0.66 | -8.67 | -4.1100 | 2.0721 | -4.4700 | 3 | -5.5590 |
| Fe I | 3 | 4291.47 | 0.05 | -1.99 | -8.87 | -4.1600 | 2.6784 | -4.6800 | 3 | -6.9682 |
| Fe I | 942 | 4325.77 | 1.60 | 0.36 | -8.67 | -4.0200 | 3.6099 | -4.0400 | 3 | -5.2276 |
| Fe I | 597 | 4327.92 | 3.03 | -0.48 | -8.67 | -4.4600 | 1.4920 | -4.9700 | 2 | -6.2974 |
| Fe I | 518 | 4369.77 | 3.03 | -0.65 | -8.67 | -4.1200 | 1.3262 | -4.5200 | 3 | -5.0611 |
| Fe I | 2 | 4375.93 | 0.0 | -2.59 | -8.87 | -4.1500 | 2.1331 | -4.5000 | 3 | -5.7736 |
| Fe I | 41 | 4383.55 | 1.48 | 0.51 | -8.72 | -4.0200 | 3.8743 | -4.0700 | 3 | -5.5723 |
| Fe I | 2 | 4389.24 | 0.05 | -3.90 | -8.87 | -4.2600 | 0.7782 | -5.0000 | 3 | -5.6253 |
| Fe I | 41 | 4404.75 | 1.55 | 0.25 | -8.72 | -4.0300 | 3.5530 | -4.1100 | 3 | -5.3653 |
| Fe I | 41 | 4415.13 | 1.60 | -0.13 | -8.72 | -4.1000 | 3.1288 | -4.2100 | 3 | -5.2706 |
| Fe I | 68 | 4430.62 | 2.21 | -1.70 | -8.78 | -4.1500 | 1.0111 | -4.5700 | 3 | -4.9579 |
| Fe I | 43 | 4420.34 | 2.19 | -1.00 | -8.78 | -4.1400 | 1.7301 | -4.5100 | 3 | -5.4184 |
| Fe I | 350 | 4443.20 | 2.85 | -0.72 | -8.78 | -4.1300 | 1.4226 | -4.5700 | 3 | -5.3695 |
| Fe I | 68 | 4447.72 | 2.21 | -1.08 | -8.78 | -4.1800 | 1.6328 | -4.5200 | 3 | -5.3677 |
| Fe I | 350 | 4454.38 | 2.82 | -1.01 | -8.78 | -4.1900 | 1.1603 | -4.6100 | 3 | -5.2486 |
| Fe I | 2 | 4489.74 | 0.12 | -3.40 | -8.87 | -4.1400 | 1.2232 | -4.6000 | 3 | -5.2781 |
| Fe I | 39 | 4531.15 | 1.48 | -1.57 | -8.67 | -3.8600 | 1.8086 | -4.1400 | 0 | -3.7058 |
| Fe I | 39 | 4602.94 | 1.48 | -1.46 | -8.72 | -4.1200 | 1.9255 | -4.5900 | 2 | -5.9458 |
| Fe I | 318 | 4871.32 | 2.85 | -0.39 | -8.67 | -4.0500 | 1.7926 | -4.3600 | 3 | -4.6952 |
| Fe I | 318 | 5006.13 | 2.83 | -0.83 | -8.67 | -4.0500 | 1.2448 | -4.6400 | 2 | -5.2138 |
| Fe I | 16 | 5051.64 | 0.91 | -2.71 | -8.77 | -4.0200 | 1.1224 | -4.5100 | 2 | -4.5933 |
| Fe I | 383 | 5068.77 | 2.93 | -1.09 | -8.67 | -4.0600 | 0.9002 | -4.6400 | 2 | -4.8692 |

TABLE XII (Continued)

| Element | RMT | λ | X(R,S) | Log GF | 2/3 Log $C_4$ | Log (H/L) | Log C | Log (W/L) | Wt. | Log N/N(H) |
|---|---|---|---|---|---|---|---|---|---|---|
| Fe I | 16 | 5083.34 | 0.95 | -2.74 | -8.77 | -4.0300 | 1.0580 | -4.6300 | 2 | -4.9913 |
| Fe I | 1 | 5110.41 | 0.0 | -3.34 | -8.87 | -4.0000 | 1.3458 | -4.5000 | 2 | -4.7767 |
| Fe I | 1092 | 5133.69 | 4.16 | 0.39 | -8.57 | -4.0500 | 1.2943 | -4.5600 | 3 | -4.9618 |
| Fe I | 383 | 5192.35 | 2.99 | -0.32 | -8.67 | -4.0800 | 1.6266 | -4.5500 | 3 | -5.2552 |
| Fe I | 36 | 5194.94 | 1.55 | -1.93 | -8.72 | -4.0800 | 1.3241 | -4.6900 | 3 | -5.4527 |
| Fe I | 36 | 5216.28 | 1.60 | -1.95 | -8.72 | -4.0500 | 1.2601 | -4.6300 | 3 | -5.1934 |
| Fe I | 1 | 5225.53 | 0.11 | -4.26 | -8.87 | -4.0000 | 0.3326 | -4.9500 | 2 | -5.0411 |
| Fe I | 383 | 5266.56 | 2.99 | -0.41 | -8.67 | -4.0900 | 1.5428 | -4.5700 | 3 | -5.2492 |
| Fe I | 383 | 5281.80 | 3.03 | -0.75 | -8.67 | -4.1100 | 1.1682 | -4.7000 | 3 | -5.3261 |
| Fe I | 553 | 5283.63 | 3.24 | -0.30 | -8.27 | -4.1000 | 1.4310 | -4.8500 | 3 | -5.9522 |
| Fe I | 36 | 5307.37 | 1.60 | -2.76 | -8.72 | -4.4800 | 0.4576 | -4.9700 | 3 | -5.1999 |
| Fe I | 553 | 5339.94 | 3.26 | -0.61 | -8.67 | -4.0500 | 1.1077 | -4.7200 | 3 | -5.3220 |
| Fe I | 1146 | 5364.87 | 4.44 | 0.41 | -8.62 | -4.3600 | 1.0883 | -4.7700 | 4 | -5.4318 |
| Fe I | 1146 | 5367.47 | 4.41 | 0.49 | -8.62 | -4.7100 | 1.1948 | -4.9200 | 3 | -5.8501 |
| Fe I | 1146 | 5369.97 | 4.35 | 0.57 | -8.62 | -4.2300 | 1.3275 | -4.6600 | 3 | -5.3633 |
| Fe I | 1146 | 5383.37 | 4.29 | 0.67 | -8.62 | -3.9900 | 1.4811 | -4.6000 | 3 | -5.3033 |
| Fe I | 553 | 5393.17 | 3.23 | -0.60 | -8.67 | 4.3300 | 0.0 | 4.8000 | 0 | 0.0 |
| Fe I | 15 | 5397.13 | 0.91 | -1.88 | -8.67 | -4.0300 | 1.9812 | -4.3900 | 3 | -4.9725 |
| Fe I | 15 | 5405.78 | 0.99 | -1.75 | -8.77 | -4.3700 | 2.0376 | -4.5100 | 3 | -5.5084 |
| Fe I | 1165 | 5410.91 | 4.45 | 0.54 | -8.62 | -4.3300 | 1.2133 | -4.8400 | 4 | -5.7140 |
| Fe I | 1146 | 5424.07 | 4.32 | 0.68 | -8.62 | -3.9500 | 1.4681 | -4.5400 | 3 | -5.0577 |
| Fe I | 15 | 5429.70 | 0.95 | -1.78 | -8.77 | -4.2500 | 2.0466 | -4.4900 | 3 | -5.4374 |
| Fe I | 15 | 5434.53 | 1.01 | -2.27 | -8.67 | -3.9300 | 1.5013 | -4.5300 | 3 | -5.0516 |
| Fe I | 1163 | 5445.05 | 4.37 | 0.17 | -8.62 | -4.1100 | 0.9160 | -4.7300 | 3 | -5.1574 |
| Fe I | 15 | 5497.52 | 1.01 | -2.79 | -8.77 | -3.8600 | 0.9864 | -4.5000 | 2 | -4.4173 |
| Fe I | 15 | 5501.47 | 0.95 | -2.66 | -8.77 | -3.8900 | 1.1723 | -4.5800 | 2 | -4.9178 |
| Fe I | 15 | 5506.78 | 0.99 | -2.44 | -8.77 | -3.9200 | 1.3556 | -4.5500 | 2 | -4.9842 |
| Fe I | 686 | 5569.63 | 3.42 | -0.43 | -8.67 | -3.9200 | 1.1632 | -4.6500 | 2 | -5.1664 |
| Fe I | 686 | 5572.85 | 3.40 | -0.22 | -8.67 | -3.8600 | 1.3913 | -4.5800 | 2 | -5.1368 |
| Fe I | 686 | 5576.10 | 3.43 | -0.81 | -8.67 | -4.0600 | 0.7748 | -4.8100 | 2 | -5.2113 |

TABLE XII (Concluded)

| Element | RMT | λ | X(R,S) | Log GF | 2/3 Log $C_4$ | Log (H/L) | Log C | Log (W/L) | Wt. | Log N/N(H) |
|---|---|---|---|---|---|---|---|---|---|---|
| Fe I | 1107 | 5762.99 | 4.19 | -0.10 | -8.57 | -4.1200 | 0.8282 | -4.7100 | 2 | -5.0147 |
| Fe I | 959 | 5976.80 | 3.93 | -1.03 | -8.57 | -4.3000 | 0.1423 | -5.0000 | 2 | -4.9334 |
| Fe I | 959 | 6003.08 | 3.86 | -0.91 | -8.57 | -4.3300 | 0.3261 | -4.9700 | 2 | -5.0684 |
| Fe I | 1178 | 6024.07 | 4.53 | 0.22 | -8.49 | -4.3100 | 0.8701 | -4.8600 | 2 | -5.4114 |
| Fe I | 207 | 6065.53 | 2.60 | -1.33 | -8.67 | -4.2100 | 1.0353 | -4.7400 | 2 | -5.3031 |
| Fe I | 1259 | 6055.99 | 4.71 | -0.12 | -8.49 | -4.3200 | 0.3764 | -5.0800 | 2 | -5.2868 |
| Fe I | 207 | 6137.70 | 2.58 | -1.26 | -8.67 | -4.2600 | 1.1284 | -4.6700 | 2 | -5.1960 |
| Fe I | 62 | 6213.40 | 2.21 | -2.45 | -8.78 | -4.3700 | 0.2792 | -4.9500 | 2 | -4.9876 |
| Fe I | 207 | 6230.73 | 2.55 | 2.36 | -8.67 | -4.1000 | 4.7820 | -4.6700 | 2 | -8.8496 |
| Fe I | 816 | 6246.33 | 3.59 | -0.81 | -8.67 | -4.2300 | 0.6821 | -4.9100 | 3 | -5.3191 |
| Fe I | 169 | 6252.56 | 2.39 | -1.79 | -8.67 | -4.1200 | 0.7784 | -4.7600 | 3 | -5.0973 |
| Fe I | 62 | 6265.14 | 2.17 | -2.50 | -8.78 | -4.2200 | 0.2691 | -4.9900 | 2 | -5.0442 |
| Fe I | 816 | 6301.54 | 3.64 | -0.72 | -8.67 | -4.2200 | 0.7317 | -4.6300 | 2 | -4.6650 |
| Fe I | 168 | 6318.02 | 2.44 | -2.06 | -8.67 | -4.2100 | 0.4675 | -4.9000 | 2 | -5.0859 |
| Fe I | 168 | 6393.61 | 2.42 | -1.60 | -8.67 | -4.1200 | 0.9509 | -4.7000 | 2 | -5.1088 |
| Fe I | 816 | 6411.66 | 3.64 | -0.51 | -8.67 | -4.0400 | 0.9492 | -4.7100 | 2 | -5.1356 |
| Fe I | 111 | 6421.36 | 2.27 | -1.84 | -8.67 | -4.2100 | 0.8490 | -4.7800 | 2 | -5.2165 |
| Fe I | 168 | 6494.99 | 2.39 | -1.16 | -8.67 | -4.2100 | 1.4249 | -4.6500 | 2 | -5.4281 |
| Fe I | 62 | 6430.85 | 2.17 | -1.87 | -8.78 | -4.2700 | 0.9104 | -4.8200 | 2 | -5.3688 |

TABLE XIII

ABUNDANCE RESULTS FOR Fe II

| Element | RMT | λ | X(R,S) | Log GF | 2/3 Log $C_4$ | Log (H/L) | Log C | Log (W/L) | Wt. | Log N/N(H) |
|---|---|---|---|---|---|---|---|---|---|---|
| Fe II | 27 | 4128.74 | 2.58 | -2.76 | -8.67 | -4.4700 | 0.9815 | -4.7900 | 3 | -5.3665 |
| Fe II | 28 | 4178.86 | 2.57 | -2.00 | -8.67 | -4.3400 | 1.7556 | -4.5200 | 2 | -5.2292 |
| Fe II | 27 | 4273.32 | 2.69 | -3.51 | -8.60 | -4.2500 | 0.1491 | -4.5900 | 0 | -3.9375 |
| Fe II | 27 | 4303.17 | 2.70 | -2.00 | -8.67 | -4.3200 | 1.6533 | -4.5300 | 3 | -5.1749 |
| Fe II | 28 | 4369.40 | 2.77 | -2.87 | -8.67 | -4.6400 | 0.7280 | -4.8600 | 2 | -5.2699 |
| Fe II | 38 | 4576.33 | 2.85 | -2.22 | -8.67 | -4.1600 | 1.3273 | -4.5500 | 3 | -4.9430 |
| Fe II | 38 | 4620.51 | 2.82 | -2.63 | -8.67 | -4.1700 | 0.9480 | -4.7100 | 2 | -5.1235 |
| Fe II | 49 | 5197.57 | 3.22 | -2.23 | -8.57 | -4.1300 | 1.0472 | -4.5900 | 3 | -4.8356 |
| Fe II | 49 | 5234.62 | 3.21 | -2.03 | -8.57 | -4.3600 | 1.2590 | -4.7100 | 3 | -5.4345 |
| Fe II | 48 | 5264.80 | 3.22 | -2.23 | -8.57 | -4.6200 | 1.0528 | -5.1300 | 2 | -6.0378 |
| Fe II | 41 | 5284.09 | 2.88 | -2.42 | -8.67 | -4.5300 | 1.1632 | -4.9300 | 2 | -5.8412 |
| Fe II | 49 | 5325.56 | 3.21 | -2.72 | -8.57 | -4.4100 | 0.5765 | -5.0200 | 3 | -5.4049 |
| Fe II | 48 | 5362.86 | 3.19 | -1.95 | -8.57 | -4.0400 | 1.3671 | -4.5800 | 3 | -5.1162 |
| Fe II | 48 | 5414.09 | 3.21 | -2.75 | -8.57 | -4.3400 | 0.5537 | -5.1800 | 2 | -5.6040 |
| Fe II | 49 | 5425.27 | 3.19 | -2.75 | -8.57 | -4.1900 | 0.5721 | -4.9000 | 2 | -5.1940 |
| Fe II | 74 | 6247.56 | 3.87 | -1.55 | -8.50 | -4.3400 | 1.2418 | -4.8400 | 2 | -5.7412 |
| Fe II | 40 | 6432.65 | 2.88 | -2.73 | -8.67 | -4.2600 | 0.9386 | -4.9500 | 2 | -5.6522 |
| Fe II | 74 | 6456.38 | 3.89 | -1.44 | -8.50 | -4.0900 | 1.3488 | -4.5800 | 2 | -5.0980 |

TABLE XIV

ABUNDANCE RESULTS FOR Mg I

| Element | RMT | $\lambda$ | X(R,S) | Log GF | 2/3 Log $C_4$ | Log (H/L) | Log C | Log (W/L) | Wt. | Log N/N(H) |
|---|---|---|---|---|---|---|---|---|---|---|
| Mg I | 15 | 4167.27 | 4.33 | 0.0 | -8.10 | 0.0 | 1.8664 | -4.550 | 2 | -5.6459 |
| Mg I | 11 | 4702.99 | 4.34 | -0.58 | -8.10 | 0.0 | 1.3303 | -4.3100 | 1 | -3.7866 |
| Mg I | 10 | 4730.03 | 4.34 | -1.88 | -8.57 | 0.0 | 0.0327 | -5.0400 | 3 | -4.9114 |
| Mg I | 2 | 5172.68 | 2.71 | -0.38 | -9.38 | 0.0 | 3.0013 | -4.0600 | 3 | -4.6101 |
| Mg I | 2 | 5183.60 | 2.72 | -0.16 | -9.38 | 0.0 | 0.0 | -3.9600 | 0 | 0.0 |
| Mg I | 9 | 5528.40 | 4.34 | -0.48 | -8.49 | 0.0 | 1.5005 | -4.4500 | 1 | -4.7928 |
| Mg I | 8 | 5711.08 | 4.34 | -1.34 | -8.57 | 0.0 | 0.6546 | -5.1440 | 2 | -5.6719 |

TABLE XV

ABUNDANCE RESULTS FOR Mn I

| Element | RMT | λ | X(R,S) | Log GF | 2/3 Log $C_4$ | Log (H/L) | Log C | Log (W/L) | Wt. | Log N/N(H) |
|---|---|---|---|---|---|---|---|---|---|---|
| Mn I | 5 | 4018.10 | 2.11 | -0.14 | -8.67 | 0.0 | 2.9284 | -4.4500 | 3 | -6.9747 |
| Mn I | 2 | 4030.76 | 0.0 | -0.84 | -8.87 | 0.0 | 4.1540 | -4.1500 | 3 | -7.0204 |
| Mn I | 2 | 4033.07 | 0.0 | -1.00 | -8.87 | 0.0 | 3.9942 | -4.2500 | 3 | -7.3618 |
| Mn I | 2 | 4034.49 | 0.0 | -1.24 | -8.87 | 0.0 | 3.7544 | -4.3500 | 3 | -7.5185 |
| Mn I | 5 | 4055.54 | 2.13 | -0.02 | -8.67 | 0.0 | 3.0346 | -4.5600 | 3 | -7.3124 |
| Mn I | 29 | 4059.39 | 3.06 | -0.37 | -8.57 | 0.0 | 1.8593 | -5.1200 | 2 | -6.9047 |
| Mn I | 5 | 4070.28 | 2.18 | -0.79 | -8.67 | 0.0 | 2.2215 | -5.0900 | 3 | -7.2319 |
| Mn I | 5 | 4079.42 | 2.18 | -0.39 | -8.67 | 0.0 | 2.6224 | -4.6700 | 3 | -7.0848 |
| Mn I | 5 | 4082.94 | 2.17 | -0.24 | -8.67 | 0.0 | 2.7817 | -4.8700 | 4 | -7.5230 |
| Mn I | 23 | 4257.66 | 2.94 | -0.20 | -8.57 | 0.0 | 2.1557 | -5.4600 | 1 | -7.5764 |
| Mn I | 23 | 4265.92 | 2.93 | -0.22 | -8.57 | 0.0 | 2.1454 | -5.2700 | 1 | -7.3600 |
| Mn I | 22 | 4453.00 | 2.93 | -0.48 | -8.57 | 0.0 | 1.9040 | -5.3900 | 1 | -7.2497 |
| Mn I | 28 | 4457.05 | 3.06 | -0.89 | -8.57 | 0.0 | 1.3799 | -5.5900 | 1 | -6.9379 |
| Mn I | 22 | 4470.14 | 2.93 | -0.39 | -8.57 | 0.0 | 1.9957 | -5.2900 | 1 | -7.2323 |
| Mn I | 22 | 4502.22 | 2.91 | -0.36 | -8.57 | 0.0 | 2.0465 | -5.2100 | 3 | -7.1944 |
| Mn I | 21 | 4709.72 | 2.88 | -0.59 | -8.57 | 0.0 | 1.8626 | -5.1900 | 3 | -6.9880 |
| Mn I | 21 | 4739.11 | 2.93 | -0.66 | -8.57 | 0.0 | 1.7511 | -5.2800 | 1 | -6.9767 |
| Mn I | 16 | 4754.04 | 2.27 | -0.36 | -8.67 | 0.0 | 2.6385 | -4.5700 | 3 | -6.9343 |
| Mn I | 21 | 4765.86 | 2.93 | -0.29 | -8.57 | 0.0 | 2.1235 | -4.8500 | 4 | -6.8385 |
| Mn I | 21 | 4766.43 | 2.91 | -0.09 | -8.57 | 0.0 | 2.3413 | -4.7500 | 4 | -6.9214 |
| Mn I | 16 | 4783.42 | 2.29 | -0.38 | -8.67 | 0.0 | 2.6033 | -4.4800 | 3 | -6.7196 |
| Mn I | 16 | 4823.52 | 2.31 | -0.34 | -8.67 | 0.0 | 2.6290 | -4.4300 | 3 | -6.6268 |

TABLE XVI

ABUNDANCE RESULTS FOR Na I

| Element | RMT | λ | X(R,S) | Log GF | 2/3 Log $C_4$ | Log (H/L) | Log C | Log (W/L) | Wt. | Log N/N(H) |
|---|---|---|---|---|---|---|---|---|---|---|
| Na I | 6 | 5682.63 | 2.10 | -0.67 | -7.65 | 0.0 | 1.3091 | -4.8300 | 3 | -5.8154 |
| Na I | 6 | 5688.21 | 2.10 | -0.42 | -7.65 | 0.0 | 1.5595 | -4.6800 | 2 | -5.6988 |
| Na I | 1 | 5889.95 | 0.0 | 0.12 | -9.80 | 0.0 | 3.9683 | -4.1900 | 2 | -5.7823 |
| Na I | 1 | 5895.92 | 0.0 | -0.18 | -9.80 | 0.0 | 3.6678 | -4.3000 | 2 | -5.9082 |

TABLE XVII

ABUNDANCE RESULTS FOR Ni I

| Element | RMT | λ | X(R,S) | Log GF | 2/3 Log $C_4$ | Log (H/L) | Log C | Log (W/L) | Wt. | Log N/N(H) |
|---|---|---|---|---|---|---|---|---|---|---|
| Ni I | 86 | 4462.46 | 3.45 | -0.95 | -8.67 | 0.0 | 0.9336 | -4.8900 | 4 | -5.5570 |
| Ni I | 86 | 4470.48 | 3.38 | -0.51 | -8.67 | 0.0 | 1.4364 | -4.8200 | 4 | -5.9228 |
| Ni I | 98 | 4604.99 | 3.47 | -0.41 | -8.67 | 0.0 | 1.4695 | -4.8100 | 3 | -5.9355 |
| Ni I | 100 | 4606.23 | 3.58 | -0.88 | -8.67 | 0.0 | 0.9028 | -5.3100 | 1 | -6.1124 |
| Ni I | 98 | 4648.66 | 3.40 | -0.40 | -8.67 | 0.0 | 1.5456 | -4.7900 | 4 | -5.9696 |
| Ni I | 98 | 4686.22 | 3.58 | -0.79 | -8.67 | 0.0 | 1.0003 | -5.1300 | 3 | -5.9927 |
| Ni I | 98 | 4714.42 | 3.37 | -0.34 | -8.67 | 0.0 | 1.6383 | -4.5400 | 3 | -5.3024 |
| Ni I | 98 | 4715.78 | 3.53 | -0.92 | -8.67 | 0.0 | 0.9169 | -4.9500 | 4 | -5.6474 |
| Ni I | 98 | 4756.52 | 3.47 | -0.79 | -8.67 | 0.0 | 1.1036 | -4.8500 | 4 | -5.6495 |
| Ni I | 163 | 4806.99 | 3.66 | -0.84 | -8.67 | 0.0 | 0.8911 | -5.1400 | 3 | -5.8961 |
| Ni I | 131 | 4829.03 | 3.53 | -0.93 | -8.67 | 0.0 | 0.9172 | -4.6900 | 4 | -5.0919 |
| Ni I | 111 | 4866.27 | 3.52 | -0.76 | -8.67 | 0.0 | 1.0993 | -4.8700 | 4 | -5.6846 |
| Ni I | 111 | 4873.44 | 3.68 | -0.93 | -8.67 | 0.0 | 0.7895 | -4.9700 | 4 | -5.5534 |
| Ni I | 129 | 4904.41 | 3.53 | -0.70 | -8.67 | 0.0 | 1.1539 | -4.9300 | 4 | -5.8499 |
| Ni I | 177 | 4918.36 | 3.82 | -0.65 | -8.57 | 0.0 | 0.9506 | -4.9800 | 3 | -5.7308 |
| Ni I | 177 | 4935.83 | 3.92 | -0.82 | -8.57 | 0.0 | 0.6944 | -5.2700 | 3 | -5.8553 |
| Ni I | 112 | 4980.16 | 3.59 | -0.66 | -8.67 | 0.0 | 1.1479 | -4.7100 | 3 | -5.3795 |
| Ni I | 143 | 4984.13 | 3.78 | -0.54 | -8.67 | 0.0 | 1.1015 | -4.7400 | 3 | -5.4103 |
| Ni I | 145 | 5000.34 | 3.62 | -1.11 | -8.67 | 0.0 | 0.6733 | -4.8100 | 3 | -5.1394 |

TABLE XVII (Concluded)

| Element | RMT | λ | X(R,S) | Log GF | 2.3 Log $C_4$ | Log (H/L) | Log C | Log (W/L) | Wt. | Log N/N(H) |
|---|---|---|---|---|---|---|---|---|---|---|
| Ni I | 111 | 5012.46 | 3.68 | -1.00 | -8.67 | 0.0 | 0.7317 | -4.9600 | 3 | -5.4790 |
| Ni I | 111 | 5017.59 | 3.52 | -0.65 | -8.67 | 0.0 | 1.2226 | -4.7100 | 3 | -5.4542 |
| Ni I | 143 | 5035.37 | 3.62 | -0.28 | -8.67 | 0.0 | 1.5064 | -4.7700 | 3 | -5.8861 |
| Ni I | 143 | 5080.52 | 3.64 | -0.27 | -8.67 | 0.0 | 1.5027 | -4.7000 | 3 | -5.7063 |
| Ni I | 194 | 5081.11 | 3.83 | -0.36 | -8.57 | 0.0 | 1.2460 | -4.8800 | 3 | -5.8505 |
| Ni I | 162 | 5084.08 | 3.66 | -0.86 | -8.67 | 0.0 | 0.8955 | -4.8500 | 3 | -5.4414 |
| Ni I | 161 | 5099.95 | 3.66 | -0.86 | -8.67 | 0.0 | 0.8968 | -4.8200 | 3 | -5.3832 |
| Ni I | 177 | 5115.40 | 3.82 | -0.86 | -8.57 | 0.0 | 0.7577 | -4.9000 | 3 | -5.3997 |
| Ni I | 162 | 5146.48 | 3.69 | -0.67 | -8.67 | 0.0 | 1.0644 | -4.7100 | 4 | -5.2960 |
| Ni I | 210 | 5155.76 | 3.88 | -0.55 | -8.57 | 0.0 | 1.0184 | -4.9000 | 4 | -5.6605 |
| Ni I | 209 | 5176.57 | 3.88 | -1.03 | -8.57 | 0.0 | 0.5402 | -5.1900 | 3 | -5.6060 |
| Ni I | 47 | 5578.73 | 1.67 | -3.20 | -8.72 | 0.0 | 0.3787 | -5.3200 | 2 | -5.6003 |
| Ni I | 69 | 5592.28 | 1.94 | -2.63 | -8.78 | 0.0 | 0.7039 | -5.4100 | 1 | -6.0325 |

TABLE XVIII

ABUNDANCE RESULTS FOR Sc II

| Element | RMT | λ | X(R,S) | Log GF | 2/3 Log $C_4$ | Log (H/L) | Log C | Log (W/L) | Wt. | Log N/N(H) |
|---|---|---|---|---|---|---|---|---|---|---|
| Sc II | 7 | 4246.83 | 0.31 | 0.28 | -8.87 | 0.0 | 6.2570 | -4.4200 | 3 | -9.2474 |
| Sc II | 15 | 4294.77 | 0.60 | -1.28 | -8.87 | 0.0 | 4.4328 | -4.6400 | 3 | -8.5174 |
| Sc II | 15 | 4314.08 | 0.62 | -0.10 | -8.87 | 0.0 | 5.5962 | -4.3600 | 3 | -8.2096 |
| Sc II | 15 | 4320.75 | 0.60 | -0.22 | -8.87 | 0.0 | 5.4954 | -4.6200 | 2 | -9.5135 |
| Sc II | 14 | 4354.61 | 0.60 | -1.50 | -8.87 | 0.0 | 0.0 | -4.7000 | 0 | 0.0 |
| Sc II | 14 | 4415.56 | 0.59 | -0.84 | -8.87 | 0.0 | 4.8940 | -4.4800 | 3 | -8.2781 |
| Sc II | 26 | 5239.82 | 1.45 | 0.56 | -8.77 | 0.0 | 0.0 | -4.9400 | 0 | 0.0 |
| Sc II | 31 | 5526.81 | 1.76 | -0.03 | -8.77 | 0.0 | 4.7295 | -4.6200 | 2 | -8.7477 |
| Sc II | 29 | 5667.16 | 1.49 | -1.35 | -8.77 | 0.0 | 0.0 | -5.1600 | 0 | 0.0 |
| Sc II | 29 | 5669.03 | 1.49 | -1.23 | -8.77 | 0.0 | 0.0 | -5.2200 | 0 | 0.0 |
| Sc II | 28 | 6245.63 | 1.50 | -1.05 | -8.77 | 0.0 | 0.0 | -5.2400 | 0 | 0.0 |

TABLE XIX

ABUNDANCE RESULTS FOR Si I

| Element | RMT | λ | X(R,S) | Log GF | 2/3 Log $C_4$ | Log (H/L) | Log C | Log (W/L) | Wt. | Log N/N(H) |
|---|---|---|---|---|---|---|---|---|---|---|
| Si I | 10 | 5708.48 | 4.93 | -1.15 | -8.42 | 0.0 | 0.1807 | -5.0200 | 1 | -4.9932 |
| Si I | 17 | 5772.26 | 5.06 | -1.38 | -8.20 | 0.0 | -0.1572 | -5.1800 | 1 | -4.8857 |
| Si I | 16 | 5948.58 | 5.06 | -1.24 | -8.20 | 0.0 | -0.0041 | -5.0000 | 1 | -4.7762 |

TABLE XX

ABUNDANCE RESULTS FOR Ti I

| Element | RMT | λ | X(R,S) | Log GF | 2/3 Log $C_4$ | Log (H/L) | Log C | Log (W/L) | Wt. | Log N/N(H) |
|---|---|---|---|---|---|---|---|---|---|---|
| Ti I | 187 | 4008.05 | 2.11 | 0.04 | -8.67 | 0.0 | 1.7109 | -5.0300 | 3 | -6.6576 |
| Ti I | 12 | 4008.93 | 0.02 | -0.83 | -8.87 | 0.0 | 2.7279 | -4.5700 | 3 | -7.0467 |
| Ti I | 186 | 4016.20 | 2.13 | -0.25 | -8.67 | 0.0 | 1.4041 | -5.7700 | 1 | -7.1431 |
| Ti I | 80 | 4060.26 | 1.05 | -0.22 | -8.77 | 0.0 | 2.4048 | -5.4400 | 2 | -7.8083 |
| Ti I | 163 | 4166.31 | 1.87 | -0.49 | -8.77 | 0.0 | 1.4108 | -5.7000 | 1 | -7.0869 |
| Ti I | 163 | 4169.33 | 1.88 | -0.19 | -8.77 | 0.0 | 1.7022 | -5.8200 | 1 | -7.4832 |
| Ti I | 129 | 4186.12 | 1.50 | 0.10 | -8.77 | 0.0 | 2.3329 | -5.3000 | 1 | -7.5850 |
| Ti I | 162 | 4265.72 | 1.87 | -0.60 | -8.77 | 0.0 | 1.3110 | -6.0300 | 1 | -7.2432 |
| Ti I | 44 | 4281.37 | 0.81 | -1.11 | -8.77 | 0.0 | 1.7554 | -5.7900 | 1 | -7.5115 |
| Ti I | 44 | 4286.01 | 0.82 | -0.18 | -8.77 | 0.0 | 2.6768 | -4.7300 | 4 | -7.2420 |
| Ti I | 44 | 4287.41 | 0.84 | -0.20 | -8.77 | 0.0 | 2.6387 | -5.0600 | 3 | -7.6207 |
| Ti I | 44 | 4305.91 | 0.84 | 0.66 | -8.77 | 0.0 | 3.5006 | -4.3300 | 3 | -7.2316 |
| Ti I | 235 | 4321.66 | 2.23 | 0.43 | -8.67 | 0.0 | 2.0276 | -5.1900 | 3 | -7.1579 |
| Ti I | 43 | 4326.36 | 0.82 | -0.95 | -8.77 | 0.0 | 1.9108 | -5.4500 | 1 | -7.3253 |
| Ti I | 161 | 4417.27 | 1.88 | 0.17 | -8.77 | 0.0 | 2.0873 | -5.5100 | 1 | -7.5672 |
| Ti I | 128 | 4427.10 | 1.50 | 0.43 | -8.77 | 0.0 | 2.6872 | -5.4900 | 1 | -8.1454 |
| Ti I | 160 | 4453.71 | 1.87 | 0.27 | -8.77 | 0.0 | 2.1998 | -5.3800 | 1 | -7.5385 |
| Ti I | 146 | 4465.81 | 1.73 | 0.14 | -8.77 | 0.0 | 2.1958 | -5.4100 | 1 | -7.5667 |
| Ti I | 42 | 4518.02 | 0.82 | -0.20 | -8.77 | 0.0 | 2.6797 | -4.8800 | 4 | -7.4431 |
| Ti I | 42 | 4533.24 | 0.84 | 0.58 | -8.77 | 0.0 | 3.4430 | -4.4800 | 3 | -7.5872 |
| Ti I | 42 | 4534.78 | 0.83 | 0.35 | -8.77 | 0.0 | 3.2222 | -4.6200 | 3 | -7.6240 |
| Ti I | 42 | 4548.76 | 0.82 | -0.24 | -8.77 | 0.0 | 2.6426 | -5.0300 | 2 | -7.5893 |
| Ti I | 42 | 4555.49 | 0.84 | -0.34 | -8.77 | 0.0 | 2.5251 | -4.8400 | 4 | -7.2382 |
| Ti I | 145 | 4617.27 | 1.74 | 0.62 | -8.77 | 0.0 | 2.6814 | -5.0200 | 3 | -7.6163 |
| Ti I | 145 | 4623.10 | 1.73 | 0.40 | -8.77 | 0.0 | 2.4709 | -5.3300 | 1 | -7.7556 |
| Ti I | 145 | 4639.37 | 1.73 | 0.0 | -8.77 | 0.0 | 2.0724 | -5.3900 | 1 | -7.4218 |
| Ti I | 145 | 4639.67 | 1.74 | -0.03 | -8.77 | 0.0 | 2.0335 | -5.6500 | 1 | -7.6601 |
| Ti I | 145 | 4645.19 | 1.73 | -0.22 | -8.77 | 0.0 | 1.8529 | -5.5100 | 1 | -7.3328 |

TABLE XX (Concluded)

| Element | RMT | λ | X(R,S) | Log GF | 2/3 Log $C_4$ | Log (H/1) | Log C | Log (W/L) | Wt. | Log N/N(H) |
|---|---|---|---|---|---|---|---|---|---|---|
| Ti I | 6 | 4656.47 | 0.0 | -1.21 | -8.87 | 0.0 | 2.4312 | -5.0800 | 3 | -7.4364 |
| Ti I | 6 | 4681.91 | 0.05 | -1.05 | -8.87 | 0.0 | 2.5478 | -4.7100 | 4 | -7.0843 |
| Ti I | 157 | 4913.62 | 1.87 | 0.24 | -8.77 | 0.0 | 2.2124 | -5.4500 | 1 | -7.6269 |
| Ti I | 200 | 4919.87 | 2.15 | 0.12 | -8.67 | 0.0 | 1.8445 | -5.6400 | 1 | -7.4611 |
| Ti I | 38 | 4981.73 | 0.84 | 0.51 | -8.77 | 0.0 | 3.4139 | -4.6100 | 2 | -7.7998 |
| Ti I | 38 | 5016.16 | 0.84 | -0.50 | -8.77 | 0.0 | 2.4069 | -4.9700 | 3 | -7.2818 |
| Ti I | 38 | 5024.84 | 0.81 | -0.53 | -8.77 | 0.0 | 2.4049 | -4.8300 | 3 | -7.1052 |
| Ti I | 173 | 5025.57 | 2.03 | 0.35 | -8.67 | 0.0 | 2.1898 | -5.0900 | 2 | -7.2065 |
| Ti I | 5 | 5039.96 | 0.02 | -1.02 | -8.87 | 0.0 | 2.6373 | -4.8800 | 3 | -7.4007 |
| Ti I | 38 | 5043.58 | 0.83 | -1.36 | -8.77 | 0.0 | 1.5584 | -5.5500 | 1 | -7.0812 |
| Ti I | 4 | 5152.19 | 0.02 | -1.79 | -8.87 | 0.0 | 1.8769 | -5.6700 | 1 | -7.5235 |
| Ti I | 4 | 5173.74 | 0.0 | -1.12 | -8.87 | 0.0 | 2.5670 | -4.8400 | 4 | -7.2801 |
| Ti I | 183 | 5194.04 | 2.09 | -0.17 | -8.67 | 0.0 | 1.6311 | -5.8600 | 1 | -7.4440 |
| Ti I | 183 | 5201.10 | 2.08 | -0.31 | -8.67 | 0.0 | 1.5005 | -5.8300 | 1 | -7.2896 |
| Ti I | 4 | 5210.39 | 0.05 | -0.96 | -8.87 | 0.0 | 2.6843 | -4.9300 | 4 | -7.5100 |
| Ti I | 183 | 5224.30 | 2.13 | 0.33 | -8.67 | 0.0 | 2.0983 | -5.4600 | 1 | -7.5237 |
| Ti I | 249 | 5689.47 | 2.29 | -0.01 | -8.67 | 0.0 | 1.6540 | -5.6800 | 1 | -7.3105 |
| Ti I | 249 | 5713.90 | 2.28 | -0.38 | -8.67 | 0.0 | 1.2947 | -5.6500 | 1 | -6.9213 |
| Ti I | 309 | 5766.33 | 3.28 | 0.63 | -8.57 | 0.0 | 1.4350 | -5.6000 | 1 | -7.0105 |
| Ti I | 72 | 5866.45 | 1.06 | -0.59 | -8.77 | 0.0 | 2.1856 | -5.6200 | 1 | -7.7817 |
| Ti I | 71 | 5918.55 | 1.06 | -1.13 | -8.77 | 0.0 | 1.6494 | -5.6100 | 1 | -7.2352 |

TABLE XXI

ABUNDANCE RESULTS FOR Ti II

| Element | RMT | λ | X(R,S) | Log GF | 2/3 Log $C_4$ | Log (H/L) | Log C | Log (W/L) | Wt. | Log N/N(H) |
|---|---|---|---|---|---|---|---|---|---|---|
| Ti II | 41 | 4300.05 | 1.18 | -0.46 | -8.77 | 0.0 | 4.5412 | -4.3000 | 3 | -8.1687 |
| Ti II | 41 | 4301.93 | 1.16 | -1.11 | -8.77 | 0.0 | 3.9095 | -4.4500 | 3 | -7.9919 |
| Ti II | 41 | 4312.86 | 1.18 | -1.06 | -8.77 | 0.0 | 3.9425 | -4.3900 | 3 | -7.8716 |
| Ti II | 94 | 4316.81 | 2.04 | -1.07 | -8.67 | 0.0 | 3.1608 | -4.9000 | 4 | -7.9519 |
| Ti II | 20 | 4337.92 | 1.08 | -0.90 | -8.77 | 0.0 | 4.1954 | -4.4400 | 3 | -8.2544 |
| Ti II | 20 | 4344.29 | 1.08 | -1.67 | -8.77 | 0.0 | 3.4261 | -4.6200 | 3 | -7.8307 |
| Ti II | 51 | 4394.06 | 1.22 | -1.47 | -8.77 | 0.0 | 3.5045 | -4.6000 | 3 | -7.8771 |
| Ti II | 19 | 4395.03 | 1.08 | -0.50 | -8.77 | 0.0 | 4.6011 | -4.2900 | 3 | -8.1886 |
| Ti II | 61 | 4395.85 | 1.24 | -1.53 | -8.77 | 0.0 | 3.4266 | -4.7100 | 4 | -7.9661 |
| Ti II | 61 | 4409.52 | 1.23 | -2.07 | -8.77 | 0.0 | 2.8969 | -5.0800 | 2 | -7.9047 |
| Ti II | 40 | 4417.72 | 1.16 | -1.18 | -8.77 | 0.0 | 3.8510 | -4.5300 | 3 | -8.1002 |
| Ti II | 93 | 4421.95 | 2.05 | -1.14 | -8.67 | 0.0 | 3.0924 | -4.8500 | 4 | -7.8209 |
| Ti II | 19 | 4443.80 | 1.08 | -0.74 | -8.77 | 0.0 | 4.3659 | -4.4100 | 3 | -8.3497 |
| Ti II | 19 | 4450.49 | 1.08 | -1.41 | -8.77 | 0.0 | 3.6966 | -4.5100 | 3 | -7.9065 |
| Ti II | 31 | 4468.49 | 1.13 | -0.65 | -8.77 | 0.0 | 4.4131 | -4.3700 | 3 | -8.2834 |
| Ti II | 50 | 4533.97 | 1.23 | -0.64 | -8.77 | 0.0 | 4.3390 | -4.2500 | 3 | -7.7524 |
| Ti II | 50 | 4563.76 | 1.22 | -0.86 | -8.77 | 0.0 | 4.1309 | -4.3700 | 3 | -8.0012 |
| Ti II | 60 | 4568.31 | 1.22 | -1.93 | -8.77 | 0.0 | 3.0613 | -5.0000 | 2 | -7.9751 |
| Ti II | 82 | 4571.97 | 1.56 | -0.34 | -8.77 | 0.0 | 4.3449 | -4.2700 | 3 | -7.8484 |
| Ti II | 92 | 4805.11 | 2.05 | -0.76 | -8.67 | 0.0 | 3.5085 | -4.4900 | 2 | -7.6773 |
| Ti II | 86 | 5129.14 | 1.88 | -0.93 | -8.77 | 0.0 | 3.5185 | -4.5700 | 2 | -7.8406 |
| Ti II | 69 | 5336.81 | 1.57 | -1.35 | -8.77 | 0.0 | 3.3931 | -4.8000 | 4 | -8.0570 |

TABLE XXII

ABUNDANCE RESULTS FOR V I

| Element | RMT | λ | X(R,S) | Log GF | 2/3 Log $C_4$ | Log (H/L) | Log C | Log (W/L) | Wt. | Log N/N(H) |
|---|---|---|---|---|---|---|---|---|---|---|
| V I | 41 | 4095.49 | 1.06 | 0.08 | -8.77 | 0.0 | 2.7661 | -5.3300 | 1 | -8.0186 |
| V I | 27 | 4111.79 | 0.30 | 0.33 | -8.87 | 0.0 | 3.7057 | -5.9500 | 2 | -9.6295 |
| V I | 52 | 4113.52 | 1.21 | -0.37 | -8.77 | 0.0 | 2.1837 | -5.4400 | 1 | -7.5616 |
| V I | 27 | 4115.19 | 0.29 | 0.0 | -8.87 | 0.0 | 3.3851 | -5.2400 | 1 | -8.5311 |
| V I | 103 | 4342.83 | 1.86 | 0.18 | -8.77 | 0.0 | 2.1784 | -5.3400 | 1 | -7.4425 |
| V I | 22 | 4379.24 | 0.30 | 0.37 | -8.87 | 0.0 | 3.7730 | -4.8000 | 4 | -8.3012 |
| V I | 22 | 4389.97 | 0.27 | -0.06 | -8.87 | 0.0 | 3.3714 | -4.9100 | 4 | -8.0833 |
| V I | 22 | 4406.64 | 0.30 | -0.36 | -8.87 | 0.0 | 3.0457 | -5.2600 | 3 | -8.2157 |
| V I | 22 | 4408.20 | 0.27 | -0.20 | -8.87 | 0.0 | 3.2332 | -5.2400 | 1 | -8.3792 |
| V I | 21 | 4437.84 | 0.29 | -0.94 | -8.87 | 0.0 | 2.4779 | -5.6600 | 1 | -8.0966 |
| V I | 21 | 4444.21 | 0.27 | -0.96 | -8.87 | 0.0 | 2.4768 | -5.3100 | 1 | -7.7059 |
| V I | 87 | 4452.01 | 1.86 | 0.56 | -8.77 | 0.0 | 2.5692 | -5.3600 | 1 | -7.8564 |
| V I | 87 | 4469.71 | 1.85 | 0.33 | -8.77 | 0.0 | 2.3498 | -5.6500 | 1 | -7.9578 |
| V I | 133 | 4553.06 | 2.35 | 0.13 | -8.67 | 0.0 | 1.7177 | -5.2400 | 2 | -6.8637 |
| V I | 109 | 4560.71 | 1.94 | 0.26 | -8.67 | 0.0 | 2.2088 | -5.4500 | 1 | -7.5978 |
| V I | 4 | 4577.17 | 0.0 | -1.38 | -8.87 | 0.0 | 2.3157 | -5.0500 | 2 | -7.2235 |
| V I | 93 | 4686.93 | 1.86 | -0.88 | -8.77 | 0.0 | 1.1516 | -5.7700 | 1 | -6.8869 |
| V I | 131 | 5234.09 | 2.35 | -0.02 | -8.67 | 0.0 | 1.6283 | -5.4900 | 1 | -7.0617 |

TABLE XXIII

ABUNDANCE RESULTS FOR V II

| Element | RMT | λ | X(R,S) | Log GF | 2/3 Log $C_4$ | Log (H/L) | Log C | Log (W/L) | Wt. | Log N/N(H) |
|---|---|---|---|---|---|---|---|---|---|---|
| V II | 9 | 4002.94 | 1.42 | -1.28 | -8.77 | 0.0 | 3.6283 | -4.7100 | 3 | -8.0033 |
| V II | 32 | 4005.71 | 1.81 | -0.22 | -8.77 | 0.0 | 4.3414 | -4.5500 | 3 | -8.2398 |
| V II | 32 | 4023.39 | 1.80 | -0.35 | -8.77 | 0.0 | 4.2222 | -4.8100 | 4 | -8.7892 |
| V II | 9 | 4036.78 | 1.47 | -1.42 | -8.77 | 0.0 | 3.4471 | -4.9300 | 3 | -8.2042 |
| V II | 32 | 4039.57 | 1.81 | -1.60 | -8.77 | 0.0 | 2.9651 | -5.3000 | 1 | -8.1901 |
| V II | 37 | 4225.23 | 2.02 | -1.07 | -8.67 | 0.0 | 3.3283 | -5.1500 | 1 | -8.3748 |
| V II | 225 | 4232.07 | 3.96 | -0.23 | -8.47 | 0.0 | 2.4976 | -5.2600 | 1 | -7.6757 |
| V II | 24 | 4234.25 | 1.68 | -2.11 | -8.77 | 0.0 | 2.5910 | -5.3900 | 1 | -7.9192 |

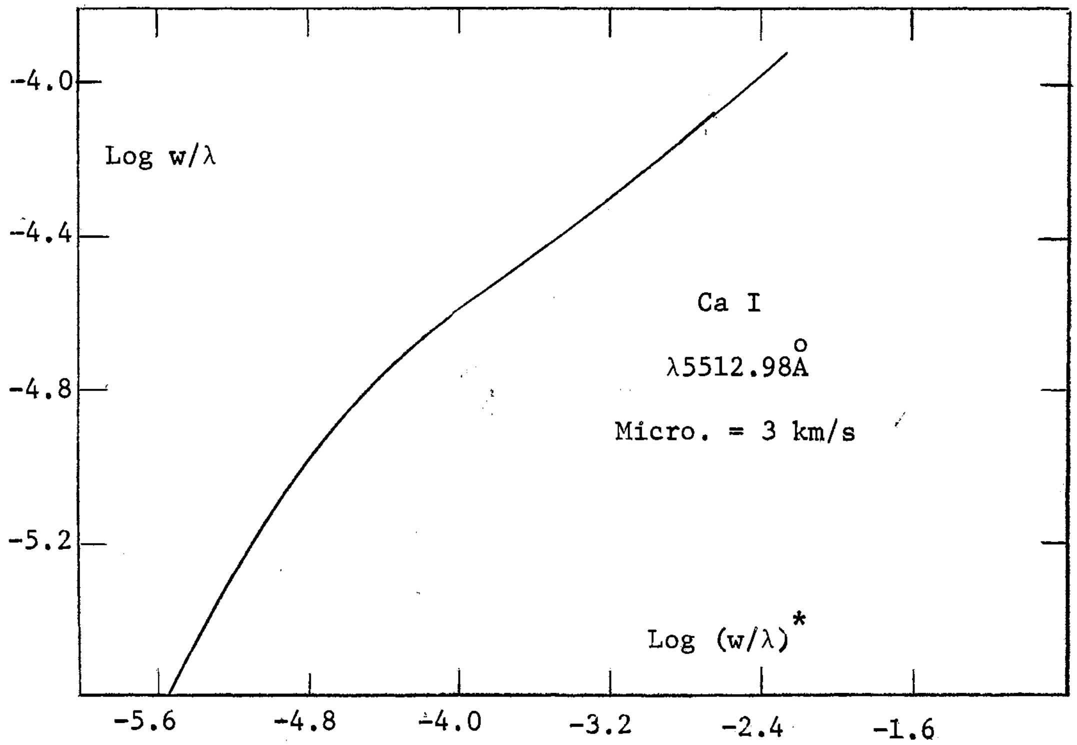


Figure 19. Theoretical Curve of Growth for Ca I

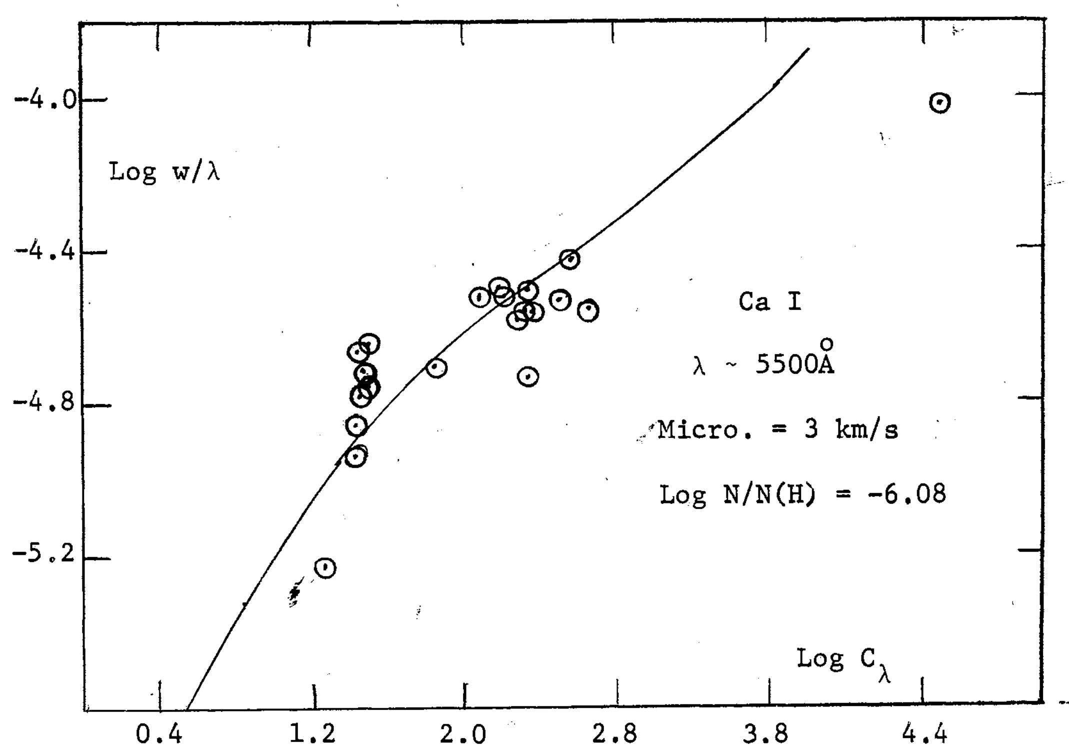


Figure 20. Empirical Curve of Growth for Ca I

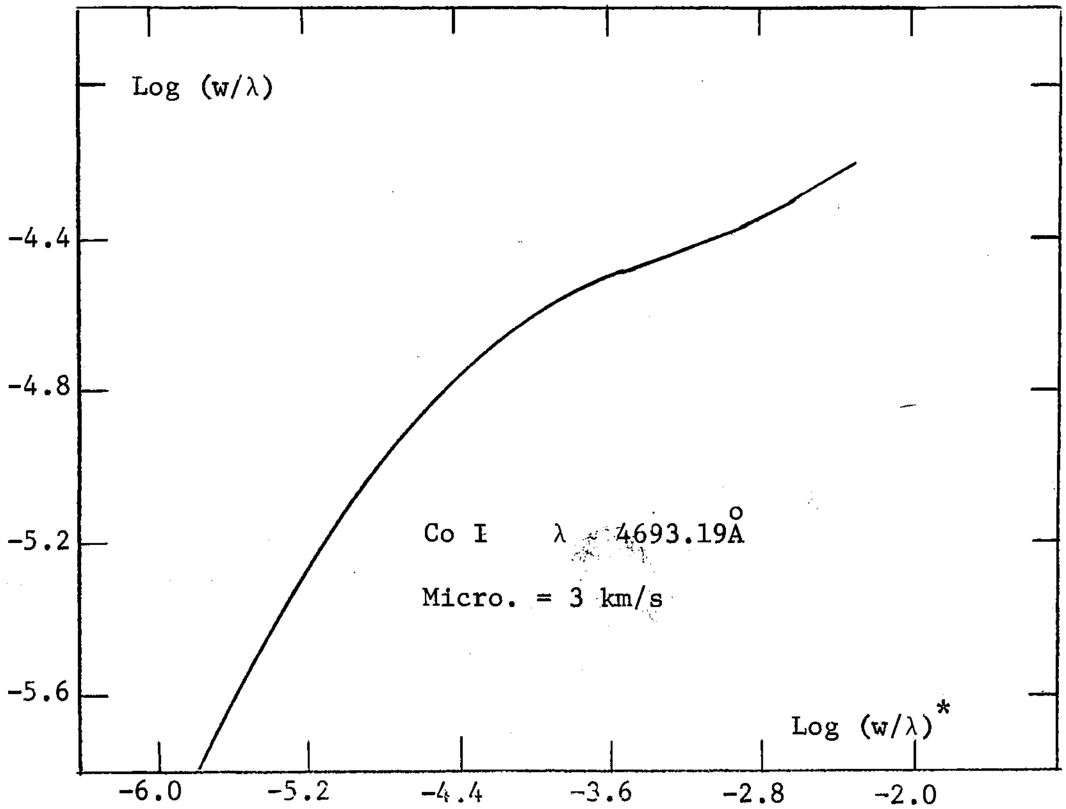


Figure 21. Theoretical Curve of Growth for Co I

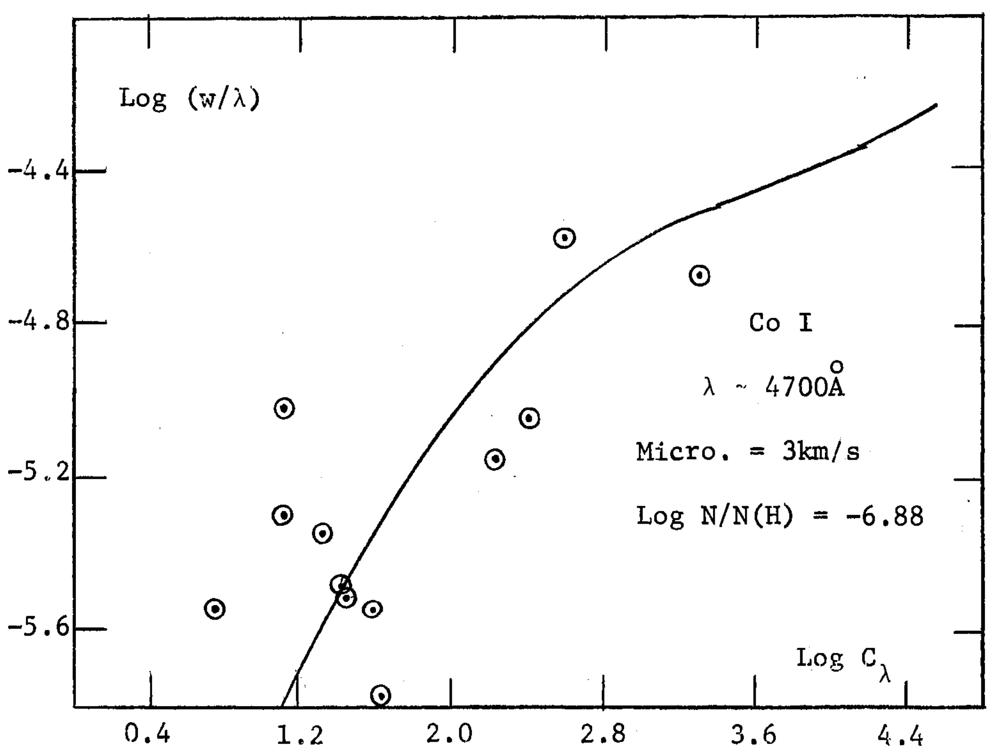


Figure 22. Empirical Curve of Growth for Co I

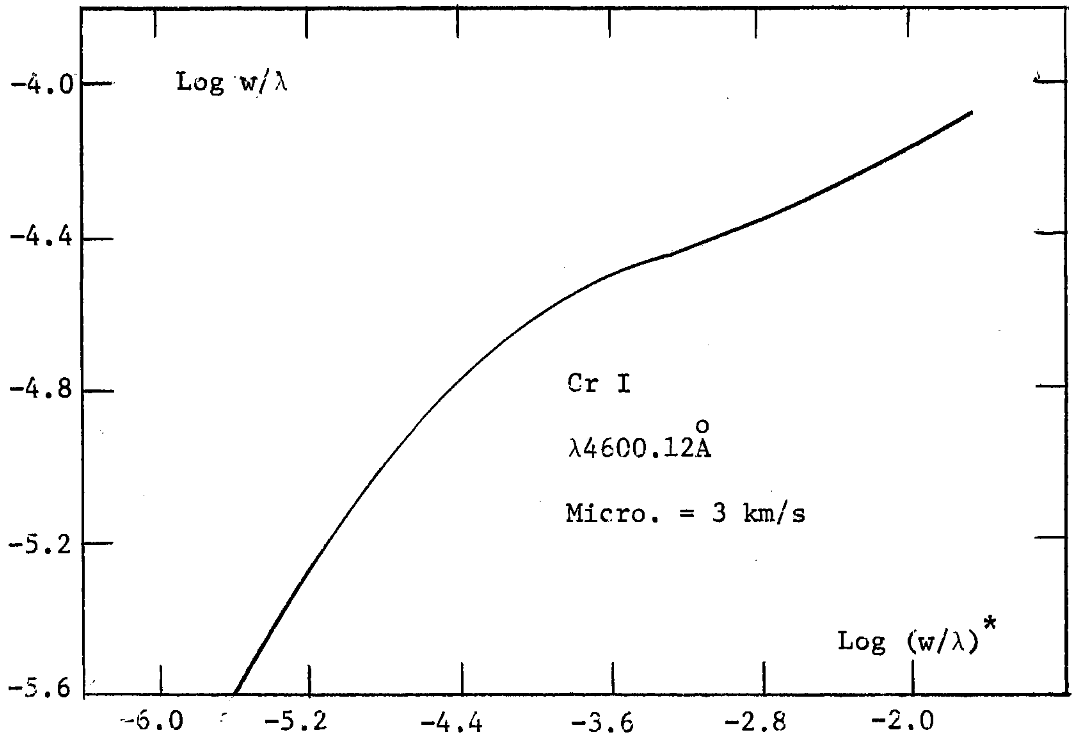


Figure 23. Theoretical Curve of Growth for Cr I

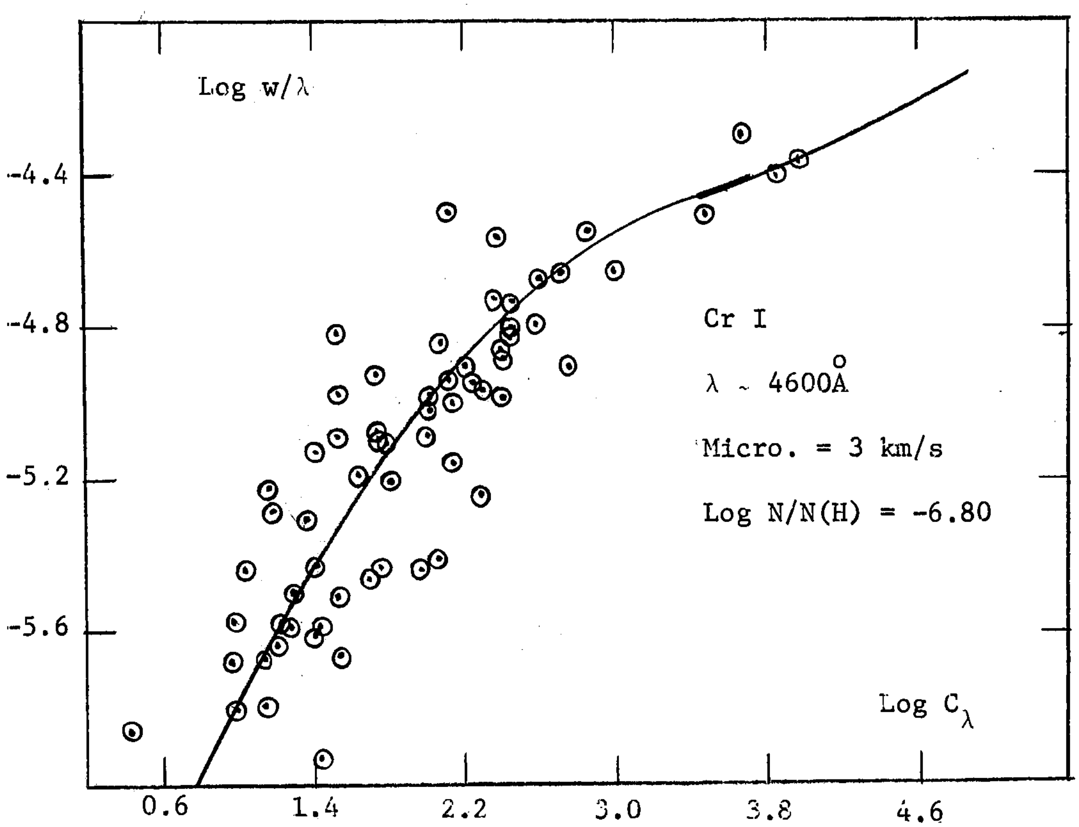


Figure 24. Empirical Curve of Growth for Cr I

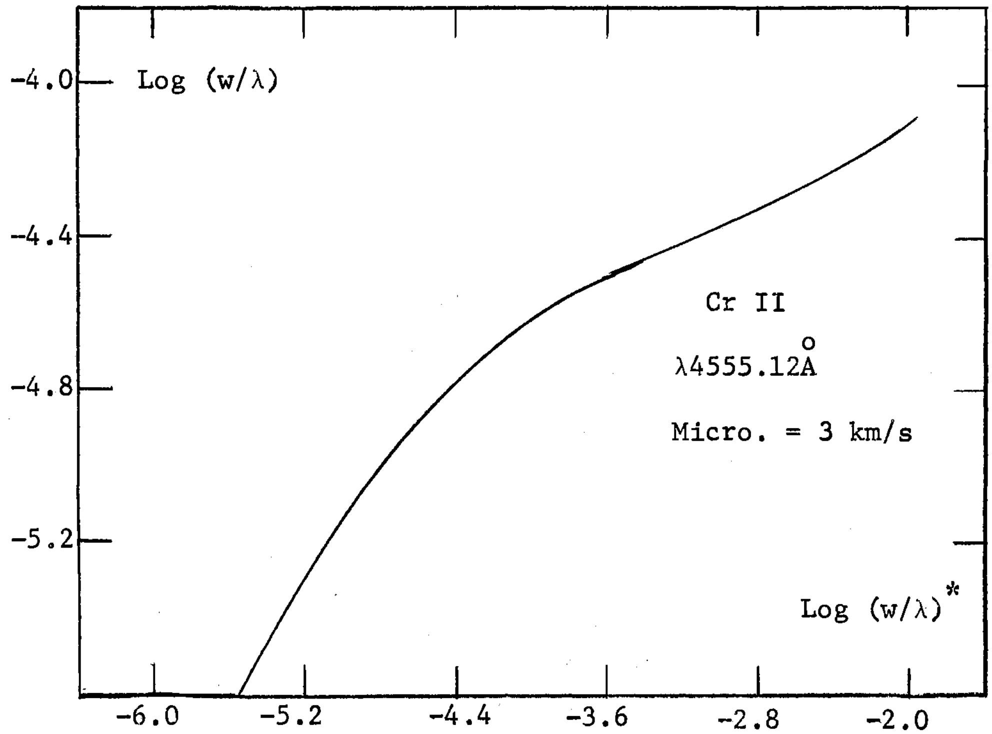


Figure 25. Theoretical Curve of Growth for Cr II

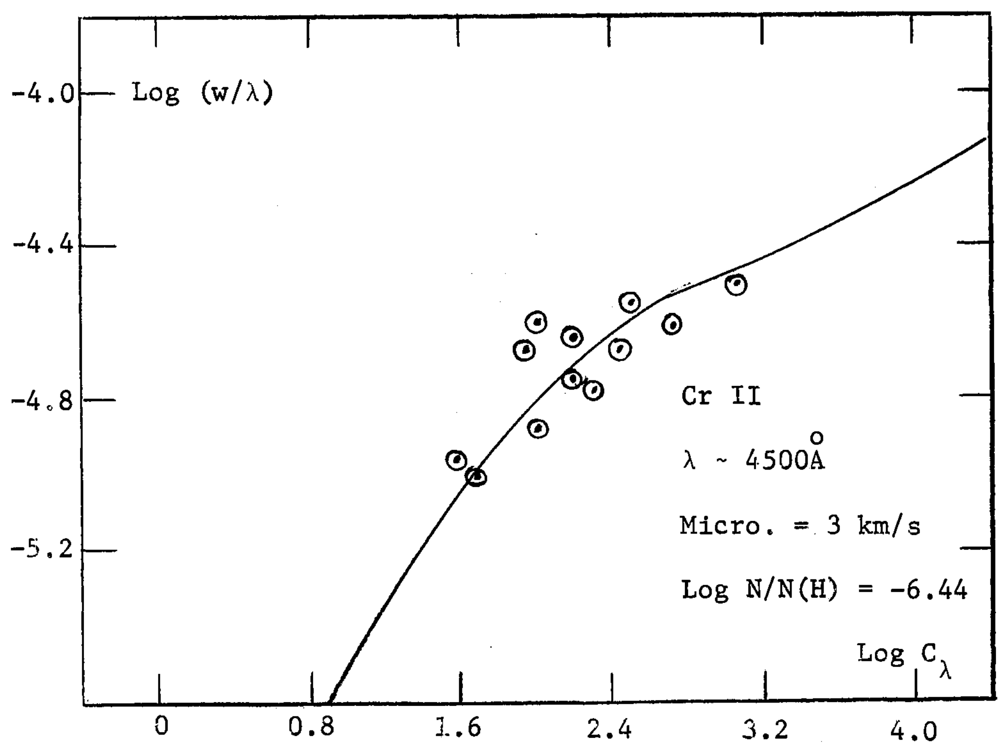


Figure 26. Empirical Curve of Growth for Cr II

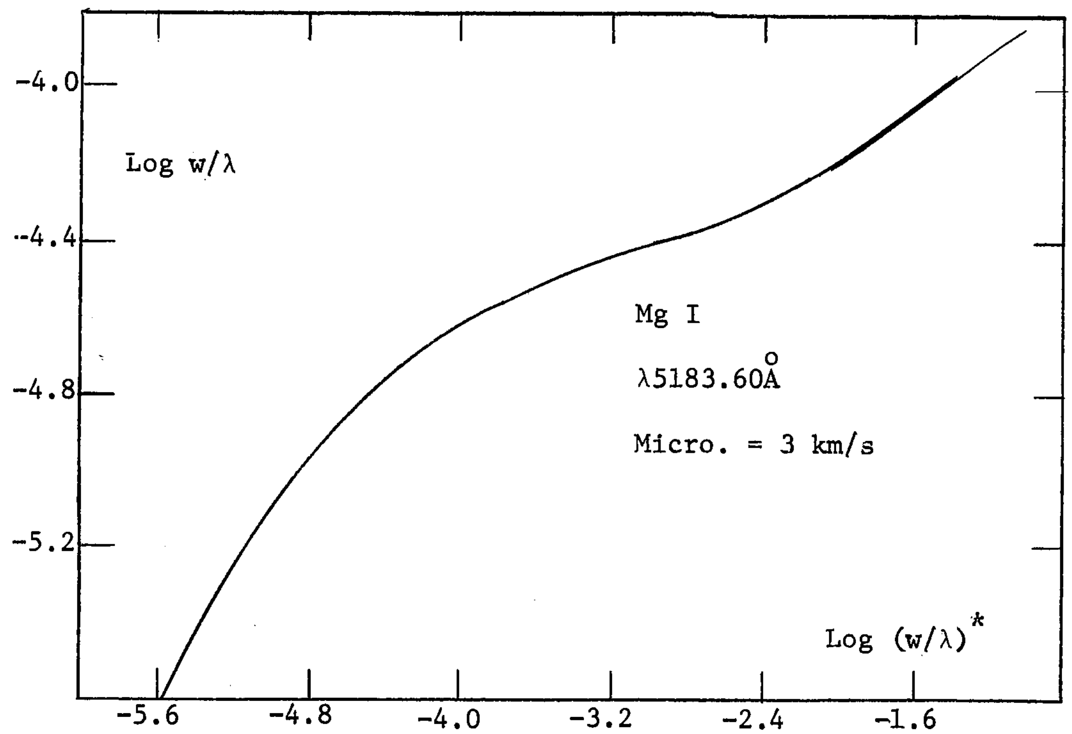


Figure 27. Theoretical Curve of Growth for Mg I

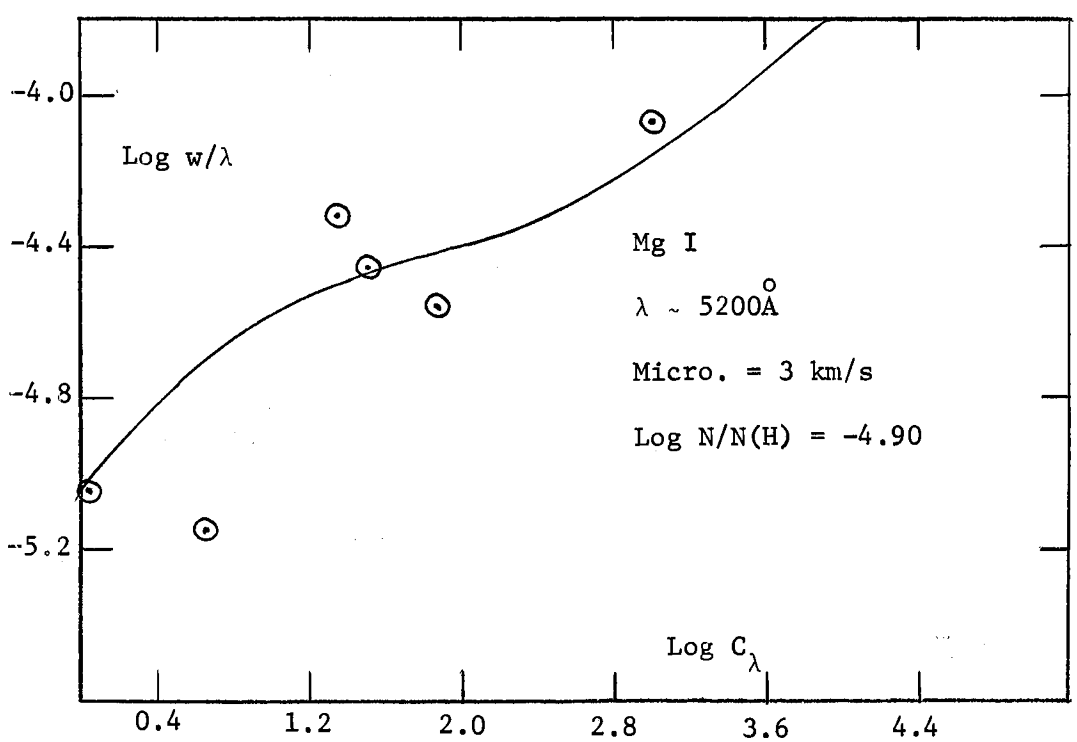


Figure 28. Empirical Curve of Growth for Mg I

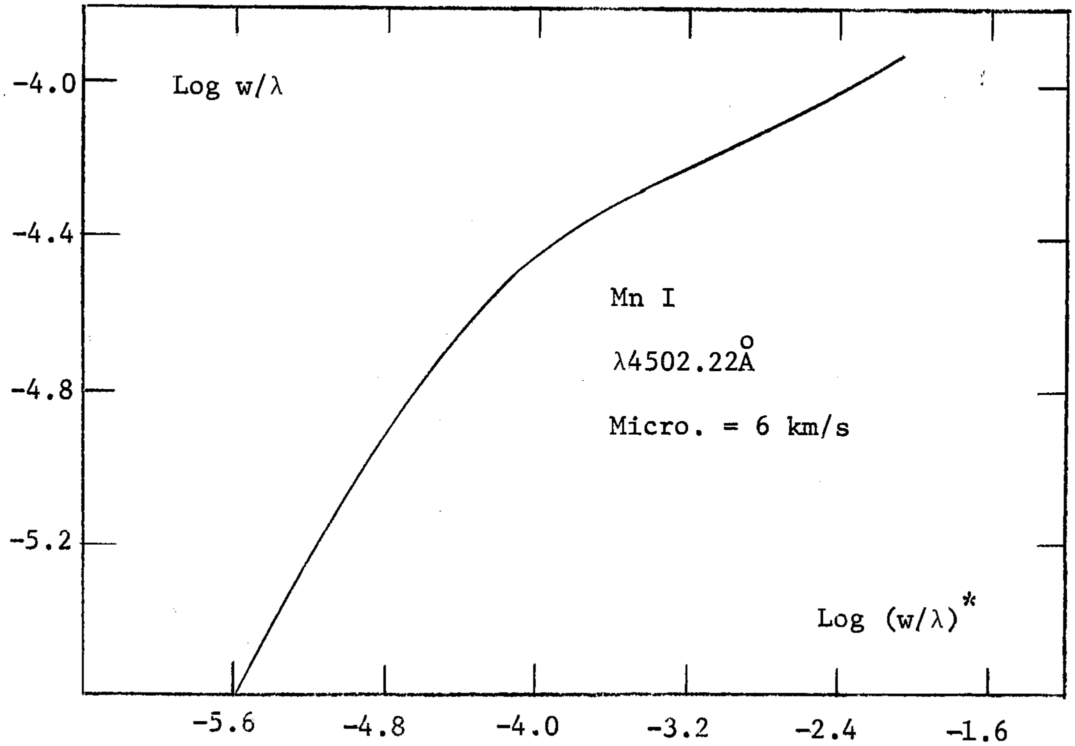


Figure 29. Theoretical Curve of Growth for Mn I

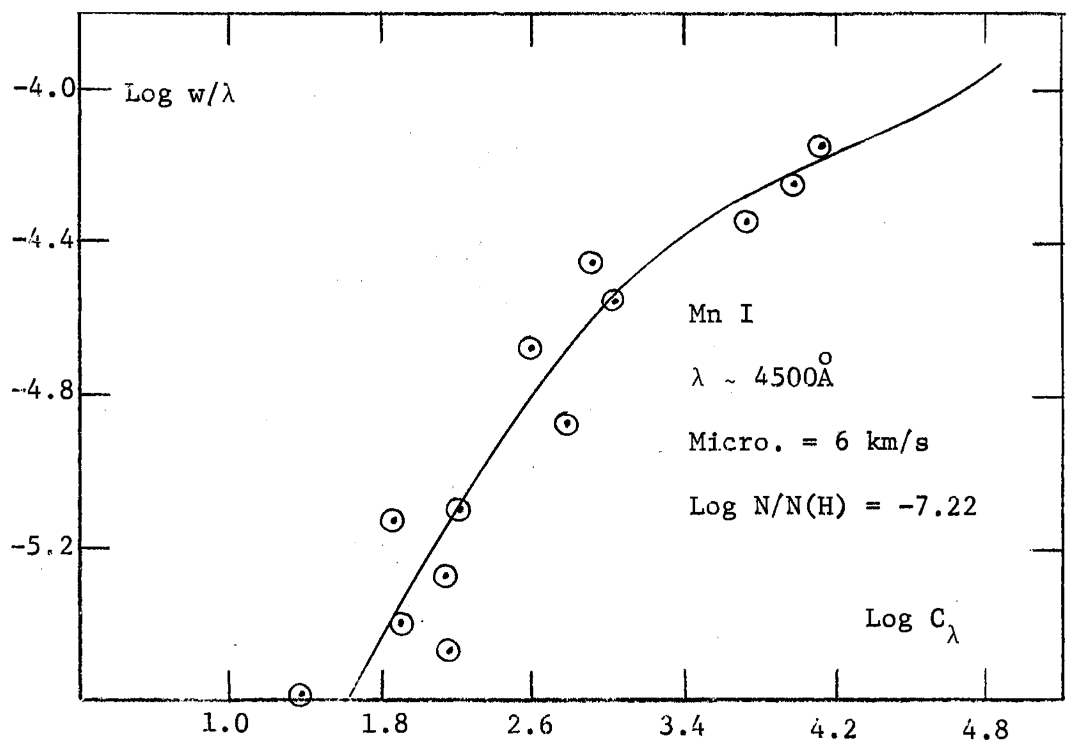


Figure 30. Empirical Curve of Growth for Mn I

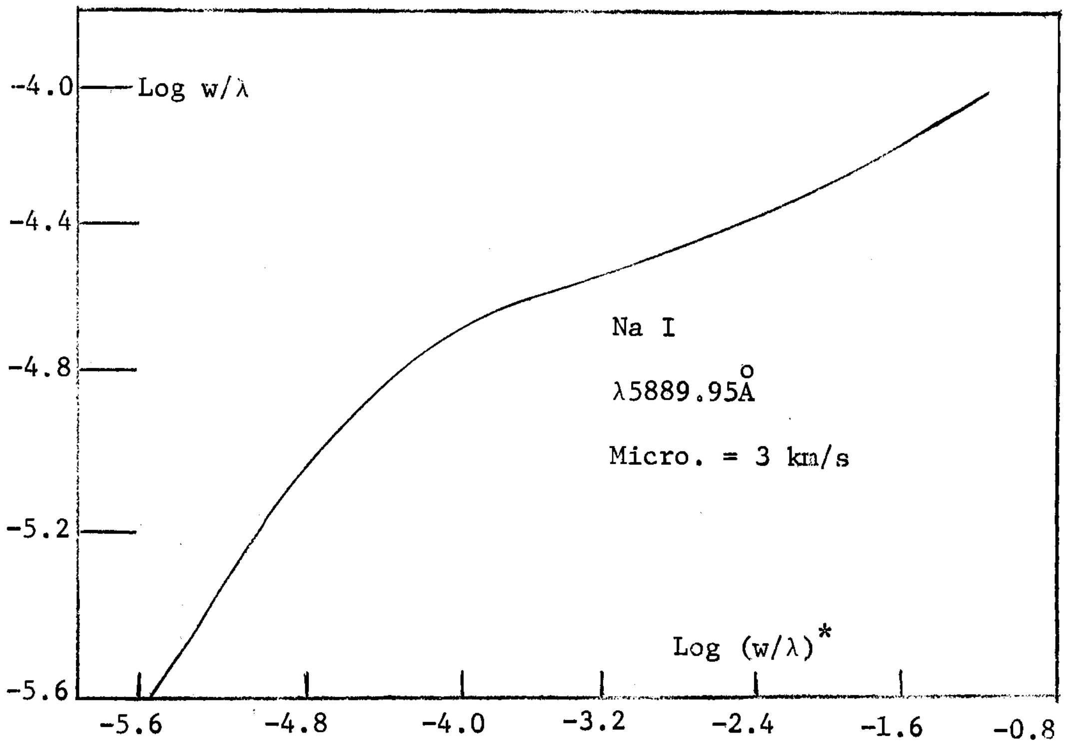


Figure 31. Theoretical Curve of Growth for Na I

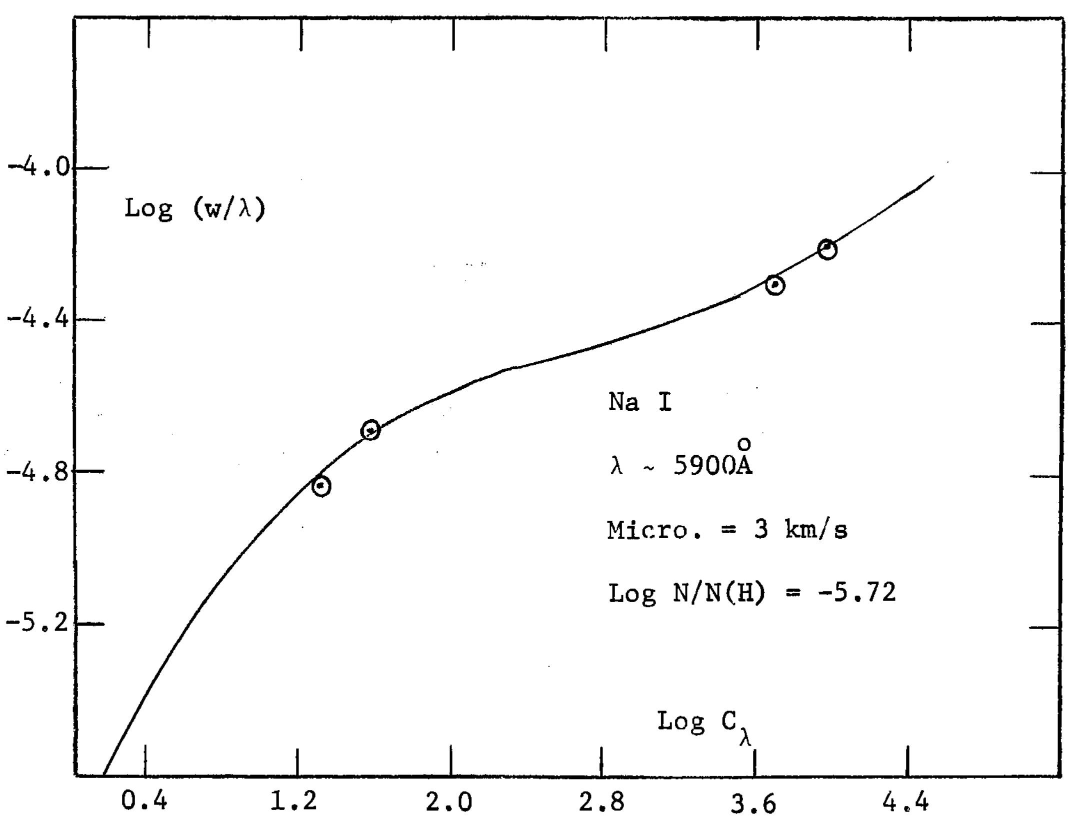


Figure 32. Empirical Curve of Growth for Na I

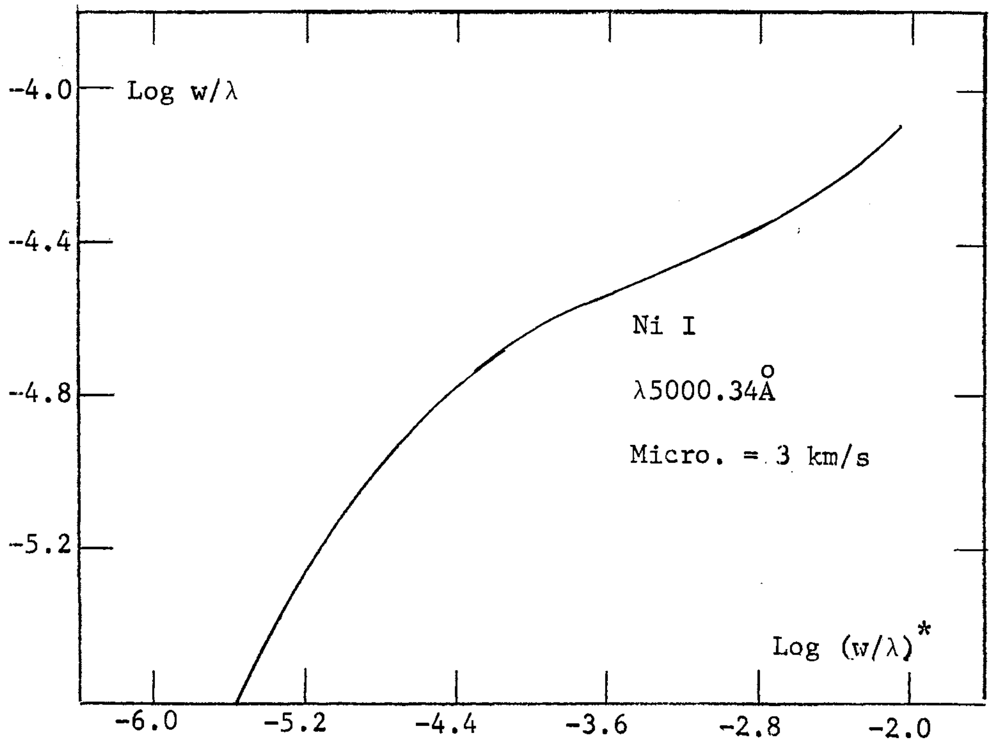


Figure 33. Theoretical Curve of Growth for Ni I

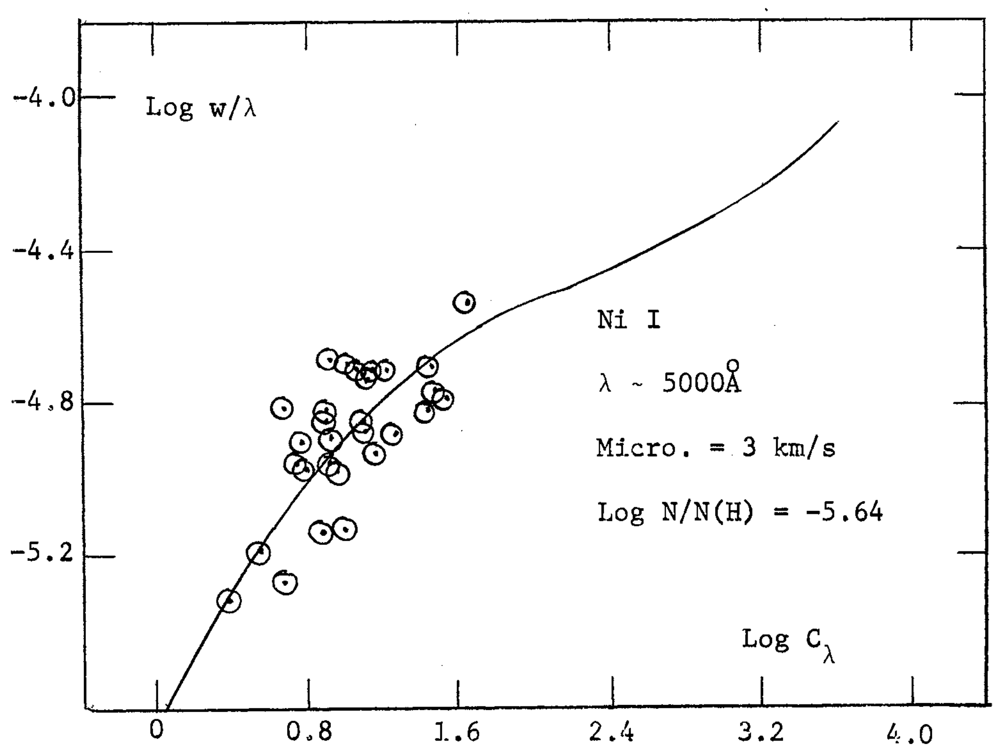


Figure 34. Empirical Curve of Growth for Ni I

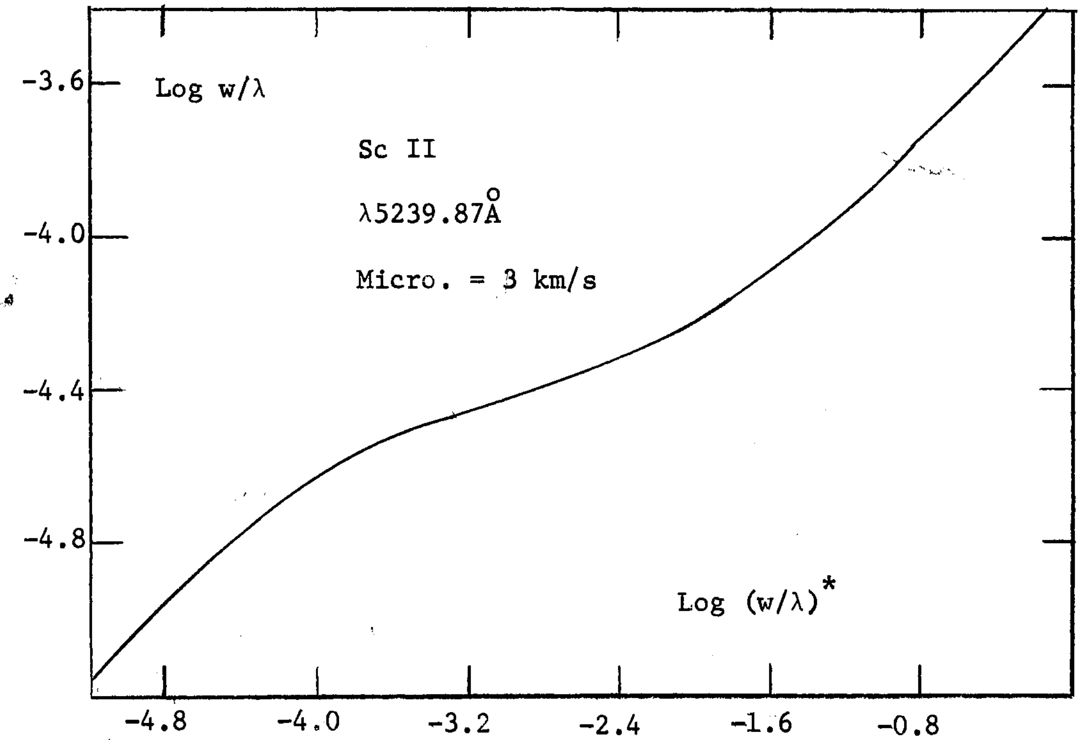


Figure 35. Theoretical Curve of Growth for Sc II

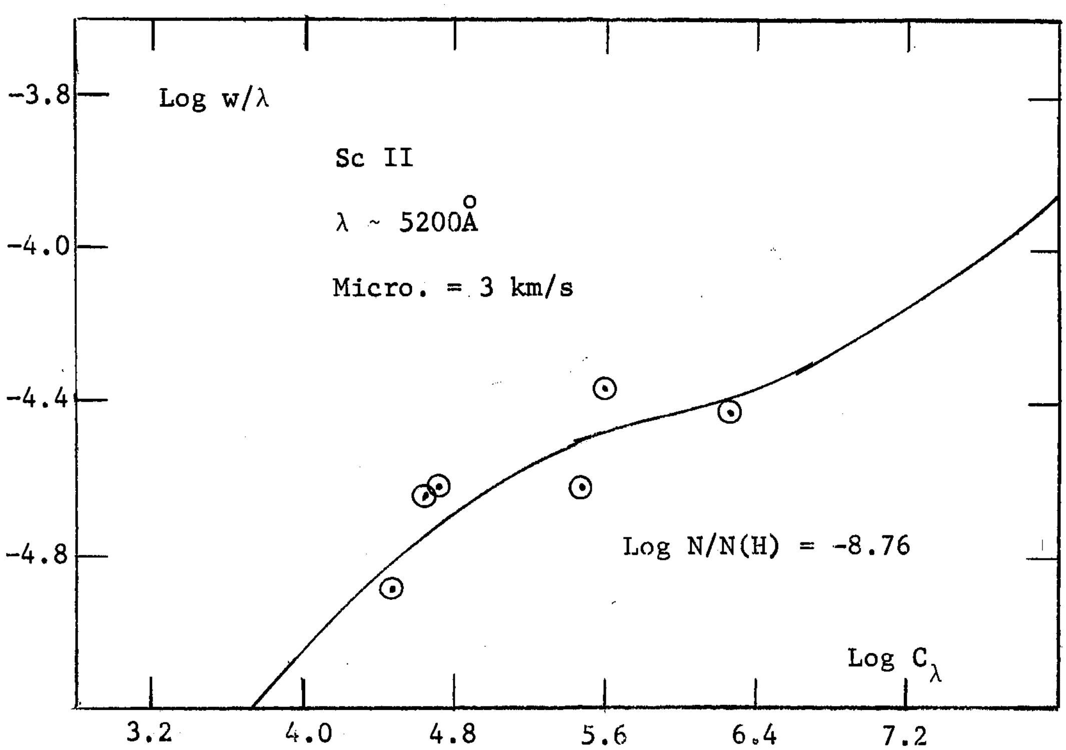


Figure 36. Empirical Curve of Growth for Sc II

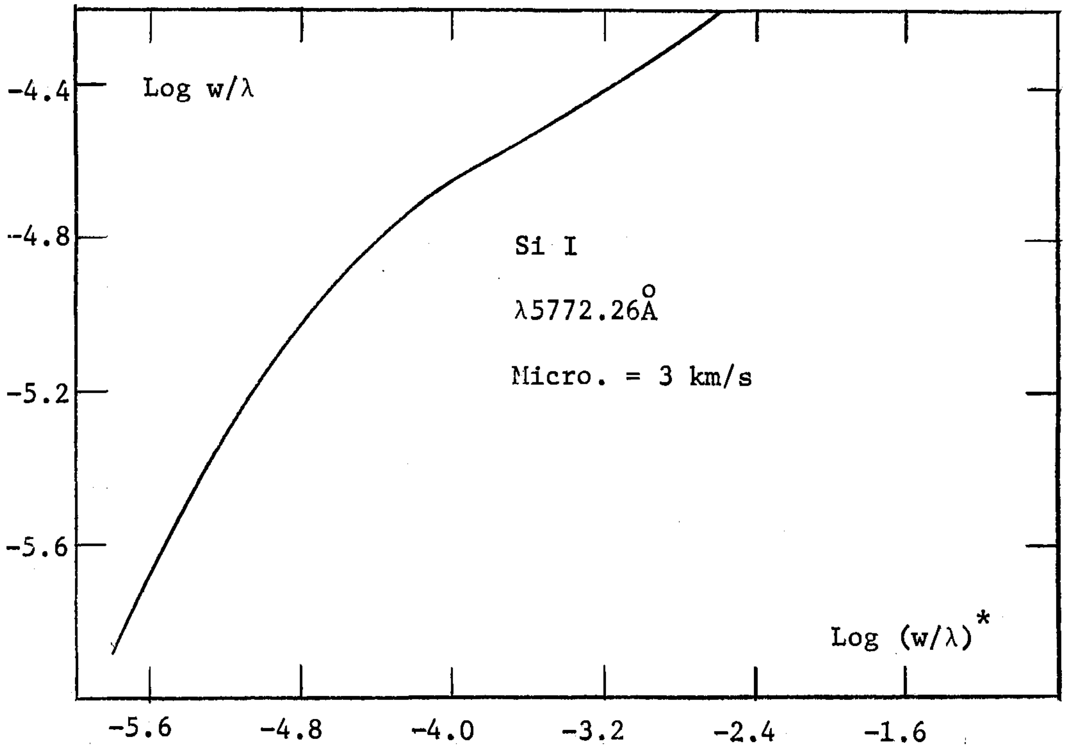


Figure 37. Theoretical Curve of Growth for Si I

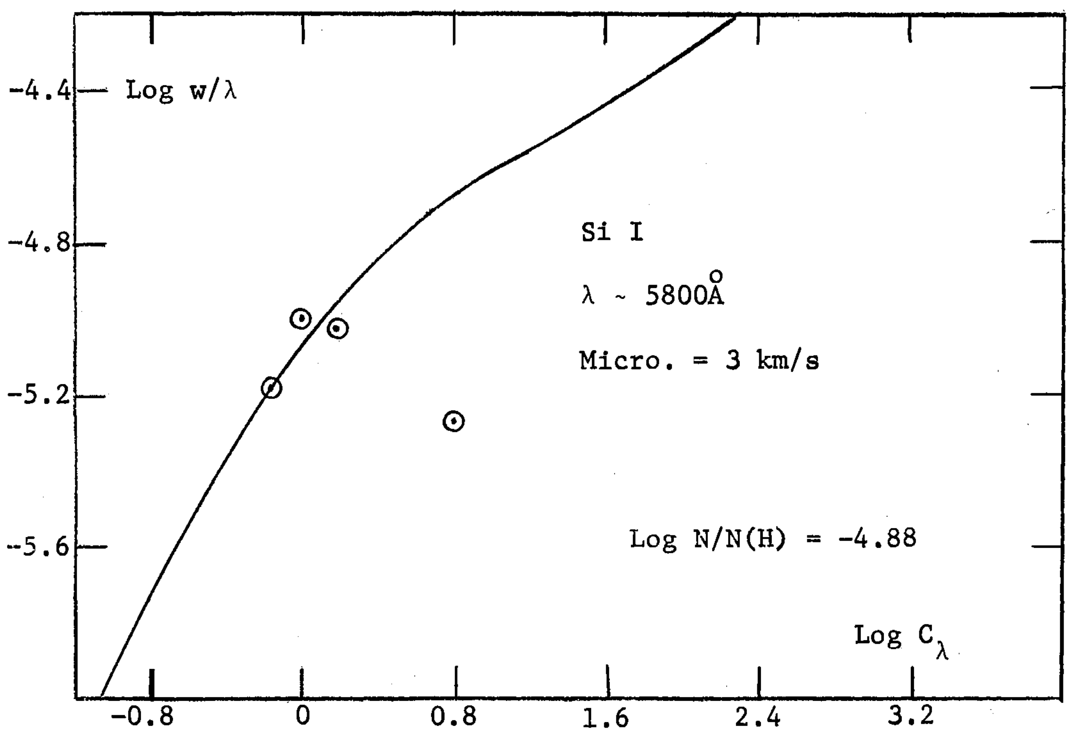


Figure 38. Empirical Curve of Growth for Si I

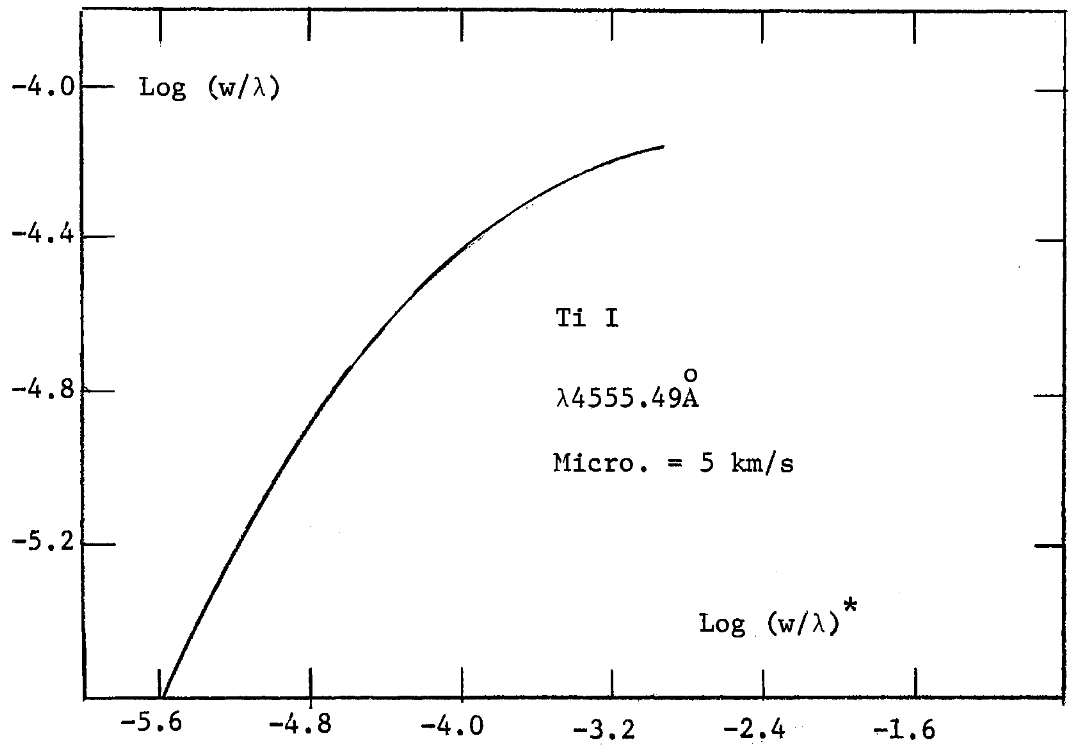


Figure 39. Theoretical Curve of Growth for Ti I

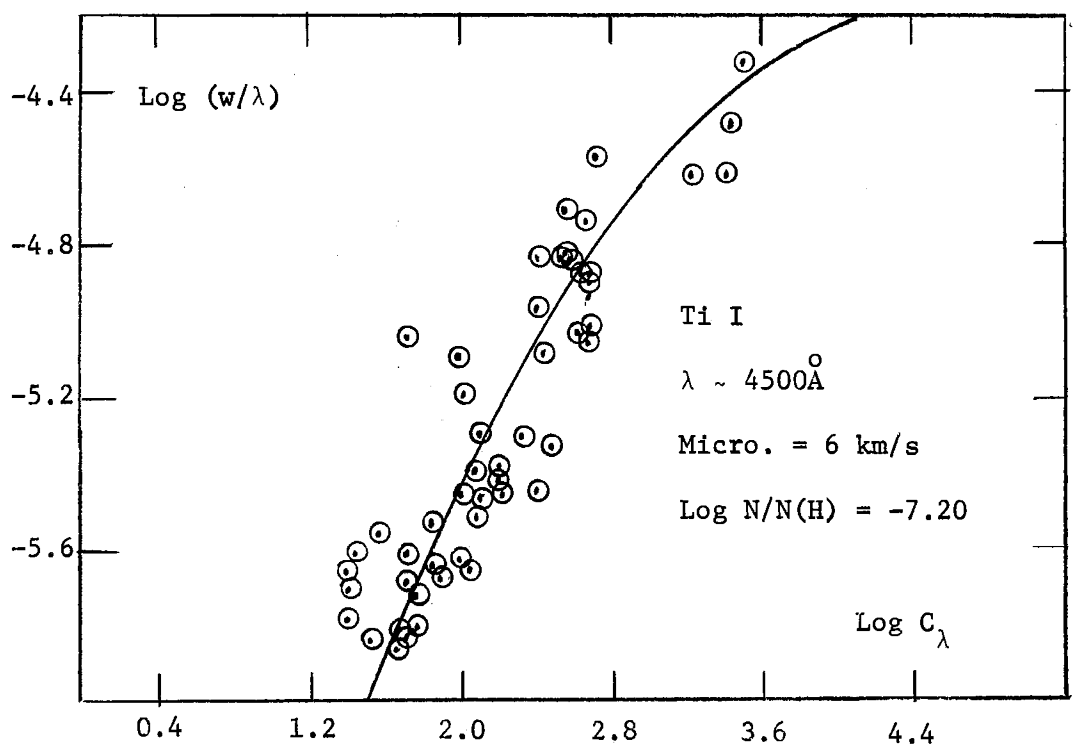


Figure 40. Empirical Curve of Growth for Ti I

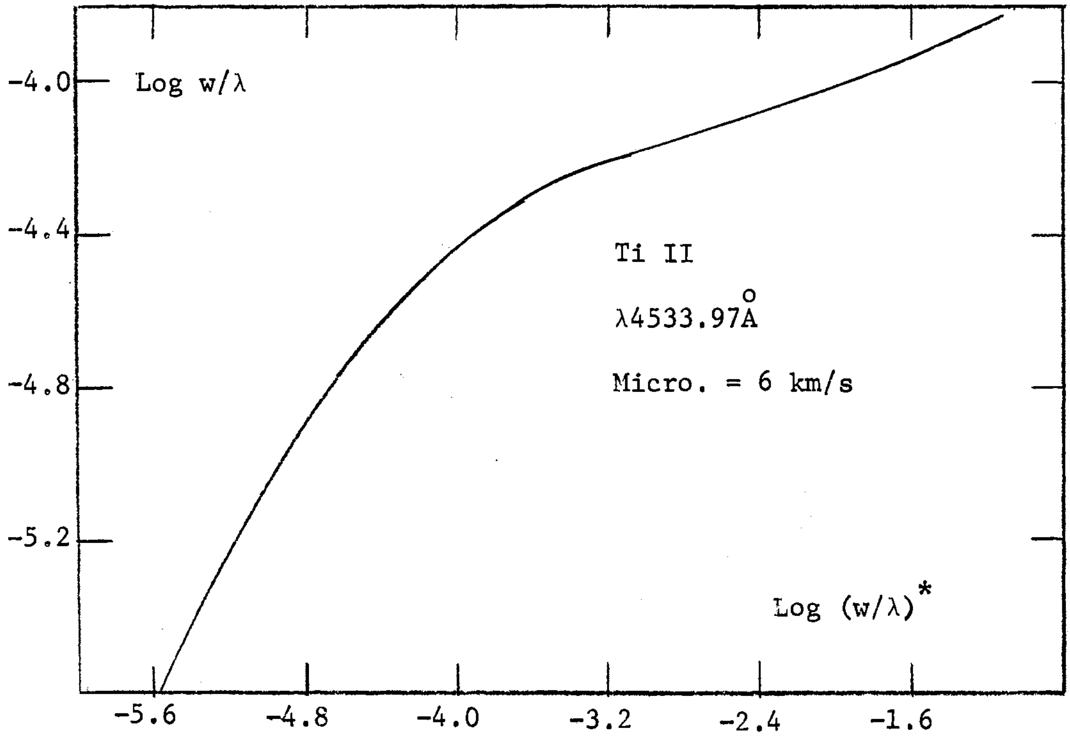


Figure 41. Theoretical Curve of Growth for Ti II

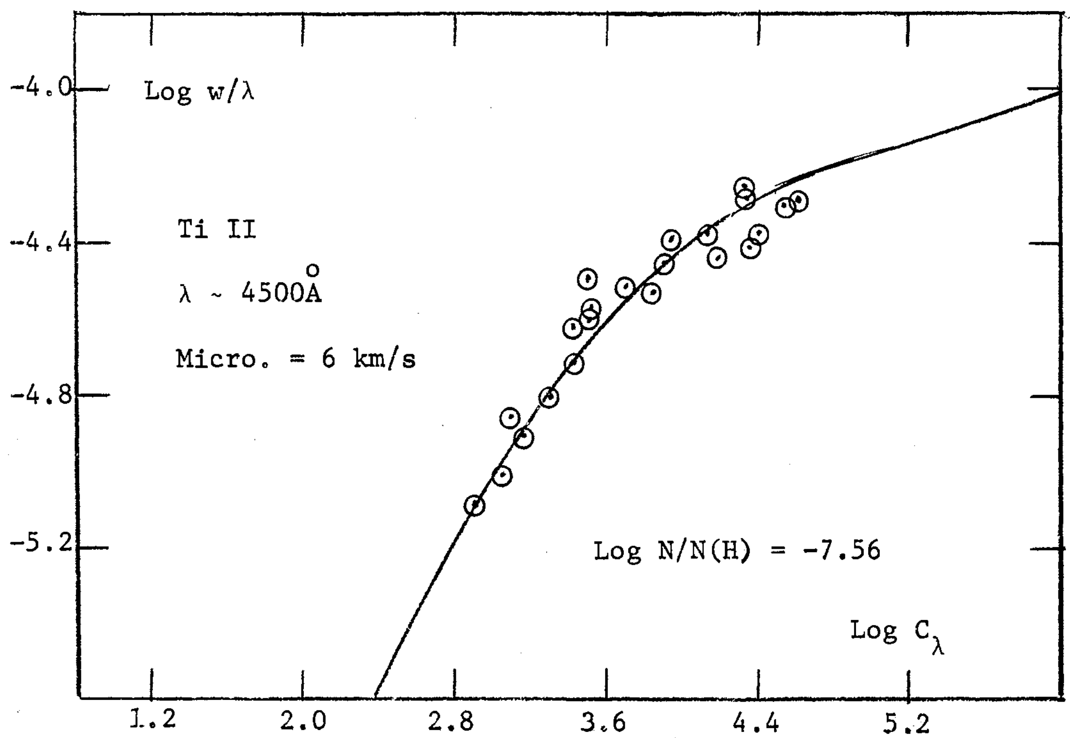


Figure 42. Empirical Curve of Growth for Ti II

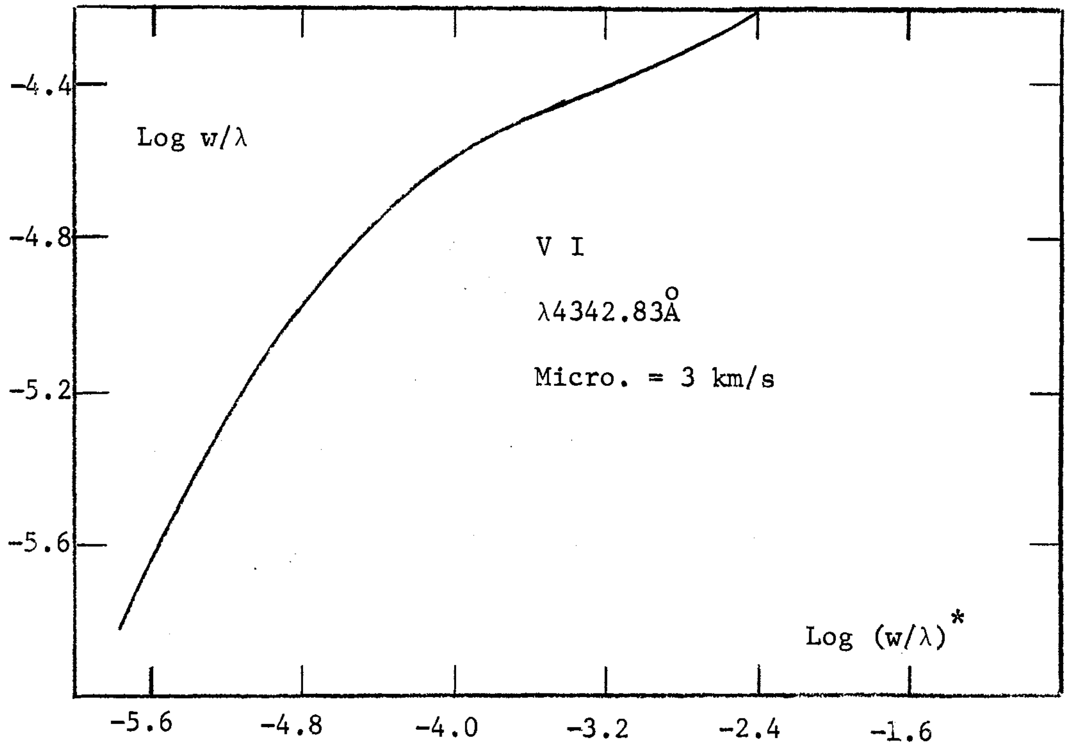


Figure 43. Theoretical Curve of Growth for V I

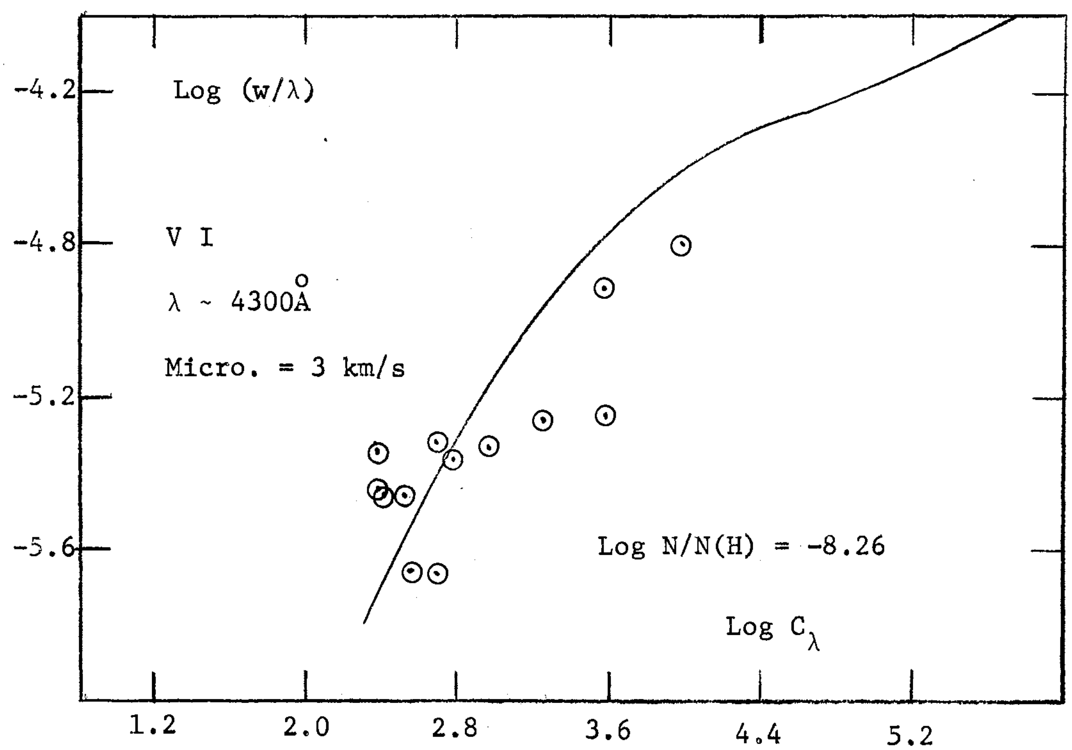


Figure 44. Empirical Curve of Growth for V I

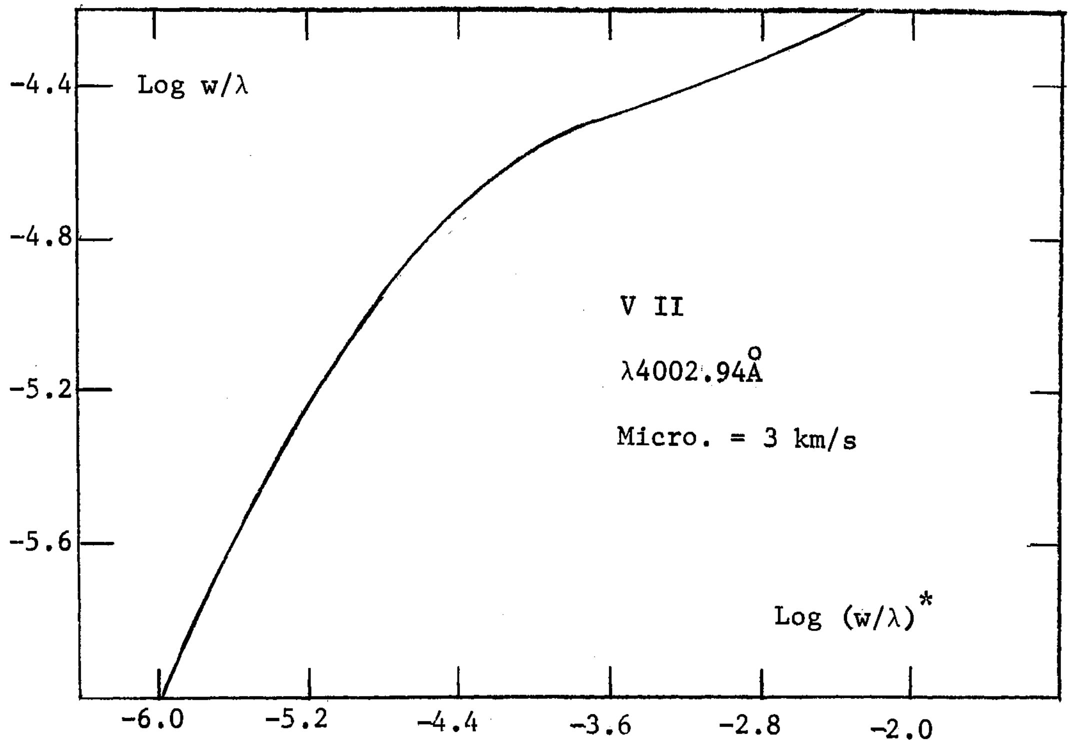


Figure 45. Theoretical Curve of Growth for V II

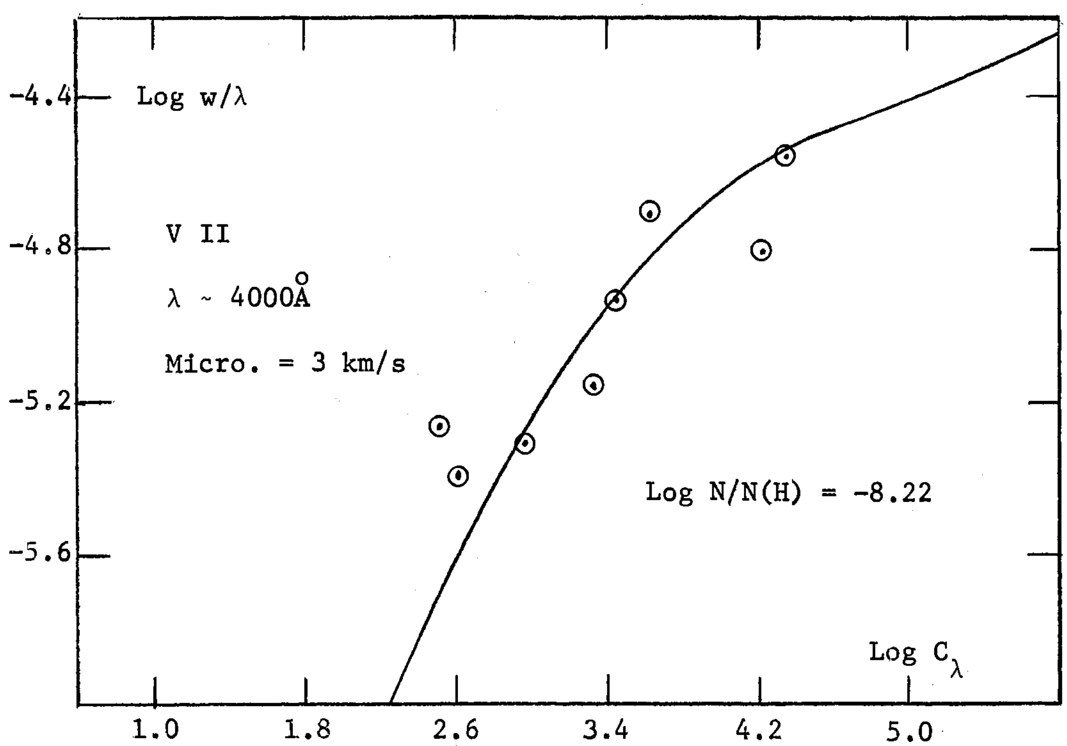


Figure 46. Empirical Curve of Growth for V II

14. The observed profile of the Fe II line indicates that it could be suffering from a serious blending effect or from a misplaced continuum. There is apparently no explanation for the discrepancy between theory and observation for the Fe I line unless this line is being formed in a region of the atmosphere not in local thermodynamic equilibrium.

## The Abundance Analysis

The ratio of the abundance of an element to hydrogen was computed for each individual observation according to the procedures outlined in Chapter III. The solar-type model atmosphere (see Chapter II) with an effective temperature of $6350^{\circ}K$ and $\log g = 4.0$, was used for the analysis employing a turbulence model having a depth independent micro-turbulent velocity of 3.0 km/s. The observational data are listed in Tables VIII through Table XXIII. In order, the labels list the element, the multiplet number, the wavelength, the excitation potential of the lower level, the logarithm of the product of the statistical weight and the oscillator strength, the damping constant for the quadratic Stark effect, the abscissa for the empirical curve of growth, the logarithm of the equivalent width divided by the wavelength, the statistical weight, and finally the logarithm of the abundance of the element relative to hydrogen. The application of a weighting procedure allows for the computation of a weighted mean abundance for all the lines of an element. Accompanying each table (Figures 19 through 46) are the theoretical curve of growth used for the determination of a mean abundance and the empirical curve of growth for the element under investigation.

The statistical weight of a line was based upon the following procedure. If the equivalent width of a line was measured three or more times, a statistical weight of two was assigned. Further, if the deviation in the measurements of the equivalent width departed significantly from the average a statistical weight of zero was given to the line. Since the uncertainty in the measurement of the equivalent width increases for the weak lines, lines with an equivalent width of approximately 20 mA were given a total statistical weight of one. An additional statistical weight was assigned to a line depending upon its position on the curve of growth. Small equivalent widths, falling on the linear portion of the curve of growth show more scatter than the stronger lines and so may be suffering from large systematic errors. Also even though moderately strong lines have equivalent widths more accurately determined they fall upon the flat portion of the curve of growth where a significant error in the abscissa can be produced by a small error in the equivalent width. Strong lines have equivalent widths very sensitive to the mechanisms for damping which occur during line formation and so are unreliable for the analysis. The most accurate results are produced from lines which fall upon the transition region of the curve of growth. These lines are assigned a statistical weight of two; all other lines carry a statistical weight of one due to their position. The total statistical weight of a line is then found by summing the statistical weights from its position and the number of measurements.

The errors involved in the determination of the abundances are very difficult to assess. The error involved in the ordinate of the curve of growth has already been discussed elsewhere in this study and attention must be turned to the abscissa of the empirical curve of growth. The most significant source of error for abundances lies in the values of log gf used for computing the empirical curve of growth. In many instances systematic errors are included in the published results in an unknown manner. Whenever possible all wavelength or excitation potential dependence was eliminated to some degree. In addition to this, little is known about the line broadening mechanism for the wings of spectral lines. This amount of uncertainty in the system of physical constants is entirely open to question. The values used for this analysis could be in error by a factor of two or more. Qualitatively, the random error reported in the measurements of the oscillator strengths gives a lower limit to the uncertainty (~ 0.3 dex) while the upper limit may be as great as 1.0 dex.

Further, limitations upon the fine-analysis procedure limit the reliability of the results. The temperature distribution was based upon a solar model which may not competely describe the state of affairs at all points in the atmosphere or account for the influence of the chromosphere. The manner in which turbulence is theoretically incorporated into the calculations may not adequately describe the physical situation. Finally, there is also the possibility of deviations from thermodynamic equilibrium to be considered, especially for the strong lines.

As a routine check upon the abundance results, a correlation of abundance with the excitation potential and wavelength was investigated for the Fe I lines observed in this study. The results of both these investigations is incorporated into Figure 47. The derived abundances should not depend upon the excitation potential of the lines used for the investigation. Any correlation here indicates that the temperature is incorrect for the region of line formation. Figure 47 shows no evidence of any such dependence of the abundance upon excitation potential.

If a systematic error with a functional dependence upon the wave-

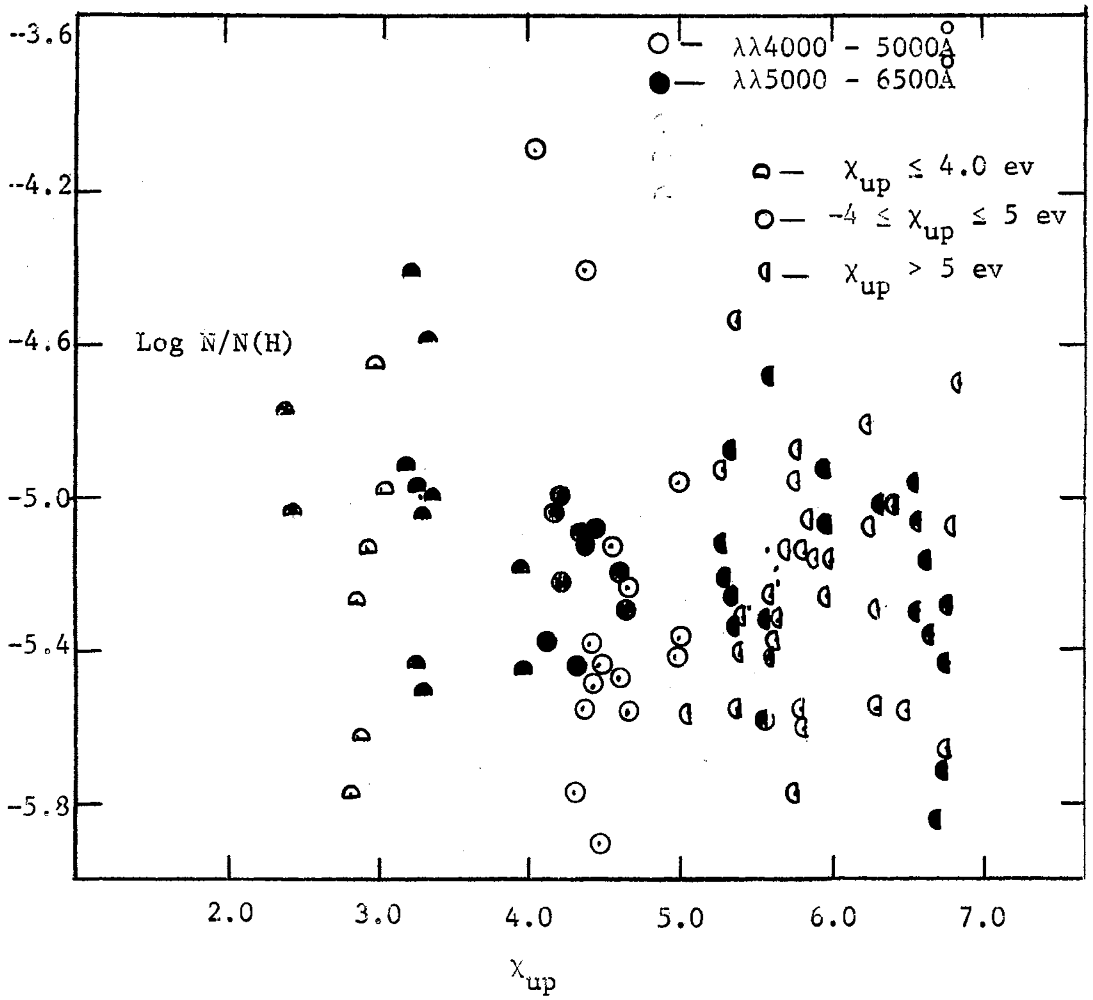


Figure 47. The Abundance of Fe I as a Function of the Excitation Potential of the Upper Level

length exists, the abundances will have an additional uncertainty. The earlier results of Evans, Weems and Schroeder (1970) indicated that some dependence might be expected; however, the results of Figure 47 show no overall correlation with the possible exception of the lines of high excitation potential falling between λλ4000-5000. In addition to this, the abundances derived for iron in both stages of ionization were the same. This lends further evidence to support the results of this study.

## Results for the Individual Elements

### Calcium

The results for neutral calcium are displayed in Table VIII and Figures 19 and 20. The f-values used for the analysis come from a tabulation by Wiese, Smith, and Miles (1969). For a large majority of the lines an accuracy of no greater than 10% and as much as 50% can be expected. Twenty-one calcium lines measured by Peebles (1964) were investigated yielding a mean abundance of

$$\log \frac{N_{Ca}}{N_H} = -6.08 \ (-6.06).$$

The weighted mean abundances is indicated above by the value in parenthesis. In some of the lines, the inaccuracy in the f-values was reflected in the statistical weight used for the analysis. However, the scatter in the data points is quite low and is reflected in the similar abundance results from both techniques. All lines were grouped together and the mean abundance determined from the λ5512.98 line.

## Cobalt

The equivalent widths of twelve lines of neutral cobalt used for the abundance determination are listed in Table IX. The source of the oscillator strengths was the compilation of Corliss and Bozman (1962). These f-values were known to contain a systematic excitation potential dependence. An attempt was made to remove this dependence by using a correction factor obtained from the publication by Takens (1970). Figure 21 and Figure 22 indicates the result of this procedure. The scatter in the data is quite large which is primarily the result of the presence of a large number of weak lines in the analysis. The possibility of large systematic errors in the data resulted in a low statistical weight which probably accounts for the difference in the reported abundances. The abundance of Co I in Theta Ursae Majoris was found to be

$$\log \frac{N_{Co}}{N_H} = -6.88 \ (-6.57) \ .$$

## Chromium

The analysis of this element was carried out upon both the neutral and the first stage of ionization. The observation data for the 65 lines of Cr I are reproduced in Table X shown by Figures 23 and 24. The data extend over a wide range of excitation potential and the equivalent widths are generally very dependable (Mangold, 1968). The f-values are those of Corliss and Bozman and have been altered to account for their excitation potential dependence using the Takens (1970) correction factor. The mean abundance of the group was determined to be -6.80 (-6.59).

For the Cr II lines indicated in Table XI, Corliss and Bozmann f-values were not available and those of Warner (1967, 1968) were utilized instead. Some of the Warner f-values are empirically derived from stellar sources and so will tend to produce less scatter in the data as indicated by Figures 25 and 26. This does not necessarily imply a better abundance result. The abundance results from the Cr II lines was -6.44 (-6.36) which was somewhat different than obtained for Cr I. The difference in reported abundances from the two stages of ionization is not significant and is probably due to the different scales used for the f-values. When both stages of ionization are considered, the abundance of chromium was determined to be

$$\log \frac{N_{Cr}}{N_H} = -6.62 \ (-6.53) \ .$$

Iron

Table XII contains a listing of the one hundred and seven lines of Fe I used for the analysis. An additional eighteen Fe II lines, shown in Table XIII, were incorporated for the evaluation of the abundance of iron. f-values from Corliss and Tech (1968) were involved in the computations. Since these values are known to have a systematic excitation potential dependence, a correction factor based upon the amount of shift needed to define a single empirical curve of growth was utilized. The actual factor used has been discussed earlier in this study (Chapter IV).

Theoretical and empirical curves of growth were constructed and the Fe I lines (see Figures 2 and 3) separated into two distinct wavelength regions, λ4200 and λ5400. The lines within each region have essentially the same curve of growth. A derived abundance was then obtained from Figures 3 and 4 of -5.20 dex, while a weighted abundance of -5.16 in the logarithm was determined from Table XII.

The Fe II lines underwent a similar investigation. The theoretical curve of growth for λ5414.09 in Figure 4 was computed and used to derive a mean abundance of -5.20. From Table XIII a value of -5.23 was computed for the weighted abundance for Fe II.

The results from both stages of ionization were combined statistically to yield a mean abundance for iron of

$$\log \frac{N_{Fe}}{N_H} = -5.20\ (-5.17)\ .$$

As usual, the weighted average abundance is shown in parenthesis.

Magnesium

Only the neutral atom was investigated for this element since few lines of this element were identified in the atmosphere of Theta Ursae Majoris. The f-values are from Wiese, Smith, and Miles (1969). Again the reported values range in accuracy from 10% to 50%; so in addition to the small number of observational data available, the uncertainty in the abscissa is large. For some unknown reason, the computation of log $C_\lambda$ for the λ5183.60 line could not be performed which explains the abundance result appearing in Table XIV for this line. From Figures 27 and 28 a mean abundance of

$$\log \frac{N_{Mg}}{N_H} = -4.90\ (-4.60)$$

was obtained. The weighted mean value is also shown in parenthesis and both results are questionable as to their accuracy.

## Manganese

Corliss and Bozman f-value were used for the analysis of the 22 lines of neutral manganese listed in Table XV. Since most of the data fall on the transition portion of the curve of growth and has been evaluated from a large number of individual measurements, the data should be quite reliable. Figures 29 and 30 show the theoretical and empirical curve of growth constructed for this element. Initially, the theoretical curve was calculated with the normal turbulence model; however, the data points fell far above this curve, suggesting a larger value of the turbulent velocity. A best fit was achieved for a microturbulent velocity of 6 km/s. This scatter in the data as well as the reliability of the f-values and the equivalent width, support the evidence of unusual microturbulence for the region of line formation of Mn I. A similar phenomenon was observed by Aller (1942) in this investigation of $\alpha$ Cyg where curves of growth for Cr II and Ti II differed substantially from that of Fe II; however, Greenstein (1948) makes no mention of any peculiarities in Mn I in his analysis of several F-type stars, including Theta Ursae Majoris. The probable physical causes for such a phenomenon cannot really be justified by a higher-than-normal microturbulent motion since the lines seem to be formed in about the same depth as for Fe I and Fe II. Also an excitation potential dependence could be overruled since the Fe I and II lines used for the turbulence analysis were within the range of those of Mn I. More probably the difficulty lies in the elementary nature of the curve of growth theory.

Using the derived microturbulent velocity of 6 km/s, the abundance determination yielded the values,

$$\log \frac{N_{Mn}}{N_H} = -7.22 \ (-7.02) \ .$$

Sodium

The four Na I lines used in the analysis are given in Table XVI, and the curves of growth are displayed as Figures 31 and 32. The theoretical curve is for $\lambda$5889.95 and $\chi(r,s) = 0$ e.v. All the observed data fall on the mean curve of growth yielding a derived abundance of

$$\log \frac{N_{Na}}{N_H} = -5.72 \ (-5.80) \ .$$

The absolute scale for the f-values is from the tabulation by Wiese, Smith and Miles (1969). The accuracy in the f-values of the sodium D-lines is three per cent and for the higher excitation potential ones, twenty-five per cent. This tends to re-enforce the reliability of the abundance result even though the number of observations is low.

Nickel

The observation data used for the analysis of this element are listed in Table XVII while the curve of growths employed for the study are shown by Figures 33 and 34. Most of the data are quite reliable, falling on the transition region of the curve of growth, and the scatter is low. The mean abundance determined for Ni I from Figures 34 is

$$\log \frac{N_{Ni}}{N_H} = -5.64 \ (-5.55) \ .$$

Differences between the results from the two abundance techniques are not significant.

The oscillator strengths come from the work of Corliss and Bozman (1962). Any dependence of the results upon the excitation potential of the line was at least partially removed by using a correction factor published by Takens (1970).

Scandium

The analysis of Sc II was performed using the corrected (Takens, 1970) f-values of Corliss and Bozman (1962); therefore, the observational data should be relatively free from any excitation potential dependence. The six lines employed in the analysis are listed in Table XVIII and the abundance determined using Figures 35 and 36. If for no other reason the luck of observations introduces some doubts about the reliability of the results. However, the scatter is low indicating the absence of any systematic errors. The mean abundance derived from the curve of growth and by the weighting method is

$$\log \frac{N_{Sc}}{N_H} = -8.76 \ (-8.51) \ .$$

Silicon

The observational data used for the analysis of this neutral element are given by Table XIX and the curve of growths employed by Figures 37 and 38. The available data are disappointing and the reliability of the f-values no better than 50%. The low scatter in the data points out the false sense of security induced by the appropriate choice of the scale of the f-values. The relative abundance of Silicon was found to be

$$\log \frac{N_{Si}}{N_H} = -4.88 \ (-4.88) \ .$$

Titanium

Fourty-nine lines of Ti I and twenty-two lines of Ti II listed in Tables XX and XXI were used for the analysis of Titanium. The results for Ti I employed the use of f-values of Corliss and Bozman. A correction factor (Takens, 1970) was utilized to remove the excitation potential dependence of the absolute scale used by these investigators. For Ti II, f-values compiled by Warner (1967, 1968) were employed. No systematic dependence upon excitation potential is known for these f-values.

Theoretical curves of growth, Figures 39 through 42, were calculated using the turbulence model suggested by the analysis of the iron lines. This yielded a curve of growth falling well below the observation points on the empirical curve of growth. The microturbulence velocity was then increased until a best fit was achieved for both Ti I and Ti II for a depth independent model with a microturbulent velocity of 6 km/s. This phenomenon was also observed for Mn I and similar effects have been observed in other stars (Aller, 1942; Greenstein, 1948). It is significant that this phenomenon is common to both stages of ionization, not just an effect due to an abnormal population difference for the two stages of ionization. That is, the ionization equilibrium is correct. Stream motions could be the physical cause or perhaps some factor unaccounted for by the theory used to compute the curve of growth.

The abundance results using a 6 km/s microturbulence velocity were determined for Ti I to be -7.20 (-7.28) and -7.56 (-7.96). The difference between the results for the two stages of ionization are probably due to differences between the absolute scales of the f-values used for the analyses. For both stages of ionization, the mean abundance is

$$\log \frac{N_{Ti}}{N_H} = -7.38 \ (-7.46) \ .$$

The accuracy of the result is high since a large number of observational data was available covering a large range of excitation potentials. The statistical weight assigned to most of the lines was large which indicates that the measured equivalent widths used in the analysis were very reliable.

Vanadium

Eighteen lines of V I are listed in Table XXII and the curves of growths in Figure 43 and 44. The theoretical curve is for λ4342.83 and $\chi_{\ell}$ = 1.86 ev. The f-values are those of Corliss and Bozman (1962) and the systematic errors removed using the appropriate correction factor (Takens, 1970) for the excitation potential of the upper level of the transition. The scatter and quality of the data is such that the abundance results probably show a substantial error. For the V I lines a derived abundance of -8.26 was obtained from Figure 44 while a weighted mean abundance of -7.54 was found.

The V II results were based upon eight observation points which are listed in Table XXIII. Because of the incompleteness of the Corliss and Bozman list of f-values, Warner's (1967, 1968) compilation was utilized. The tendency of the Warner scale is to produce less scattering; however, the accuracy is not necessarily increased.

Figures 45 and 46 yielded V II abundances with a mean value of -8.77 (-8.17).

When the results from both stages of ionization were incorporated, an abundance of

$$\log \frac{N_V}{N_H} = -8.24 \ (-7.68)$$

was determined. Of the two techniques the weighted mean abundance, enclosed in parenthesis above, is more reliable.

# CHAPTER VI

# CONCLUSIONS

## The Model Atmosphere

The spectral analysis of the star Theta Ursae Majoris was performed using a pressure-opacity flux model with a scaled solar temperature distribution. From a grid of models, selection of the representation model was based upon an analysis of the hydrogen line profiles as well as U-B-V and multi-color photometry. A representative model atmosphere with an effective temperature of 6350$^{\circ}$K and logarithm of the surface gravity of 4.0 was employed for the analysis.

Observed profiles of the iron-peak elements were measured and compared to those calculated on the basis of the assumed model. Near the cores of the lines, the temperature distribution predicted stronger intensities than were observed. This suggests that the empirical solar temperature distribution fails to adequately represent the temperature stratification of Theta Ursae Majoris near the boundary of the atmosphere.

## The Turbulence Model

The presence of large and small scale mass motions in the atmosphere of Theta Ursae Majoris was investigated from an analysis of the iron lines. All theoretical calculations assume local thermodynamic equilibrium and employ the Planckian gradient technique.

Both theoretical and empirical curves of growth were computed for the model atmosphere selected for Theta Ursae Majoris. In order to achieve a fit between the empirical and calculated curve, it was necessary to include a small microturbulent velocity of 3 km/s. This value is somewhat smaller than was reported in an earlier analysis (Evans, Weems and Schroeder, 1970). The value of the microturbulent velocity was derived from the curve of growth using a homogeneous, depth-independent model.

From the correlation existing between the halfwidth of a line and its equivalent width, an assessment of the amount of macroturbulent motion in the stellar atmosphere was derived. In order to achieve the results indicated by the empirical curve of Fe I, an apparent 3.5 km/s macroturbulent velocity was found to be necessary. The difference which exist between this result and the value reported earlier (Evans, Weems, and Schroeder, 1970) are due to a correction for instrument broadening of the lines introduced by the spectrographs at Dominion Observatory.

The macroturbulence calculations were performed assuming cells with velocity components satisfying a dispersion relation. The result obtained from the iron lines was evaluated using a macroturbulence model of the atmosphere having homogeneous, depth-independent components.

## The Analysis of the Line Profile

Using the model atmosphere selected for this star, line profiles were computed for a few selected lines of Fe I and Fe II. In a comparison with the observed profiles, it was necessary to include the turbulence model and increase the damping in the wings of the lines to achieve a fit. The observed profiles of Theta Ursae Majoris show abnormally weak metal lines compared to other stars in the same spectral class. This was demonstrated in the difference between central intensities predicted by the model and the observed quantity. A portion of this effect was also thought to be due to an incomplete temperature distribution near the outer boundary of the atmosphere.

## The Abundances

The abundances of twelve elements found to exist in Theta Ursae Majoris were determined. Selection was based upon the availability and the quality of observational data for this star. The abundance of each individual line was computed using a theoretical curve of growth based upon the analysis of the Fe I lines.

The evaluation of the titanium and manganese lines produce an interesting anomaly in the size of the predicted microturbulent velocity. The analysis of all elements, some in two stages of ionization confirm the conclusion derived from the Fe I and Fe II lines that the microturbulence in the atmosphere is very close to 3 km/s; however, the empirical curves of growth for Ti I, Ti II, and Mn I could only be described by the addition of a velocity distribution twice as large. Curiously enough, this effect may not be physical in nature since the abundances reported by Mangold and Weems do not differ by a significant amount.

For the sake of completeness, the abundance results from this study are compared to those obtained in a coarse analysis of Theta Ursae Majoris by Mangold (1968) and to the solar abundances derived by Goldberg, Muller, and Aller (1960). The abundances listed in Table XXIV are determined relative to the hydrogen abundance in the stellar atmosphere. The first column lists the element for which an abundance was derived.

TABLE XXIV

A COMPARISON OF ABUNDANCE RESULTS

| Element | GMA Solar Abundances | Mangold ΘU Ma | Weems ΘU Ma | | Δ Log $N/N_H$ | |
|---|---|---|---|---|---|---|
| | | | Derived | Weighted | Derived | Weighted |
| Ca | -6.12 | -6.26 | -6.08 | -6.06 | +0.18 | +0.20 |
| Co | -7.36 | -7.87 | -6.88 | -6.57 | +0.99 | +1.30 |
| Cr | -6.64 | -6.93 | -6.62 | -6.53 | +0.31 | +0.40 |
| Fe | -5.43 | -5.69 | -5.20 | -5.17 | +0.49 | +0.53 |
| Mg | -4.60 | -5.54 | -4.90 | -4.60 | +0.64 | +0.94 |
| Mn** | -7.10 | -7.51 | -7.22 | -7.02 | +0.29 | +0.49 |
| Na | -5.70 | -5.96 | -5.72 | -5.80 | +0.34 | +0.16 |
| Ni | -6.09 | -6.48 | -5.64 | -5.55 | +0.84 | +0.93 |
| Si | -4.50 | -5.20 | -4.88 | -4.88 | +0.32 | +0.32 |
| Sc* | -9.18 | -8.79 | -8.76 | -8.51 | +0.03 | +0.28 |
| Ti** | -7.32 | -7.49 | -7.38 | -7.46 | +0.11 | +0.03 |
| V | -8.30 | -8.60 | -8.24 | -7.68 | +0.36 | +0.92 |

*The results from Mangold were calculated on the basis of the Sc II lines.

**The result reported by Weems was calculated using a 6 km/s microturbulent velocity.

Column two gives the solar abundances of Goldberg, Muller and Aller for the element in its first stage of ionization. The third column contains the abundances derived by Mangold for the first stage of ionization except for Scandium. Because of insufficient data, the results for Scandium are based upon the Sc II lines. The abundances listed by Mangold were determined relative to their respective values in the sun and so had to be converted to the form used in this analysis by the expression

$$\log(\frac{N}{N_H}) = \log(\frac{N}{N_H})_{sun} + \log(\frac{N_{star}}{N_{sun}}) .$$

Solar values for the abundances of the elements with respect to hydrogen were obtained from the tabulation of Goldberg, Muller and Aller (1960). The column heading, Weems, lists the derived abundances relative to hydrogen as determined from the mean curve of growth and also the statistically weighted value. The final column,

$$\Delta \log N/N_H \equiv \log(N/N_H)_{Weems} - \log(N/N_H)_{Mangold} .$$

The abundances determined for Theta Ursae Majoris are very much like those in the sun. This result has been confirmed by other investigations of stars in the same spectral category. A slight tendency towards over abundance exists for the observed elements except for sodium, silicon, and titanium; however, direct comparison of the Goldberg, Muller and Aller solar abundances is inconclusive because of a difference in the choice of f-values used for the studies. Table XXIV also indicates that the abundances obtained by using the differential curve of growth techniques of Mangold were consistently smaller than their corresponding values as determined from the detailed analysis technique utilized in this study. This effect is probably the result of an inclusion of a microturbulent velocity as an integral part of the calculations as well as an elimination of most of the systematic errors in the oscillator strengths.

In summary, this investigation produced evidence to suggest that the atmosphere of Theta Ursae Majoris contains several important sources of line broadening. Both turbulent effects, microturbulence and macroturbulence, play important roles during line formation in this stellar object and are present in this star in about equal amounts.

An analysis of the line profiles indicates that in the line wings damping from other line broadening mechanisms plays just as dominant a role as does turbulence in the reproduction of the observed triangular profiles of Theta Ursae Majoris. Further, the profiles suggests that the scaled-solar temperature distribution does not adequately fit that of Theta Ursae Majoris near the outer boundary of the atmosphere.

Intensity anomilies were confirmed for Titanium and Manganese. Both of these elements show curves of growth which indicate microturbulent velocities twice as large as the value predicted by the iron lines.

Finally, this study confirms earlier reports of no large abundance differences between the sun and stars in the spectral class F; and the results are somewhat larger than those predicted by the curve of growth analysis of Mangold.

## SELECTED BIBLIOGRAPHY

Allen, C. W. and Asaad, A. S. 1957, M. N. 117, 36.

Aller, L. H. 1942, Ap. J. 95, 73.

__________. 1949, Ap. J. 109, 244.

__________. 1960, Stellar Atmospheres, ed. J. L. Greenstein (Chicago: University of Chicago Press), p. 156.

__________. 1963, Astrophysics (2nd. ed.; New York: The Ronald Press Company).

__________. 1966, I.A.U. Symposium No. 26, Abundance Determinations in Stellar Spectra, ed. H. Hubenet (New York: Academic Press).

Aller, L. H., Elste, G. and Jugaku, J. 1957, Ap. J. Suppl. 3, 1.

Aller, M., Elste, G. and Williams, J. 1970, The University of Michigan Abundance Catalogue, (Ann Arbor: Astronomy Department, The University of Michigan).

Ambartsumyan, V. A. 1958, Theoretical Astrophysics, (London: Pergamon Press).

Babcock, H. W. 1960, Stellar Atmospheres, ed. J. L. Greenstein (Chicago: University of Chicago Press), p. 282.

Böhm, K. 1960, Stellar Atmospheres, ed. J. L. Greenstein (Chicago: University of Chicago Press), p. 88.

Boyarchuck, M. E. 1960, Isv. Crim. Astrophysics Obs., 24, 115.

Boyarchuck, M. E. 1961, Isv. Crim. Astrophysics Obs., 26, 287.

Bulman, J. A. 1971, Ph.D. Thesis, Oklahoma State University, unpublished.

Chandrasekhar, S. 1950, Radiative Transfer, (New York: Dover Publications, Inc.).

Chiu, H.-Y., Warasila, R. L., and Remo, J. L. 1969, Stellar Astronomy, Vol. 1 and 2.

Corliss, C. H. and Bozman, W. R. 1962, NBS Monograph No. 53 (Washington, D.C.: Department of Commerce).

Corliss, C. H. and Tech, J. L. 1968, NBS Monograph No. 108, (Washington, D.C.: Department of Commerce).

Cowley, C. R. 1970, The Theory of Stellar Spectra (New York: Gordon and Breach).

David, K. 1961, Z. f. Ap. 53, 37.

Elste, G. 1953, Z. f. Ap. 33, 39.

__________. 1955, Z. f. Ap. 37, 184.

__________. 1967, Ap. J. 148, 857.

Evans, J. C. 1966, Ph.D. Thesis, University of Michigan, unpublished.

__________. 1970, 1971, private communication.

Evans, J. C. and Schroeder, L. W. 1969, Bull. Am. Astron. Soc. Vol. 1, No. 1, p. 341.

Evans, J. C., Weems, M. L. B., and Schroeder, L. W. 1970, Bull. Am. Astron. Soc. Vol. 3, No. 1, pt. 1, p. 10.

Gingerich, O. 1964, First Harvard-Smithsonian Conference on Stellar Atmospheres (Smithsonian Special Report No. 767), p. 17.

__________. 1969, Theory and Observation of Normal Stellar Atmospheres (Cambridge: The M.I.T. Press).

Glennon, B. M. and Wiese, W. L. 1962, NBS Monograph No. 50 (Washington, D.C.: Department of Commerce).

Goldberg, L., Kopp, R. A. and Dupres, A. K. 1964, Ap. J. 140, 707.

Goldberg, L., Muller, E. A. and Aller, L. W. 1960, Ap. J. Suppl. 5, 1.

Griem, H. R. 1964, Plasma Spectroscopy (New York: McGraw-Hill Book Company).

Greenstein, J. L. 1948, Ap. J. 107, 151.

Gussman, E. A. 1963, Naturwissenschaften 50, 495.

Heuvel, E. P. J. van den. 1963, B. A. N. 17, 148.

Huang, S. S. and Struve, O. 1952, Ap. J. 116, 410.

Huang, S. S. and Struve, O. 1960, Stellar Atmospheres, ed. J. L. Greenstein (Chicago: University of Chicago Press) p. 321.

Hulst, H. C. van de and Reesinck, J. J. M. 1947, Ap. J. 106, 121.

Jeffries, J. T. 1968, Spectral Line Formation, (Waltham, Massachusetts: Blaisdell Publishing Company).

Jeffries, J. T. and White, O. R. 1967, Ap. J. 150, 1051.

Johnson, H. L. and Morgan, W. W. 1953, Ap. J. 114, 522.

Jugaku, J. 1957, Ph.D. Thesis, University of Michigan, unpublished.

Keenan, P. C. and Morgan, W. W. 1951, Astrophysics, ed. J. A. Hynek (New York: McGraw-Hill Book Co.), pp. 12, 27.

Kourganoff, V. 1952, Basic Methods in Transfer Problems, (Oxford: Oxford University Press).

Mangold, E. C. 1968, Ph.D. Thesis, Oklahoma State University, unpublished.

Mangold, E. C., Peebles, H. O. and Schroeder, L. W. 1968, Astron. J. 73, S190.

Mattig, W. and Schröter, E. H. 1961, Z. f. Ap. 52, 195.

Matsushima, S. 1964, Proc. Harvard-Smithsonian Conf. Stellar Atmospheres, 1st (Cambridge: The M.I.T. Press), p. 5.

Mihavas, P. 1970, Stellar Atmospheres, (San Francisco: W. H. Freeman and Company).

Miles, B. M. and Wiese, W. L. 1970, NBS Special Publication No. 320 (Washington, D.C.: Department of Commerce).

Minnaert, M. S. and Slob, C. 1931, Proc. Amsterdam Acad. 3A, pt. 1, 542.

Mitchell, R. I. and Johnson, H. L. 1962, Comm. of the Lunar and Planetary Lab. 1, 73.

Moore, C. E. 1959, Revised Multiplet Table (NBS Tech Note 36 [Washington: Government Printing Office]).

Moltz, L. 1970, Astrophysics and Stellar Structure (Waltham, Massachusetts: Ginn and Company).

Mugglestone, D. 1958, Mon. Not. R. Astr. Soc. 118, 432.

__________. 1965, Second Harvard-Smithsonian Conference on Stellar Structures (Smithsonian Special Report No. 174).

Muller, E. A. and Mutschlecner, J. P. 1964, Ap. J. Suppl. 9, 1.

Myrick, E. G. 1970, Master's Thesis, Oklahoma State University, unpublished.

Parsons, S. B. 1967, Ap. J. 150, 263.

Pecker, J. C. 1965, Annual Review of Astronomy and Astrophysics (Palo Alto: Annual Reviews, Inc.), Vol. 3, p. 135.

Peebles, H. O. 1964, Ph.D. Thesis, Oklahoma State University, unpublished.

Rogerson, J. B. 1969, Ap. J. 158, 797.

Regemorten, H. van. 1965, Annual Review of Astronomy and Astrophysics (Palo Alto: Annual Reviews, Inc.), Vol. 3, p. 71.

Strobel, R. Cayrel and G. Cayrel de. 1966, Annual Review of Astronomy and Astrophysics (Palo Alto: Annual Review, Inc.), Vol. 4, p. 1.

Stromgren, B. 1940, Pub. Copenhagen Obs., Vol. 1, 127.

Takens, R. J. 1970, Astron. and Astrophys. 5, 244.

Underhill, A. B. 1954, Mon. Not. R. Astr. Soc. 114, 558.

__________. 1966, I.A.U. Symposium No. 26, Abundance Determination in Stellar Spectra, ed. H. Hubenet, (New York: Academic Press), p. 118.

Unsold, A. 1955, Physik der Sternatmospharen (Berlin: Springer-Verlag).

Wallerstein, G. 1966, I.A.U. Symposium No. 26, Abundance Determinations in Stellar Spectra, ed. H. Hubenet (New York: Academic Press), p. 238.

Wares, G. W., Wolnick, S. S. and Berthel, R. O. 1970, Ap. J. 162, 1037.

Warner, B. 1967, Mem. R. Astr. Soc. 70, 165.

__________. 1968, Mon. Nat. R. Astr. Soc. 138, 229.

Weidmann, V. 1955, Z. f. Ap. 36, 101.

Wiese, W. L., Smith, M. W. and Miles, B. M. 1969, NSRDS-Natl. Bur. Stds. No. 22 (Washington, D.C.: U.S. Government Printing Office), Vol. 2, p. 1.

Withbroe, G. L. 1969, Solar Physics 9, 19.

Wright, K. O. 1948, Pub. Dom. Ap. Obs. Victoria, VII, No. 1.

__________. 1962, Astronomical Techniques, ed. W. A. Hiltner (Chicago: The University of Chicago Press), p. 83.

__________. 1966, I.A.U. Symposium No. 26, Abundance Determinations in Stellar Spectra (New York: Academic Press), pp. 15-35.

__________. 1971, private communication.

## APPENDIX A

## THE MODEL ATMOSPHERE: THEORY AND COMPUTATIONAL PROCEDURE

This appendix covers the details of the theory used for a fine analysis of a stellar atmosphere. The model atmospheric program is based upon a computer program developed by Elste and Evans (1966, 1969). All the programs used for the analysis may be obtained through Dr. J. C. Evans, Kansas State University.

### Excitation and Ionization of Atoms in Stellar Atmospheres

In a gaseous atmosphere in which a condition of local thermodynamic equilibrium exists at each layer, the atoms, ions, and electrons all interact to bring about a distribution among the various levels to which the atoms may be excited. Considering only the neutral and singly ionized particles, the Saha equation, the Boltzmann equation, and the perfect gas law specify the contribution to the total gas pressure and the electron gas pressure of the various species occurring in the atmosphere. Through the Saha equation, Aller (1963) expresses the number of ionized atoms in the rth excited state for a given temperature and electron pressure as

$$\frac{n_1}{n_o} = 10^{\log (u_1/u_o) + (9.0801 - 2.5 \log \Theta - \log P_e) - \chi_o\Theta} \equiv \frac{\Phi_i}{P_e} \qquad \text{(A-1)}$$

Here $n_1$ = the number of singly ionized atoms of species i per unit volume,

$n_o$ = the number of neutral atoms of species i per unit volume,

$u_1(\Theta)$ = the partition function for singly ionized atoms,

$u_o(\Theta)$ = the partition function for neutral atoms,

$\Theta = 5040/T(^o k)$,

$P_e = N_e kT$ = the electron pressure in the atmosphere.

Now defining the degree of ionization to be the ratio of the number of ionized atoms to the total number of atoms irrespective of their state of ionization gives,

$$X_i \equiv \frac{n_1}{n_o + n_1} = \frac{n_1/n_o}{1 + n_1/n_o} = \frac{\Phi_i/P_e}{1 + \Phi_i/P_e}, \tag{A-2}$$

and for the ratio of all atoms, ions, and electrons to electrons,

$$\frac{N}{N_e} = n_{He} + \frac{\sum_i (n_o + n_1 + n_e)i}{\sum_i (n_e)i} = n_{He} + \frac{\Sigma (1 + X_i)(n_o + n_1)i}{\Sigma X_i (n_o + n_1)i}, \tag{A-3}$$

where $n_{He}$ is the number of helium atoms. If there is but one stage of ionization, $n_e = n_1$ and using the ideal gas relation, Equation (A-3) becomes

$$\frac{N}{N_e} = \frac{P_g}{P_e} = \frac{\sum_i (1 + X_i)\,\varepsilon_i}{\Sigma X_i\,\varepsilon_i}, \tag{A-4}$$

where $\varepsilon_i \equiv \frac{N_i}{N_H} = \frac{(n_o + n_i)i}{n_H}$ represents the number abundance of species i. $X_{He} \equiv 0$ because of the assumption of no helium ionization, and the summation is over all elements. For computational purposes Weidmann (1955) has shown that the ratio $P_g/P_e^2$ is more important so

$$\frac{P_g}{P_e^2} = \frac{\sum_i (1 + X_i)\varepsilon_i}{\sum X_i \varepsilon_i P_e} . \tag{A-5}$$

## The Continuous Absorption Coefficient

To calculate a model atmosphere, it is sufficient, once the effective temperature and surface gravity are defined, to know the opacity as functions of the physical parameters. The calculation of the continuous absorption coefficient for the continuum proceeds under the following assumptions: (1) all molecular absorption is negligible with the exception of $H_2^+$; (2) all negative ion absorption is neglected except $H^-$; and (3) the absorption by metals can be treated in the same manner as hydrogen. The principal source of absorption in the continuum is due to bound-free (bf) and free-free (ff) absorption due to $H^-$, H, $H_2^+$. In addition to these, the metals may become appreciable absorbers and there may be Thompson scattering by electrons and Rayleigh scattering by hydrogen. Gingerich (1969) gives the following expression for the Rayleigh scattering coefficient per hydrogen atom: $\sigma_R = 5.799 \times 10^{-3}\lambda^{-4} + 1.422 \cdot 10^{-6}\lambda^{-6} + 2.784\lambda^{-8}$. The Thompson scattering coefficient per electron is (Unsold 1955): $\sigma_T = \frac{8\pi e^4}{3m^2\lambda^4} = 0.66515 \times 10^{-24}$. While the relative importance of the positive hydrogen molecule as a function of the temperature and is never very great (Matsushima, 1964) its contribution is included in the total absorption coefficient. Evans (1966) has tabulated the continuous absorption coefficient data for hydrogen for various wavelength intervals ranging from λ2000 to λ21000. The total absorption coefficient per hydrogen particle per unit electron pressure may then be expressed as (Evans 1966):

$$\frac{K_\lambda}{P_e} = \left[\frac{K_\lambda(\text{Hydrogen})}{P_e} + \frac{K_\lambda(\text{Metals})}{P_e}\right](1 - 10^{-\chi_\lambda \Theta}) + \frac{\sigma}{P_e}\,, \tag{A-6}$$

where the term in parenthesis represents the stimulated emission factor which must be incorporated into all absorption processes.

## Hydrostatic Equilibrium

The expression invoking hydrostatic equilibrium, may be stated in terms of the variable of depth, the logarithm of the continuum optical depth at 5000Å, as

$$dP_g(x) = \frac{g\, m_o}{K_o} \Sigma\, \varepsilon_i\, \mu_i \left(\frac{\tau_o}{\log_{10} e}\right) dx\ . \tag{A-7}$$

This expression is most easily integrated, from the top of the atmosphere ($P_g \equiv 0$) to the depth x, to obtain the gas pressure by first multiplying by $P_g^{\,2}$ (Evans, 1966).

$$\int_o^{P_g} P_g^{\frac{1}{2}}\, dP_g = \frac{g\, m_o \sum_i \varepsilon_i\, \mu_i}{\log e} \int_{-\infty}^{x} \left(\frac{P_g}{P_e^{\,2}}\right)^{\frac{1}{2}} \frac{\tau_o\, dx}{\left(\frac{K_o}{P_e}\right)}\ . \tag{A-8}$$

The integrand on the right hand side of the above expression has been rearranged so as to employ the known function $P_g/P_e^{\,2}$. Integration of the left hand side yields

$$\frac{2}{3} \cdot P_g^{\,3/2} = \frac{g\, m_o \sum_i \varepsilon_i\, \mu_i}{\log e} \int_{-\infty}^{x} \left(\frac{P_g}{P_e^{\,2}}\right)^{\frac{1}{2}} \frac{\tau_o}{K_o/P_e}\, dx, \tag{A-9}$$

or in the more convenient form

$$\log P_g = \frac{2}{3} \log \{\frac{3}{2} \frac{g\, m_o\, \Sigma\, \varepsilon_i\, \mu_i}{\log e}\}$$

$$+ \; 2/3 \log \{\int_{-oo}^{x} (\frac{P_g}{P_e^{\,2}})^{\frac{1}{2}} \; \frac{\tau_o}{K_o/P_e} \; dx\} \; . \tag{A-10}$$

Writing the electron pressure as

$$P_e = [P_g(P_e^{\,2}/P_g)]^{\frac{1}{2}}, \tag{A-11}$$

and taking the logarithm of the expression gives the electron pressure in terms of the gas pressure and the function $P_g/P_e^{\,2}$,

$$\log P_e = \frac{1}{2}[\log P_g - \log P_g/P_e^{\,2}]. \tag{A-12}$$

Surface Flux

The equation of transfer of radiation through a stellar atmosphere has been solved by Kourganoff (1952) to yield an integral equation for the radiative flux

$$F_\lambda(0) = 2 \int_o^\infty S_\lambda(\tau_\lambda') \; E_2(\tau_\lambda') \; d\tau_\lambda' \; . \tag{A-13}$$

The quantity $S_\lambda$ appearing in the integrand is the source function which under the assumption of LTE is none other than the Planck function. $E_2(\tau_\lambda)$ represents the exponential-integral function,

$$E_n(x) = \int_1^\infty e^{-x\omega} \; \frac{d\omega}{\omega^n} \; ,$$

while the optical depth is defined as

$$\tau'_\lambda = \int_{-\infty}^{x} \frac{K_\lambda}{K_o} \left(\frac{\tau_o}{\text{Mod}}\right) dx \; . \qquad \text{(A-14)}$$

Mod is defined so as to represent the logarithm to base ten of e and is 0.43429.

Assuming that $B_\lambda(\tau_\lambda)$ remains constant over the range $0 \leq \tau_\lambda \leq \varepsilon$, Equation (A-13) becomes,

$$F_{\underline{\lambda}}(0) = 2B_\lambda(\varepsilon) \int_{\tau_\lambda=o}^{\tau_\lambda=\varepsilon} E_2(\tau_\lambda)d\tau_\lambda + \int_{\tau_\lambda=\varepsilon}^{\tau_\lambda=\infty} 2B_\lambda(\tau_\lambda)\, E_2(\tau_\lambda)d\tau_\lambda \; . \qquad \text{(A-15)}$$

From the definition of the exponential-integral function, the first integral on the right hand side of Equation (A-15) is

$$\int_{\tau_\lambda=o}^{\tau_\lambda=\varepsilon} E_2(\tau_\lambda)d\tau_\lambda = - E_3(\tau_\lambda) + \frac{1}{2} \, ,$$

while the second integral, when evaluated by integration by parts, is found to be

$$\int_{\tau_{\lambda=\varepsilon}}^{\tau_\lambda=\infty} 2B_\lambda(\tau_\lambda)\, E_2(\tau_\lambda)d\tau_\lambda = \int_{\log\, \tau_o(\varepsilon)}^{\infty} 2\, E_3(\tau_\lambda) \frac{dB_\lambda(\tau_\lambda)}{d(\log\, \tau_\lambda)} \frac{\text{Mod}}{\tau_\lambda} d\tau_\lambda .$$

When these two results are combined, they yield the expression for the flux,

$$F_\lambda(0) = B_\lambda(\varepsilon) + \int_{\log\, \tau_o(\varepsilon)}^{\infty} 2E_3(\tau_\lambda) \frac{dB_\lambda(\tau_\lambda)}{d(\log\, \tau_\lambda)} \left(\frac{\text{Mod}}{\tau_\lambda}\right) d\tau_\lambda \; . \qquad \text{(A-16)}$$

Equation (A-16) has been derived under the assumption that $B_\lambda(\tau_\lambda)$ increases less than exponentially over the range $\varepsilon \le \tau_\lambda \le \infty$. For small enough intervals in $x = \log \tau_0$, the gradient of the source function can be assumed to be independent of $\tau_\lambda$ (Evans, 1966) so the integration can be replaced by summations of the type

$$F_\lambda(0) \quad = \quad B_\lambda(\varepsilon) + \mathrm{Mod} \sum_x^\infty \frac{dB_\lambda}{d(\log \tau_\lambda)} \Delta(x), \qquad \text{(A-17)}$$

where

$$\Delta(x) \quad = \quad \int_{\tau_\lambda(x_1)}^{\tau_\lambda(x_2)} 2E_3(\tau_\lambda) \frac{d\tau_\lambda}{\tau_\lambda},$$

$$= \quad \int_{\tau_\lambda(x_1)}^{\tau_\lambda(x_2)} 2\left[\int_1^\infty e^{-\tau_\lambda \omega} \frac{d\omega}{\omega^3}\right] \frac{d\tau_\lambda}{\tau_\lambda},$$

$$= \quad \frac{1}{2}\left[E_1(\tau_\lambda)(2 - \tau_\lambda^{\,2}) - e^{-\tau_\lambda}(1 - \tau_\lambda)\right]_{\tau_\lambda(x_1)}^{\tau_\lambda(x_2)} .$$

As the optical depth increases, $\Delta$ decreases rapidly (Evans, 1966) so that the summation in Equation (A-17) need only cover the contributions from the deepest contributing layers, $-4.0 \le x \le +1.2$. The gradient of the Planck function is evaluated from Sterlings interpolation formula

$$\left.\frac{dB_\lambda}{d \log \tau_\lambda}\right|_{\tau_{\lambda(x)}} \quad = \quad \frac{1}{2}\left[\frac{B_\lambda[\tau_\lambda(x + \Delta x)] - B_\lambda[\tau_\lambda(x - \Delta x)]}{\Delta(\log \tau_\lambda)}\right]. \qquad \text{(A-18)}$$

## The Computational Procedure

For a given chemical composition, effective surface gravity, and temperature distribution a model atmosphere is calculated using an iterative procedure based upon an initial estimate of the electron pressure.

The first two input parameters as well as the electron pressure were obtained from a coarse analysis performed upon Theta Ursae Majoris by Peebles (1964) while the temperature distribution was a scale model of Elste's solar model. The computer program was developed by Elste and modified by Evans (1969).

The iterative scheme begins with a computation of the ionization equilibrium, $P_g/P_e^2$, for the initial estimate of the electron pressure, using Equation (A-5). The effective temperature and electron pressure are then used to calculate the absorption coefficeint at $\lambda 5000$, i.e., the quantity $K_o/P_e$ from Equation (A-6). Once these quantities have been determined an initial estimate of the total gas pressure $P_g$ may be determined through Equation (A-10). From the total gas pressure and the function $P_g/P_e^2$, another estimate of the electron pressure is made. A second iteration on the gas pressure is then accomplished through recycling of the entire process. The computations will continue until convergence of the electron pressure is reached. Commonly this requires but a few iterations because the behavior of the significant functions, $P_g/P_e^2$ and $K_o/P_e$, fluctuate more rapidly for variations in temperature than in pressure (Bulman, 1971).

The computation of the opacity uses an identical iterative scheme except that before the calculation of the optical depth at various wavelengths from Equation (A-14) the absorption coefficient must be determined. The absorption coefficient for wavelength $\lambda$ is computed from Equation (A-6), placed in Equation (A-14) and integrated to find $\tau_\lambda(x)$. Through Equation (A-17), the flux model is calculated at wavelength intervals of 150Å for the interval $\lambda\lambda 2,000$-$10,000$ and one each for $\lambda 15,000$

and $\lambda 21,000$. The results, the variation of the parameters specifying the model atmosphere with depth, then form the basis for the input data which will enable the calculation of line profiles and chemical abundances to be made.

## APPENDIX B

## THE COMPUTER PROGRAMS USED IN THE ANALYSIS

### The Metal Line Program

The expression for the absorption coefficient per absorbing particle for simultaneous damping and Doppler broadening as convolution of the two effects acting separately is (Aller 1963; Cowley, 1970)

$$K_{atomic}\,(x,\ \Delta\lambda) = \frac{\sqrt{\pi}e^2}{mc^2}\,\frac{\lambda^2}{\lambda_D}\,f_{r,s}\,H(a,v), \tag{B-1}$$

where

$f_{r,s}$ = the oscillator strength, for the transition, from level s, for the rth stage of ionization,

$\Delta\lambda_D$ = the Doppler width (Equation (3-22)),

$$a(x) = \frac{\Gamma_T}{4\pi}\,\frac{\lambda}{\sqrt{\frac{83.83}{\mu_i\theta} - \varepsilon^2_{turb}}},$$

$$\Gamma_T(x) = \Gamma_{rad.} + \Gamma_{Stark} + \Gamma_{van\ der\ Waals},$$

$$v(x) = \Delta\lambda/\Delta\lambda_D,$$

and $H(a,v)$ = the Voight function

$$\equiv \frac{a}{\pi}\int_{-\infty}^{+\infty} \frac{e^{-y^2}}{(v-y)^2 + a^2}\,dy\ .$$

The line absorption coefficient per hydrogen particle is then, from Equation (3-25),

$$K^{\ell} = \frac{n_{r,s}}{N_H} K_{atomic} = (\frac{n_{r,s}}{n_r})(\frac{n_r}{\Sigma n_r})(\frac{N_i}{N_H}) K_{atomic} , \qquad \text{(B-2)}$$

where the summation is carried out over all stages of ionization and excitation for the atoms of a given element and is just equal to $N_i$. The factor $n_{r,s}/\Sigma n_r$ is quite sensitive to the depth of the atmosphere and it varies from one level to the next (Aller, 1960). For a given model atmosphere the depth dependence is calculated with the help of the Saha and Boltzmann equations.

For most stellar applications, there are only three important stages of ionization of an element, say r-1, r, r+1. If s represents the lower level of the transition being considered and $u_r$ the partition function for the $r^{th}$ stage of ionization, then the first two terms of Equation (B-2) may be expressed as

$$\frac{n_{r,s}}{n_r} \cdot \frac{n_r}{\Sigma n_r} = \frac{n_{r,s}}{n_r} (\frac{n_r}{n_{r-1} + n_r + n_{r+1}}),$$

$$= (\frac{n_{r,s}}{n_r/u_r})(\frac{1}{u_r})(\frac{1}{n_{r-1}/n_r + 1 + n_{r+1}/n_r}) . \qquad \text{(B-3)}$$

Defining

$$U_r \equiv u_r \frac{n_{r-1}}{n_r} + u_r + u_r \frac{n_{r+1}}{n_r} , \qquad \text{(B-4)}$$

allows Equation (B-3) to be written as

$$\frac{n_{r,s}}{n_r}\,\frac{n_r}{\Sigma n_r} = \left(\frac{n_{r,s}\,u_r}{n_r}\right)\frac{1}{U_r}\,. \tag{B-5}$$

The Saha ionization equation,

$$\log \frac{n_{r+1}}{n_r} P_e = -\frac{5040}{T}\,\chi_r + \frac{5}{2}\log T - 0.48 + \log \frac{2\mu_{r+1}}{\mu_r},$$

can be written as

$$\log u_r \frac{n_{r+1}}{n_r} = \log u_{r+1} - \chi_r\Theta + (9.080 - \frac{5}{2}\log\Theta - \log P_e), \tag{B-6}$$

and

$$\log u_r \frac{n_{r-1}}{n_r} = \log u_{r-1} + \chi_{r-1}\Theta - (9.080 - \frac{5}{2}\log\Theta - \log P_e). \tag{B-7}$$

Substitution of Equations (B-6) and (B-7) into (B-4) gives

$$\begin{aligned} U_r &= 10\log^{u_{r-1} + \chi_{r-1}\Theta - (9.080 - 5/2\log\Theta - \log P_e)} \\ &\quad + 10\log^{u_r} \\ &\quad + 10\log^{u_{r+1} - \chi_r\Theta + (9.080 - 5/2\log\Theta - \log P_e)}\,. \end{aligned} \tag{B-8}$$

The term in parenthesis in Equation (B-5) depends upon the stage of ionization and using the combined Boltzmann and Saha equations can be written as (Evans, 1966)

$$\log \left(\frac{n_{r',s}}{n_r}\,u_r\right) = \log g_{r',s} + \Delta\chi\Theta + h(9.0801 - \frac{5}{2}\log\Theta - \log P_e), \tag{B-9}$$

where

$$h = \begin{cases} -1 & \text{if} \quad r' = r-1, \\ 0 & \text{if} \quad r' = r, \\ +1 & \text{if} \quad r' = r+1, \end{cases}$$

and

$$\Delta\chi = \begin{cases} \chi_{r-1} - \chi_{r-1,s}, & \text{for } (r-1,s), \\ -\chi_{r,s}, & \text{for } (r,s), \\ \chi_{r+1,s} - \chi_r & \text{for } (r+1,s) \ . \end{cases}$$

From Equations (B-1), (B-2), (B-5), (B-8) and (B-9) the line absorption coefficient per hydrogen particle becomes,

$$K^{\ell}(x,\Delta\lambda) = \frac{\sqrt{\pi}e^2}{mc^2}\frac{\lambda^2}{\lambda_D}(gf)_{r,s}\frac{H(a,v)}{U}\cdot\frac{N_i}{N_H}[10^{\Delta\chi\Theta+h(9.0801-\frac{5}{2}\log\Theta-\log P_e}] \ . \tag{B-10}$$

Using Equation (B-10), the optical depth in the line is computed as a function of x and $\Delta\lambda$. It is common practive to facilitate discussion (Aller, 1963) by writing the integrand of Equation (3-3) as a product of four functions,

$$\frac{K^{\ell}}{K_o}\left(\frac{\tau_o}{\text{Mod}}\right)(1 - 10^{-\chi_{\lambda_m}\Theta}) = \varepsilon_i \ Z_i(x,\lambda) \ H(a,v), \tag{B-11}$$

where $Z_i(x,\lambda) = M(x) \ N_i(x) \ L_{r,s}(x,\lambda)(1 - 10^{-\chi_{\lambda_m}\Theta})$. The advantage of this is that it allows for a more rapid and complete computational scheme when applied to an electronic computer. The first of the terms in $Z_i(x,\lambda)$ is defined as

$$M(x) = \frac{\sqrt{\pi}e^2}{mc}\frac{P_e}{K_o}\left(\frac{1}{P_e}\right)\frac{\tau_o}{\text{Mod}}, \tag{B-12}$$

and is constant for all elements and wavelength regions, $\lambda_m$. $N_i(x)$ is given by,

$$N_i(x) = \frac{1}{U_i} \frac{10^{h(9.0801 - 2.5 \log \Theta - \log P_e)}}{\sqrt{\frac{83.83}{\mu_i \Theta} - \varepsilon^2_{turb.}}}, \tag{B-13}$$

and is also free of any wavelength dependence. Finally, $L_{r,s}$ contains the dependence of the line optical depth upon the explicit transition under consideration and is defined as

$$L_{r,s}(x,\lambda) = 10^{\log (gf\lambda)_{r,s} + \Delta\chi\Theta} . \tag{B-14}$$

For lines forming doublets, the computational scheme relies on the assumption that the broadening of the separate components are independent of each other (Evans, 1966). Then Equation (B-11) can be written as

$$\left(\frac{K^{\ell_1}}{K_o} + \frac{K^{\ell_2}}{K_o}\right)\left(\frac{\tau_o}{Mod}\right)\left(1 - 10^{-\chi_{\lambda_m}\Theta}\right) = \varepsilon_i[Z_i(x,\lambda_1)\ H(a_1,v_1)$$

$$+ (x,\lambda_2)\ H(a_2,v_2)]. \tag{B-15}$$

However, the two functions, $Z_1(x,\lambda_1)$ and $Z_2(x,\lambda_2)$ are not linearly independent if the wavelengths are assigned an identical value and the damping constant is the same for both. The two functions are then connected through

$$Z_2(x,\lambda) = \frac{(gf)_{r_2 s_2}}{(gf)_{r_1 s_1}} Z_1(x,\lambda),$$

and Equation (B-15) becomes

$$\left(\frac{K^{\ell_1}}{K_o} + \frac{K^{\ell_2}}{K_o}\right)(1-10^{-\chi_{\lambda_m}\Theta}) = \epsilon_i[Z_1(x,\lambda)][H(a,v_1) + \frac{(gf)_{r_2,s_2}}{(gf)_{r_1,s_1}} H(a,v_2)], \quad \text{(B-16)}$$

where $v_2 = \frac{\Delta\lambda - d}{\Delta\lambda_D}$ ,

$d$ = the separation of the centers of the individual components of the doublet,

$= \lambda_2 - \lambda_1$ .

## The Damping Parameters

Aller (1963) has discussed the importance of radiation damping. For most stellar application, he indicates that the contribution to the total damping constant (Equation (3-24)) due to this mechanism is of least importance and can be represented by the classical formula,

$$\Gamma_{rad} = \frac{8\pi^2 e^2}{3mc}\left(\frac{1}{\lambda^2}\right) = \frac{0.22234 \times 10^{16}}{\lambda^2}, \quad \text{(B-17)}$$

where $\lambda$ is expressed in Angstrom units.

The Lindholn theory is utilized to establish an order of magnitude effect for collisional broadening due to electrons and ions and is given by (Aller, 1963)

$$\Gamma_{Stark} = \Gamma_{electrons} + \Gamma_{ions} = 38.8\ C_4^{2/3}(v_e^{1/3}Ne + v_{ions}^{1/3}N_{ions}), \quad \text{(B-18)}$$

where $v_e$ and $v_{ions}$ represents the velocity of the perturbing particles and the constant is given by

$$C_4 = 6.21 \times 10^{-10} \, (\Delta\tilde{\nu}/F^2) \, . \qquad \text{(B-19)}$$

$\Delta\tilde{\nu}$ = the shift of the energy levels expressed in wavenumbers,

$F$ = the electric field strength in kvolts/cm.

Evans (1966) has calculated the numerical value of this constant for a few lines of C, Na, Mg, and Si. Since the experimental and theoretical data are inadequate for almost all of the observed lines in Theta Ursae Majoris, the range of the values of the constant was extended to include all of the observed lines for all the elements utilized in this study.

The damping constant for van der Waals interactions (Aller, 1963) is given by the Lindholm theory as,

$$\Gamma_{\text{van der Waals}} = 17.0 \, C_6^{2/5} \, v_{\text{atoms}}^{3/5} \, N_{\text{atoms}} , \qquad \text{(B-20)}$$

where the constant, $C_6$, is the van der Waals interaction constant. The numerical value of $C_6$ can be approximated (Aller, 1963), assuming a hydrogen-like particle, as

$$C_6 = 1.61 \times 10^{-23} \left[ \left( \frac{13.5 \, Z}{\chi_r - \chi_{r,s'}} \right)^2 - \left( \frac{13.5 \, Z}{\chi_r - \chi_{r,s}} \right)^2 , \qquad \text{(B-21)}$$

where $Z$ = the effective nuclear charge,

$\chi_r$ = the ionization potential of the atom,

$\chi_{r,s}$ = excitation potential of the lower level,

$\chi_{r,s'}$ = the excitation potential of the upper level .

## The Theoretical Curve of Growth

In the expression for log C from Equation (3-28), the absorption coefficient at the line center is taken from a publication by Aller, Elste, and Jugaku (1957); so that

$$\frac{K^{\ell c}}{K_o} \left(\frac{\tau_o}{\text{Mod}}\right)\left(1 - 10^{-\chi_{\lambda_m}\Theta}\right) = \varepsilon_i \sqrt{\pi} \left(\frac{\Delta\lambda_D}{\lambda}\right) Z ,$$

and the quantity log C becomes

$$\log C = \log \left[\sqrt{\pi} \int_{-\infty}^{\infty} \left(\frac{\Delta\lambda_D}{\lambda}\right) Z \, G_{\lambda_m} dx\right] . \tag{B-22}$$

The flux weight function is given by the expression (Aller, 1960)

$$G_{\lambda_m}(\tau_\lambda) = \frac{2}{F_T{}^c(o)} \int_x^{\infty} \frac{dB_{\lambda_m}}{dx} E_2(\tau_{\lambda_m}) dx . \tag{B-23}$$

The integration is carried out over a finite range, $-4.0 \leq x \leq +1.2$, since the behavior of the exponential integral is to decrease rapidly with increasing optical depth. The saturated equivalent width is calculated from the line depth, Equation (3-29). Since the line depth for large values of $\Delta\lambda$ is negligible for weak and medium strong lines, integration of Equation (3-29) may be truncated after relatively few calculations.

## The Metal Line Program

The computer program used for the analysis of the metal lines in stellar atmospheres was origionally developed by Evans (1966). The program is designed to compute a single line profile and curve of growth for a given model atmosphere; however, it will calculate this for a variety of parameters.

The program initially begins by evaluating all quantities which are dependent only upon the model atmosphere, microturbulence model, and macroturbulence model. With the gas pressure, the electron pressure, the temperature, and the continuous absorption coefficient given as functions of the optical depth at 5000Å, the optical depth in the continuum for other necessary wavelengths is computed. The integration is performed over the range in depth of $-4.0 \leq x \leq +1.2$ in steps of 0.2. The stimulated emission factor and the weighting function can also be determined at this time for the range of wavelengths covering the observed spectral region. The gradient of the source function is obtained through Stirlings interpolation formula expressed as

$$\left(\frac{dB}{dx}\right)_x = \frac{B_\lambda(x + \Delta x) - B_\lambda(x - \Delta x)}{2\Delta x} .$$

The line absorption coefficient is then evaluated as a function of x and $\Delta\lambda$ from Equation (B-10) in order that the optical depth in the line may be computed from Equation (3-3). The retain the necessary accuracy, the third exponential integral is approximated by a Taylor series expansion to yield

$$E_3(\tau^c) - E_3(\tau^c + \tau^\ell) = \tau^\ell E_2(\tau^c) \quad \text{if} \quad \tau^\ell << \tau^c ,$$

and by

$$E_3(\tau^c) - E_3(\tau^c + \tau^\ell) = E_3(\tau^c) \quad \text{if} \quad \tau^\ell >> \tau^c .$$

If $\tau^c$ is on the order of $\tau^\ell$, the straight difference in the functions,

$$E_3(\tau^c) - E_3(\tau^c + \tau^\ell),$$

is evaluated. Then for the element of interest $U_r$ may be determined from Equation (B-8) for the energy levels of interest. For this step appropriate tables of the partition functions for the elements have been tabulated by Evans (1966). This completes the calculation of all quantities which are independent of the individual transition under investigation.

At this point, computations are made for all terms which depend only upon the depth in the atmosphere and the individual line under investigation. This includes the Doppler width $\Delta\lambda_D$ from Equation (3-23), the damping constant $\Gamma_T(x)$ and the damping parameter a(x) from Equation (B-1), the abscissa for the empirical curve of growth, log $C_\lambda$, from Equation (B-22) and, finally, log Z(x,λ) from Equations (B-11), (B-12), (B-13), and (B-14).

At this point a cycling procedure is initialized for the computation of the theoretical curve of growth. An initial abundance estimate is utilized to compute the optical depth in the line from Equations (3-3) and (B-11) as a function of Δλ. The values of Δλ are arbitrarily selected up to a maximum of 20 equal increments across the line. A variety of possible scaled values can be chosen by the user. The integration of the line optical depth is accomplished in the same manner as for the continuum. Both employ a Gauss-Encke formula with a starting integration formula of Elste (Evans, 1966). The ordinate for the theoretical curve of growth, log (w/λ), is then computed using the line depth expression (Equation (3-21)) in conjunctions with Equation (3-29). The macroturbulent calculations are carried out over forty-one different macroturbulence cells assuming a dispersion function for the individual velocity components. The calculation is carried out to plus and minus four times the observed halfwidth for the line. This procedure is then repeated for twice and half the initial abundance. If the observed value of the equivalent width for the line fails to lie within this range, additional multiples of the initial abundance estimate are used to compute additional points so that the observed value falls on the curve of growth.

The output of the metal line program has a number of options available. Upon command, the line profiles for the estimated abundance may be graphed and the mean value of the integrand of the line depth, sometimes referred to as the contribution function for the line, may be obtained. The recycling of the entire program is accomplished by first reading in all the lines and ordering them in their respective wavelength regions. After the lines in one wavelength have been exhausted, the computer progresses to the next region. This process is repeated up to a maximum of ten wavelength regions. The metal line program in its entirity can be obtained through communication with Dr. John C. Evans, Department of Physics, Kansas State University or Dr. Leon W. Schroeder, Department of Physics, Oklahoma State University.

## The Abundance Program

For a given model atmosphere, the empirical curve of growth consists of a plot of the saturated equivalent width against log $C_\lambda$ where

$$\log C_\lambda = \log g_{r,s} f_{r,s} \lambda + \log L_\lambda^* (\chi_{r,s}).$$

With the aid of Equation (3-27), the abundance of an element may be determined from the horizontal displacement of the axis with no vertical translation. If $\Delta_x$ represents the linear transformation necessary to bring the empirical curve of growth into coincidence with the theoretical curve of growth, then

$$\Delta_x = \log (w/\lambda)^* - \log C_\lambda = \log \varepsilon .$$

This procedure has been systemized with the development of a computer program (Evans, 1970), capable of determining the abundance for from one to fifty lines, of a single element based upon a theoretical curve of growth for a line representative of the range of wavelengths of interest.

For the selected model, the computation begins with the computation of the theoretical curve of growth to be used for mean abundance calculations. For this step, the optical depth is computed and the weighting functions are evaluated for the range of wavelengths of interest. For the desired element $U_r$ and log Z are computed for the energy levels of interest. The details of the calculation are identical with those outlined previously for the metal line program. The abscissa for the theoretical curve of growth is computed from Equation (3-26) while the ordinate is evaluated utilizing Equation (3-21). With the aid of Equation (3-31) $\log L_\lambda(\chi_{r,s})$ is computed for each level $\chi_{r,s}$ of interest and for the range of wavelengths covering the observed lines. Then for each individual line, or $\log g_{r,s} f_{r,s} \lambda$, $\log C_\lambda$ is determined from Equation (3-30). The observed value of $\log(w/\lambda)$ is read into the computer and the shift in the abscissa necessary to place the point on the mean theoretical curve of growth is determined. The abundance for the line thus evaluated, the program recycles until all observed lines have been read into the computer and each individual abundance calculated. At this point, the weighted mean abundance is calculated in the standard manner and the program terminated. The printed output consists of the model atmosphere, the turbulence model, the flux curve of growth, the abscissia for the empirical curve of growth, and the results of the abundance analysis.

## APPENDIX C

## THE CORRECTION FOR INSTRUMENTAL BROADENING IN A SPECTRAL LINE USING THE METHOD OF VOIGHT FUNCTIONS

From the observation of stellar spectra, it is well known that the intensity distribution of a spectral line broadened by two separate mechanisms can be expressed as the convolution

$$f(x) = \int_{-\infty}^{+\infty} f'(x-y)\, f''(y)\, dy, \tag{C-1}$$

of the profiles, $f'(x)$ and $f''(x)$, that the line would describe if only one of the effects were present. If $f(x)$ represents the observed line profile and $f'(x)$ the profile of the spectrograph, the true profile $f''(x)$ can be obtained from Equation (C-1).

One method of solving this equation is to approximate all profiles with an analytic function, the Voight function. Voight functions result from a convolution of a dispersion profile

$$f(x) = \frac{1}{\pi}\,\frac{\beta_1}{\beta_1^{\,2} + x^2}, \tag{C-2}$$

with halfwidth $\beta_1$, and a Gaussian profile

$$f(x) = \frac{1}{\sqrt{\pi}\,\beta_2}\, e^{-(x/\beta_2)^2}, \tag{C-3}$$

with a 1/e-width of $\beta_2$. The function described by Equations (C-2) has the property that the convolution of two such profiles, f' and f", results in a third function of the same type with the halfwidth equal to the sum of the halfwidths.

$$\beta_1 = \beta_1' + \beta_1'' . \tag{C-4}$$

If the functions f' and f" in Equation (C-1) are Gaussian, the profile f(x) is Gaussian and the 1/e-widths are related by the well known relation

$$\beta_2^{\,2} = \beta_2^{\,2'} + \beta_2^{\,2''} . \tag{C-5}$$

Voight functions, which are a more general type of function and include as extreme cases both types of profiles, follow similar processes under convolution and their parameters satisfy the relations given by Equation (C-4) and (C-5) (Van de Hulst and Reesinck, 1947). The area is denoted by

$$A = \int_{-\infty}^{+\infty} f(x)\, dx \equiv phc, \tag{C-6}$$

where h = the halfwidth of the profile,

c = central depth of the profile,

p = area parameter.

A Voight function is completely determined by the parameters, A, $\beta_1$, and $\beta_2$. It is sometimes more convenient to represent a standard set of Voight functions in terms of the form parameter $b_1 \equiv \beta_1/h$ where h represents the halfwidth of the profile. Then the quantities, $b_2 \equiv \beta_2/h$, $\alpha \equiv \beta_1/\beta_2$, and p are unique functions of the form parameter $b_1$ and have been produced in tabular form (Elste, 1953) in Table XXV. The first five

TABLE XXV

THE VOIGHT PARAMETERS AS FUNCTIONS OF THE FORM PARAMETER

| $b_1$ | $b_2$ | $b_2^2$ | $\alpha$ | p | $b_{0.1}/h$ |
|---|---|---|---|---|---|
| 0.00 | 0.6006 | 0.3607 | 0.0000 | 1.0645 | 1.820 |
| 0.01 | 0.5941 | 0.3529 | 0.0168 | 1.0732 | 1.825 |
| 0.02 | 0.5876 | 0.3452 | 0.0340 | 1.0819 | 1.835 |
| 0.03 | 0.5810 | 0.3375 | 0.0516 | 1.0907 | 1.850 |
| 0.04 | 0.5744 | 0.3299 | 0.0696 | 1.0996 | 1.860 |
| 0.05 | 0.5677 | 0.3223 | 0.0881 | 1.1085 | 1.870 |
| 0.06 | 0.5609 | 0.3147 | 0.1070 | 1.1175 | 1.880 |
| 0.07 | 0.5541 | 0.3071 | 0.1263 | 1.1265 | 1.895 |
| 0.08 | 0.5473 | 0.2995 | 0.1462 | 1.1356 | 1.920 |
| 0.09 | 0.5404 | 0.2920 | 0.1666 | 1.1448 | 1.925 |
| 0.10 | 0.5334 | 0.2845 | 0.1875 | 1.1540 | 1.940 |
| 0.11 | 0.5263 | 0.2770 | 0.2090 | 1.1633 | 1.950 |
| 0.12 | 0.5192 | 0.2695 | 0.2311 | 1.1727 | 1.970 |
| 0.13 | 0.5120 | 0.2621 | 0.2539 | 1.1822 | 1.980 |
| 0.14 | 0.5047 | 0.2547 | 0.2774 | 1.1918 | 1.995 |
| 0.15 | 0.4973 | 0.2473 | 0.3017 | 1.2015 | 2.020 |
| 0.16 | 0.4898 | 0.2399 | 0.3267 | 1.2112 | 2.040 |
| 0.17 | 0.4822 | 0.2325 | 0.3526 | 1.2210 | 2.050 |
| 0.18 | 0.4745 | 0.2251 | 0.3793 | 1.2309 | 2.070 |
| 0.19 | 0.4667 | 0.2178 | 0.4071 | 1.2409 | 2.080 |
| 0.20 | 0.4588 | 0.2105 | 0.4359 | 1.2509 | 2.100 |
| 0.21 | 0.4508 | 0.2032 | 0.4658 | 1.2610 | 2.130 |
| 0.22 | 0.4426 | 0.1959 | 0.4970 | 1.2711 | 2.140 |
| 0.23 | 0.4343 | 0.1887 | 0.5295 | 1.2813 | 2.150 |
| 0.24 | 0.4259 | 0.1814 | 0.5635 | 1.2915 | 2.175 |
| 0.25 | 0.4174 | 0.1742 | 0.5990 | 1.3018 | 2.190 |
| 0.26 | 0.4087 | 0.1670 | 0.6363 | 1.3122 | 2.220 |
| 0.27 | 0.3998 | 0.1598 | 0.6754 | 1.3226 | 2.245 |
| 0.28 | 0.3907 | 0.1526 | 0.7168 | 1.3331 | 2.250 |
| 0.29 | 0.3814 | 0.1454 | 0.7604 | 1.3436 | 2.275 |
| 0.30 | 0.3719 | 0.1383 | 0.8067 | 1.3541 | 2.285 |
| 0.31 | 0.3622 | 0.1312 | 0.8559 | 1.3647 | 2.310 |
| 0.32 | 0.3522 | 0.1241 | 0.9084 | 1.3754 | 2.335 |
| 0.33 | 0.3420 | 0.1170 | 0.9648 | 1.3861 | 2.350 |
| 0.34 | 0.3315 | 0.1099 | 1.0255 | 1.3968 | 2.375 |
| 0.35 | 0.3208 | 0.1029 | 1.0913 | 1.4076 | 2.400 |
| 0.36 | 0.3097 | 0.0959 | 1.1629 | 1.4185 | 2.425 |
| 0.37 | 0.2982 | 0.0889 | 1.2414 | 1.4294 | 2.450 |
| 0.38 | 0.2863 | 0.0820 | 1.3270 | 1.4403 | 2.475 |
| 0.39 | 0.2739 | 0.0750 | 1.424 | 1.4512 | 2.520 |

TABLE XXV (Concluded)

| $b_1$ | $b_2$ | $b_2^2$ | $\alpha$ | p | $b_{0.1}/h$ |
|---|---|---|---|---|---|
| 0.40 | 0.2609 | 0.0681 | 1.533 | 1.4623 | 2.540 |
| 0.41 | 0.2473 | 0.0612 | 1.658 | 1.4733 | 2.575 |
| 0.42 | 0.2330 | 0.0543 | 1.803 | 1.4843 | 2.620 |
| 0.43 | 0.2177 | 0.0474 | 1.975 | 1.4952 | 2.650 |
| 0.44 | 0.2014 | 0.0405 | 2.185 | 1.5062 | 2.700 |
| 0.45 | 0.1836 | 0.0337 | 2.451 | 1.5171 | 2.740 |
| 0.46 | 0.1641 | 0.0269 | 2.804 | 1.5280 | 2.795 |
| 0.47 | 0.1419 | 0.0201 | 3.312 | 1.5388 | 2.840 |
| 0.48 | 0.1158 | 0.0134 | 4.147 | 1.5495 | 2.875 |
| 0.49 | 0.0817 | 0.0067 | 5.994 | 1.5602 | 2.950 |
| 0.50 | 0.000 | 0.000 | 0.000 | 1.5708 | 3.000 |

columns are self explanatory while the sixth contains the breath of the line profile at one-tenth the central intensity divided by the half-width.

To find the parameters for a given profile, the central ordinate C, the halfwidth h, and the breadth of the profile at one-tenth of the central ordinate are obtained. The ratio $b_{0.1}/h$ is calculated and the corresponding values of $b_1 = \beta_1/h$, $b_2 = \beta_2{}^2/h$ and p are obtained from Table XXV, Appendix C. In addition, the area of the profile can be computed from Equation (C-6). If this is done for both the apparatus profile f'(x) and the observed profile f"(x) then the integral Equation (C-1), can be solved for the values of the true profile

$$\beta_1 = \beta_1'' - \beta_1' , \tag{C-7}$$

and

$$\beta_2{}^2 = \beta_2'' - \beta_2', \tag{C-8}$$

and

$$\alpha = \frac{\beta_1}{\beta_2}. \tag{C-9}$$

Using Table XXV, Appendix C, the appropriate values $b_1$, $b_2$, and p for the true profile can be obtained. The halfwidth of the true profile can be calculated using

$$h = \beta_1/b_1 = \beta_2/b_2 . \tag{C-10}$$

Once the central depth is obtained from

$$C = \frac{p''h''c''}{p\ h}, \tag{C-11}$$

then the area of the true profile can be found from Equation (C-6). If the height of the continuum at the line center is known then the equivalent width for the true line profile can be computed using the relation

$$W = \frac{AD}{HC}, \tag{C-12}$$

where HC represents the height of the continuum and D the dispersion of the spectrum for the wavelength considered.

## The Instrumental Broadening Program

The calculations outlined above become extremely tredious if a large quantity of data is being analyzed. This task was improved by the development of a computer program, shown in Tables XXVI and XXVII, capable of evaluating the true halfwidth and equivalent width, given the Voight parameters of the instrument and the observed profile, for an undetermined number of observed lines.

The program begins by first reading into core storage the appropriate Voight parameters of the instrument profile and the standard set of parameters as functions of the form parameter $b_1$ from Table XXV, Appendix C. Two sets of Voight parameters (see Table III, Chapter IV) of the instrumental profile were utilized for this study corresponding to the quality of the intensitometer tracing. Next the central line depth, the halfwidth, the breadth at one tenth the central intensity, and the height of the continuum of the observed profile are entered and the ratio $b_{0.1}/h$ is computed. A linear interpolation of the values in Table XXV, Appendix C is performed and the values of $\beta_1''/h'$, $\beta_2''^2/h''^2$, and $p''$ for the observed profile are obtained from which $\beta_1''$ and $\beta_2''$ are computed. Using Equations (C-7), (C-8) and (C-9), the values for the true profile are calculated and a linear interpolation of the quantities in Table XXV,

## TABLE XXVI

## INSTRUMENTAL BROADENING CORRECTION PROGRAM

```
C      INSTRUMENTAL BROADENING CORRECTION PROGRAM
       INTEGER FLAG
       DIMENSION TBI(50), TBIISQ(50), TALPHA(50), TP(50), TBOI(50)
C      READ TABLE LOOK UP INFORMATION
       NTABLE=50
       READ(5,101)(TBI(I),I=1,NTABLE)
       READ(5,101)(TBIISQ(I),I=1,NTABLE)
       READ(5,101)(TALPHA(I),I=1,NTABLE)
       READ(5,101)(TP(I),I=1,NTABLE)
       READ(5,101)(TBOI(I),I=1,NTABLE)
       WRITE(6, 30)
C      READ IN VALUES FOR EACH LINE
       READ(5,102)NDATA
       DO 50 K=1,NDATA
       READ(5,1)CO,HO,B,HC,WVLG,TRACNO,DISP, EL
C  SET VALUES FOR APPARATUS PROFILE
       AI=0.100
       AII=0.232
       AIII=2.32
       AIV=0.235
       AV=0.190
       AVI=0.505
       AVII=1.295
       AVIII=0.0235
       AIX=1.9E-3
C CONVERT DATA FROM CM TO ANGSTROMS
       CO=CO*DISP/2.54
       HO=HO*DISP/2.54
       B=B*DISP/2.54
       HC=HC*DISP/2.54
C      CALCULATION OF VOIGHT PARAMETERS FOR THE OBSERVED LINE
       BOI=B/HO
       BIO=TLU(NTABLE, TBI, TBOI, BOI,FLAG)
       BIISQ=TLU(NTABLE, TBIISQ, TBOI, BOI, FLAG)
       POB=TLU(NTABLE, TP, TBOI, BOI, FLAG)
       OBI=BIO*HO
       OBIISQ=BIISQ*(HO**2)
C CALCULATION OF VOIGHT PARAMETERS FOR THE TRUE LINE
       TRBI=OBI-AVIII
       TRBIIS=OBIISQ-AIX
       IF(TRBIIS .LE. 0.) GO TO 50
       TRBII=SQRT(TRBIIS)
       ALTR=TRBI/TRBII
       BITR=TLU(NTABLE, TBI, TALPHA,ALTR,FLAG)
       PTR=TLU(NTABLE, TP, TALPHA, ALTR, FLAG)
       BIITRS=TLU(NTABLE,TBIISQ,TALPHA,ALTR,FLAG)
       IF(BIITRS .LE. 0.)GO TO 50
       BIITR=SQRT(BIITRS)
       HTR=TRBII/BIITR
       GAMMA=POB*HO/(PTR*HTR)
       CTR=GAMMA*CO
C CALCULATION OF EQUIVALENT WIDTH AND LOG(W/L) AND LOG(H/L)
       EQW=PTR*HTR*CTR/HC
       X=ALOG10(EQW/WVLG)
       Y=ALOG10(HTR/WVLG)
       WRITE(6,10)EL,WVLG,X,Y
    50 CONTINUE
     1 FORMAT(F8.2,F8.2,F8.2,F8.2,F10.3,I10,F10.3,A6)
```

TABLE XXVI (Concluded)

```
0051         10 FORMAT(1H0,11HELEMENT ** ,A4,10X,13HWAVELENGTH = ,F10.3,10X,
              112HLOG (W/L) = ,F8.3,10X,12HLOG (H/L) = ,F8.3,//)
0052         30 FORMAT(1H1,30X,30H INSTRUMENTAL PROFILE ANALYSIS,////)
0053        101 FORMAT(7F10.4)
0054        102 FORMAT(I3)
0055            STOP
0056            END



0001            FUNCTION TLU(NTABLE,Z,X,XSTAR,FLAG)
          C     ONE-DIMENSIONAL TABLE LOOK-UP PROGRAM.  CORRESPONDING VALUES
          C     OF X (ALWAYS INCREASING) AND Z ARE STORED IN THE ARRAYS
          C     X(1)...X(NTABLE) AND Z(1)...Z(NTABLE).  USING LINEAR INTER-
          C     POLATION, THIS FUNCTION WILL GENERATE A VALUE OF Z CORRESPON-
          C     DING TO A SPECIFIED VALUE OF X=XSTAR
0002            INTEGER FLAG
0003            DIMENSICN X(50), Z(50)
          C     .....CHECK TO SEE ID XSTAR LIES WITHIN THE SCOPE OF THE TABULATED
          C       VALUES X(1)...X(NTABLE)......
0004            FLAG=0
0005            IF(XSTAR .LT. X(1))GC TO 2
0006            IF(XSTAR .LE. X(NTABLE)) GO TO 3
0007          2 FLAG = 1
0008            TLU=0.0
0009            RETURN
          C     .....SEARCH TO FIND TWO SUCCESSIVE ENTRIES, X(I-1) AND X(I),
          C     BETWEEN WHICH XSTAR LIES.....
0010          3 I=1
0011          4 IF(X(I) .GT. XSTAR)GO TO 7
0012            IF(I .GE. NTABLE) GO TO 7
0013            I=I+1
0014            GO TO 4
          C     .....LINEARLY INTERPOLATE TO FIND CORRESPONDING VALUE OF Z.....
0015          7 TLU=Z(I-1)+(XSTAR-X(I-1))*(Z(I)-Z(I-1))/(X(I)-X(I-1))
0016            RETURN
0017            END
```

# TABLE XXVII

INSTRUMENTAL PROFILE ANALYSIS

| | | | |
|---|---|---|---|
| ELEMENT ** FE I | WAVELENGTH = 4045.815 | LOG (W/L) = -3.971 | LOG (H/L) = -4.069 |
| ELEMENT ** FE I | WAVELENGTH = 4063.597 | LOG (W/L) = -4.024 | LOG (H/L) = -4.106 |
| ELEMENT ** FE I | WAVELENGTH = 4071.740 | LOG (W/L) = -4.085 | LOG (H/L) = -4.071 |
| ELEMENT ** FEI | WAVELENGTH = 4325.762 | LOG (W/L) = -3.974 | LOG (H/L) = -3.972 |
| ELEMENT ** FE I | WAVELENGTH = 4383.547 | LOG (W/L) = -4.068 | LOG (H/L) = -4.019 |
| ELEMENT ** FE I | WAVELENGTH = 4404.750 | LOG (W/L) = -4.148 | LOG (H/L) = -4.120 |
| ELEMENT ** FE I | WAVELENGTH = 4415.648 | LOG (W/L) = -4.217 | LOG (H/L) = -4.105 |
| ELEMENT ** FE I | WAVELENGTH = 4871.320 | LOG (W/L) = -4.362 | LOG (H/L) = -4.054 |
| ELEMENT ** FE I | WAVELENGTH = 5429.695 | LOG (W/L) = -4.494 | LOG (H/L) = -4.248 |
| ELEMENT ** FE I | WAVELENGTH = 4531.148 | LOG (W/L) = -4.138 | LOG (H/L) = -3.859 |
| ELEMENT ** FE I | WAVELENGTH = 4415.125 | LOG (W/L) = -4.200 | LOG (H/L) = -4.103 |
| ELEMENT ** FE I | WAVELENGTH = 4271.762 | LOG (W/L) = -4.184 | LOG (H/L) = -4.113 |
| ELEMENT ** FE I | WAVELENGTH = 4260.477 | LOG (W/L) = -4.222 | LOG (H/L) = -4.138 |
| ELEMENT ** FE I | WAVELENGTH = 4227.434 | LOG (W/L) = -4.315 | LOG (H/L) = -4.181 |
| ELEMENT ** FE I | WAVELENGTH = 4202.027 | LOG (W/L) = -4.257 | LOG (H/L) = -4.229 |

Appendix C is again made to produce $b_1$, $b_2$, and p for the true profile. The halfwidth of the true profile is calculated from Equation (C-10) and reproduced as output in the more useful form, log $h/\lambda$. With the aid of Equations (C-11) and (C-12), the equivalent width corrected for the apparatus function is evaluated. This quantity is then converted to the form $\log(w/\lambda)$ and listed in the output along with the element, wavelength, and log $h/\lambda$ for the individual line considered. At this point, the program progresses to the next line and repeats the computations until the entire set of observational data has been exhausted.

VITA

Malcolm Lee Bruce Weems

Candidate for the Degree of

Doctor of Philosophy

Thesis: A DETAILED ANALYSIS OF THE CHEMICAL ABUNDANCES FOR THE STAR THETA URSAE MAJORIS

Major Field: Physics

Biographical:

Personal Data: Born in Nashville, Kansas, the son of Bryan W. and Katherine M. Weems.

Education: Attended grade school in Sawyer, Collyer and Mahaska, Kansas; graduated from Mahaska High School in May, 1963; awarded the Bachelor of Science degree from Kansas State Teachers College, Emporia, Kansas, in May, 1967 with a major in Physical Science and Mathematics; received the Master of Science degree from Kansas State Teachers College in May, 1969 with an emphasis in physics; completed requirements for the Doctor of Philosophy degree in May, 1972.

Professional Experience: Graduate Teaching Assistant, Kansas State Teachers College, Department of Physical Science, 1963-65; Lecturer, Department of Physical Science, Kansas State Teachers College, 1966-67; Graduate Teaching Assistant, Department of Physics, Oklahoma State University, 1969-1972.